Valuing Green Infrastructure Technical Appendices

WORLD BANK GROUP | Korea Green Growth Trust Fund | natural capital PROJECT

1818 H Street NW
Washington DC 20433
Telephone: 202-473-1000
Internet: www.worldbank.org

[Cover photo: Aleksei Kazachok/Shutterstock.com | Dave Primov/Shutterstock.com

Valuing Green Infrastructure Technical Appendices

CONTENTS

APPENDIX 1: DEVELOPING A BASELINE SEDIMENT BUDGET: KALI GANDAKI, NEPAL

1. BASELINE SEDIMENT BUDGET FOR KALI GANDAKI

Understanding the sediment budget of the Kali Gandaki, i.e., the provenance and the processes generating sediment in the catchment, is crucial to design effective sediment management strategies. This section describes data collection efforts in the Kali Gandaki Basin and the henceforth derived sediment budget of the basin.

2. SAMPLING STATIONS AND DATA AVAILABILITY

A sediment sampling campaign was performed under supervision of Kathmandu University for five gauging stations Jomsom, Tatopani, Manghalgat, Nayapul and Modibeni. There are three stations on the main stem of the Kali Gandaki River. Jomsom is located at the end of the Mustang Plateau. Tatopani roughly marks the end of Kali Gandaki Gorge and Modibeni is located upstream of the confluence of the Kali Gandaki and the Modi River. Two additional stations are located on the major eastern and western tributaries. Manghalgat is located on the Myagdi River and Nayapul is located on the Modi River. The location of gauging stations is shown in Figure 1. Figure 1 also shows the drainage area of a sixth gauging station at the location of the Kali Gandaki reservoir. However, it should be noted that this station was not part of the current sampling and all analysis are based on past values reported by NEA and others. The sub-catchments covered by the drainage area are very heterogeneous in terms of their climatic and morphologic conditions. Possibly important factors related to the possible sediment generation from each catchment are, for example, the overall elevation and relief, the precipitation and the glaciation. Glaciation and precipitation, as well as relief is highest in watersheds draining the main chain of the Himalayas (Modi Beni, Manghalghat and Nayapul).

Figure - 1: Topography of the Kali Gandaki basin, location of gauging stations and their respective drainage area. Note that no sampling was taken at Kali Gandaki Reservoir but values were interpolated from upstream observations

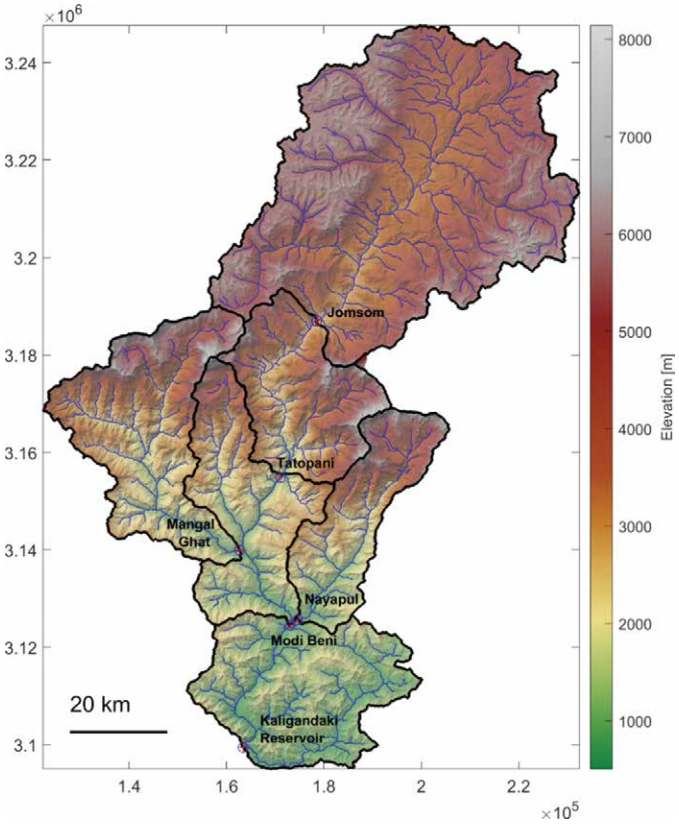

Figure 2 shows a simplified overview of the drainage network in the catchment and the location of the gauging stations. It should be noted that there are no direct observations of discharge for Kali Gandaki (only sediment concentration) and no measurements at all in the Aadhi Khola River which enters into the reservoir of Kali Gandaki. Otherwise, it should be noted that Modi Beni station receives sediment from the entire

Mustang, the Kali Gandaki Gorge, and the Upper Kali Gandaki and the Myagdi Khola. The combined load from the Modi Khola and the Upper Kali Gandaki then presents the inflow into the lower Kali Gandaki reach with Kali Gandaki A at the downstream end.

Figure - 2: Schematic of the river network and the gauging stations in Kali Gandaki. Points and italic names indicate gauging stations and bold names refer to sub-catchments. It should be noted that there are no joint measurements for sediment and discharge in Kali Gandaki and no data at all for the Aadhi Khola river

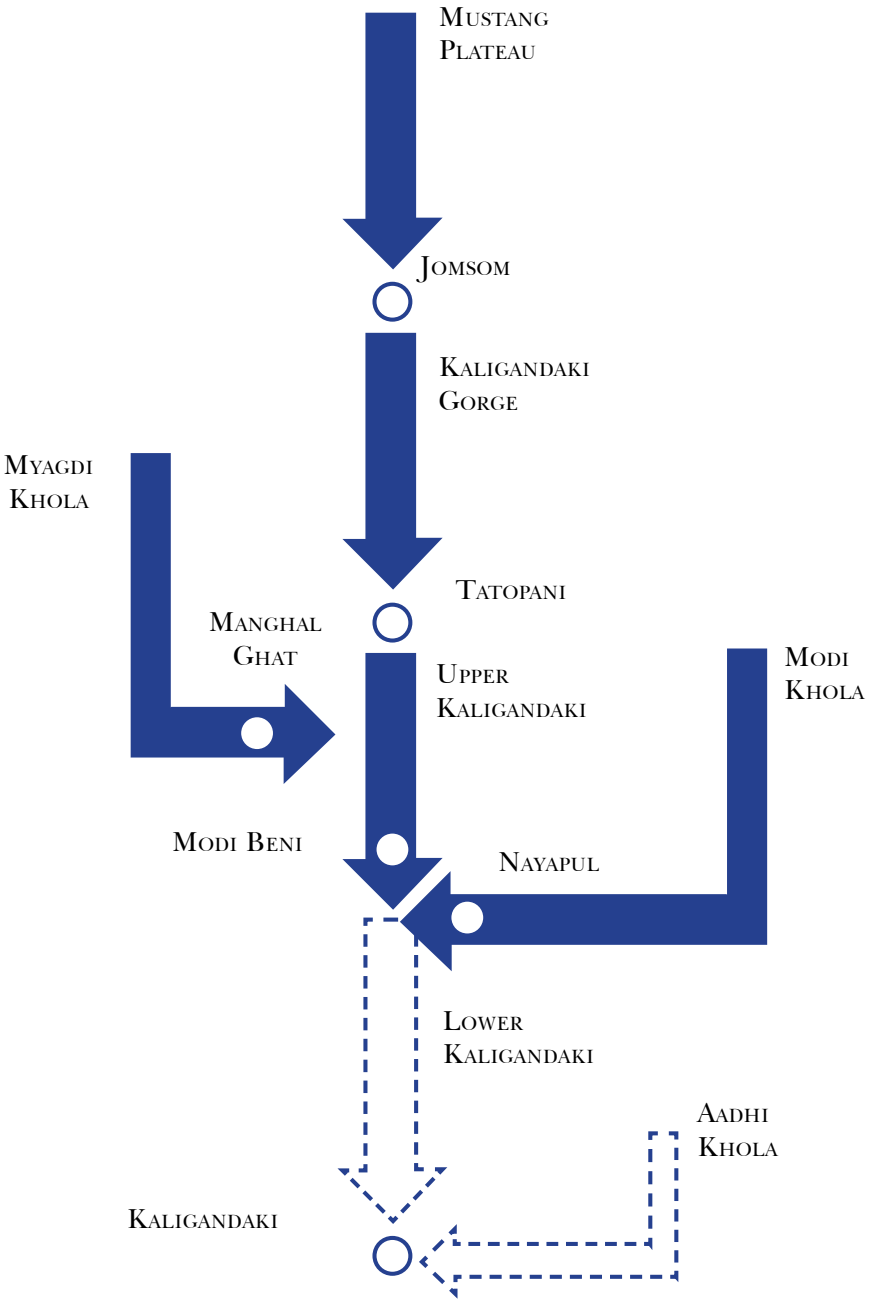

Table - 1: Overview over sub-basin characteristics of gauging stations used in this study. Elevated symbols indicate data sources +: derived from the DEM (30 m resolution), *: ICMOD glacier dataset, # interpolated from DHM rain gauges using Kriging

Name	River	Description	Drainage area [km²]+	Mean Elevation [m]+	σ elevation [m]+	Glaciation [%]*	Mean annual precipitation [mm]#
Jomsom	Kali Gandaki	Mustang Plateau	3165	4786	845	7.9	426.0
Tatopani	Kali Gandaki	Upper Kali Gandaki Gorge	782	3946	1251	9.8	1191.1
Manghalghat	Myagdi Khola	Myagdi Khola and Dhaulagiri Range	1095	3357	1509	12.6	2260.3
Modi Beni	Kali Gandaki	Middle Kali Gandaki	840	2405	1092	1.5	2076.1
Nayapul	Modi Khola	Modi Khola and Annapurna Range	648	3192	1645	11.8	2988.0
Kali Gandaki Reservoir	Kaligand-aki Reservoir	Not covered in current sampling campaign, lower Kali Gandaki	1034	1245	365	0.0	2394.7

Table - 2: Available data on discharge and sediment concentration. Sources are: * Kathmandu University sampling campaign, +: DHM, #: NEA

Name	Q (2018 - 2019)	CS (2018 - 2019)	Q (Other)	QS (Other)
'Jomsom'	n/a	65 weekly samples+	Daily 2009 – 2014+	n/a
'Tatopani'	65 weekly samples*	65 weekly samples+	Daily 2010 – 2014+	n/a
'Manghalghat'	65 weekly samples*	65 weekly samples+	Daily 2011 – 2015+	n/a
'Modi Beni'	65 weekly samples*	65 weekly samples+	Daily 2009 – 2013+	n/a
'Nayapul'	65 weekly samples*	65 weekly samples+	Daily 2011 – 2015+	n/a
'Kali Gandaki Reservoir'	n/a	n/a	n/a	Sand and mud concentration from 2003 – 2015 at different locations in the reservoir and plant. Separated by sand and finer fractions. Mostly daily but partially fragmentary#

3. METHODS

3.1. Deriving sediment rating curves

The discharge record for all stations is much more comprehensive than the sampling of sediment concentrations. For most stations, there are at least three more years of relatively recent discharge observations (Table 2). These data sets can be used to extrapolate the sediment transport in past years without sediment observations by using sediment rating curves. A common way to generalize the non-linear relationship between discharge Q and sediment concentration C_S is to fit a non-linear regression of the form

$$C_S = a * Q^b$$

The such derived equation can be used to estimate sediment loads from past discharge records. To derive the regression parameters a and b we used a least average residual (LAR) method, rather than the common sum of square errors (SSE) approach, to find an optimal fit between the observed Q and C_S at each station. This choice was to give less weight to some outliers observed for some stations (notably in Nayapul) and to derive rating curves with characteristics mirroring the basic understanding of sediment transport processes, e.g., that C_S increases overproportionately with Q (i.e., $b>1$).

It should be noted that the rating curve approach creates an analytic link between Q and C_S but also introduces some uncertainty (Asselman 2000). Nonetheless it is still widely used in engineering and water management applications.

3.2. Sediment sampling and load calculations

Sampling took place from February 2018 – January 2019. Samples were taken at 5 gauging stations throughout the basin with a roughly weekly frequency. Sediment concentrations were derived using standard procedures and multiple repetitions per site and date. As the staff derived samples wading in the river, it should be noted that samples are not taken across the entire cross section as high flows make crossing the rivers and wading impossible during most of the monsoon season. Discharge was derived for all sampling locations from the DHM gauging stations, so that total sediment discharge for each station can be calculated as

$$Q_s(t) = Q(t) * C_S(t)$$

With Q_s[t/d] and Q[m³/d] being the discharge of sediment and water, C_S being the sediment concentration [t/m³] and t denoting the day of the year when a sample was taken. To calculate the total annual load, we assumed that the load is constant between measurement dates. In addition to sediment samples and discharge observations, there were various other data available from previous studies and DHMs long term monitoring (Table 2).

3.3. Handling missing data

It should be noted that there were no reliable measurements for the most upstream station (Jomsom, Table 2), which is a major limitation, given that the drainage area of Jomsom station covers nearly half of the total drainage area and that that particular area is subject to very specific hydro- climatic conditions (high desert) (Figure 1, Table 1).

We analyzed past discharge observations for Jomsom and the next downstream station, Tatopani, to estimate Q_{Jomsom} and hence to calculate Q_s for Jomsom for the 2018 – 2019 sampling campaign. To do so, we compared the discharge for each day with a discharge record in Jomsom with the discharge in Tatopani. The comparison shows that the ratio $\frac{Q_{Jomsom}}{Q_{Tatopani}}$ is variable over the year but can be well described by an average 0.44. Hence, we calculated the sediment load in Jomsom for the 2018/2019 sampling campaign from the observed sediment concentration in Jomsom and assuming that $Q_{Jomsom} = 0.44\ Q_{Tatopani}$

It should also be noted that the most downstream station (Modi Beni) is still significantly upstream from KGA. The available gauging stations cover only around 6500 of 7500 km2 of the total drainage area of KGA. While there are many years of sediment concentration measurements available in KGA (Table 2), we did not have access to discharge data at KGA. To estimate discharge at the KGA, we assumed that the discharge between the confluence of the Kali Gandaki and the Modi Khola and KGA scales linearly with drainage area so that for any given day

$$Q_{KG} = (Q_{Modi\ Khola} + Q_{Modi\ Beni}) * \frac{AD_{Kaligandaki\ A}}{A_{Modi\ Khola} + A_{Modi\ Beni}}$$

3.4. Sediment budget for Kali Gandaki

The average sediment budget for different parts of the Kali Gandaki catchment can hence be calculated for different periods of time from the different stations; specifically, we can calculate:

- Sediment budget for 2018/2019 from the measured concentration and observed discharge at the five gauging stations upstream of KGA
- Sediment budget for the 2009 – 2015 period calculated from discharge data for that period and 2018/2019 sediment rating curves.

4. RESULTS

4.1. Sediment rating curves for Kali Gandaki

Table 3 shows the parameters fitted to discharge and sediment observations from the years 2018/2019. It should be noted that the parameters vary greatly between stations. Possibly, these parameters carry some information about each station's drainage area. Specifically, the *a* parameter can be interpreted as indicator for the erodibility of a catchment. The *b* factor can be interpreted as indicator for the erosive forces (Asselman 2000). Some of the most outstanding parameter values are the *a* values for Jomsom and Tatopani, which indicate a much greater erodibility there than in the other parts of the catchment. This finding is largely in line with our understanding as these parts of the catchment are being rapidly uplifting and eroding, respectively consisting of erodible rock types (Fort 2015; Lavé J. and Avouac J. P. 2001).

Table - 3: Parameters of sediment rating curves for gauging stations in the Kali Gandaki catchment

	Jomsom	Tatopani	Manghalghat	Nayapul	Modibeni
a	17.09	3.13	0.62	0.82	2.39
b	1.40	1.49	1.47	1.30	1.19

Figure - 3: Observed daily load (top) and cumulative load in the Kali Gandaki basin.

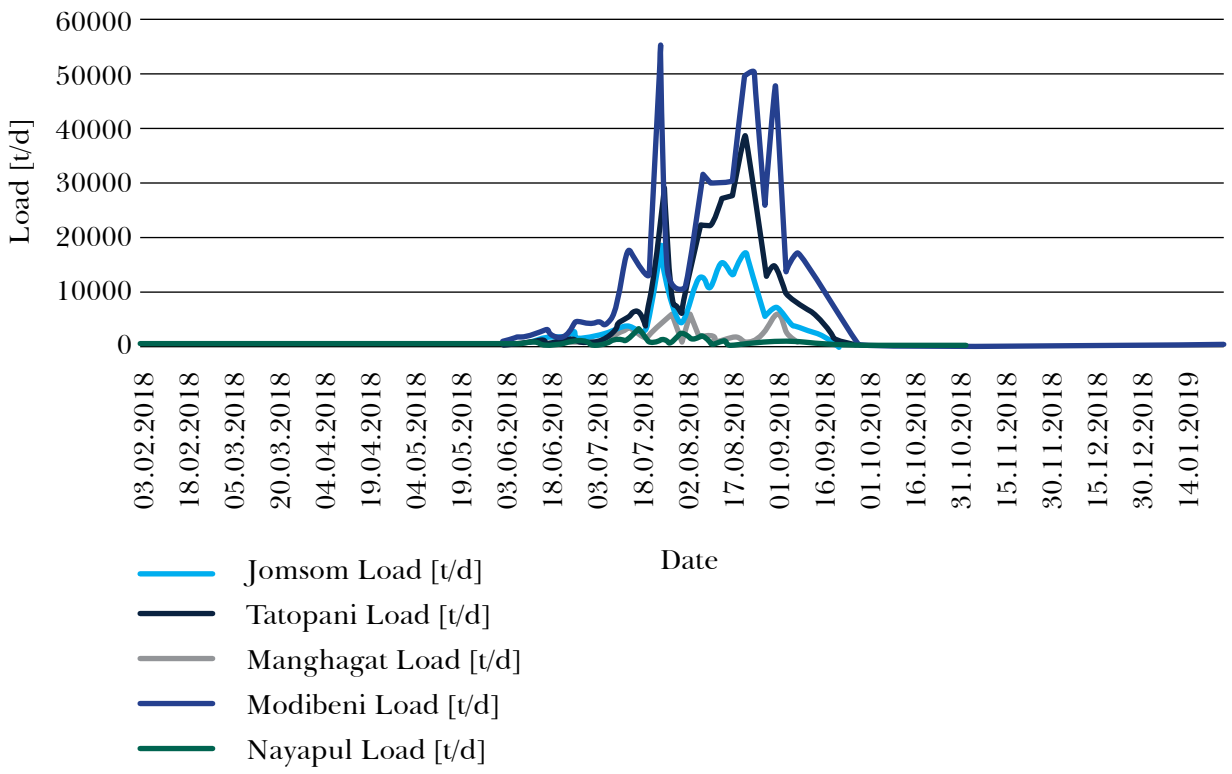

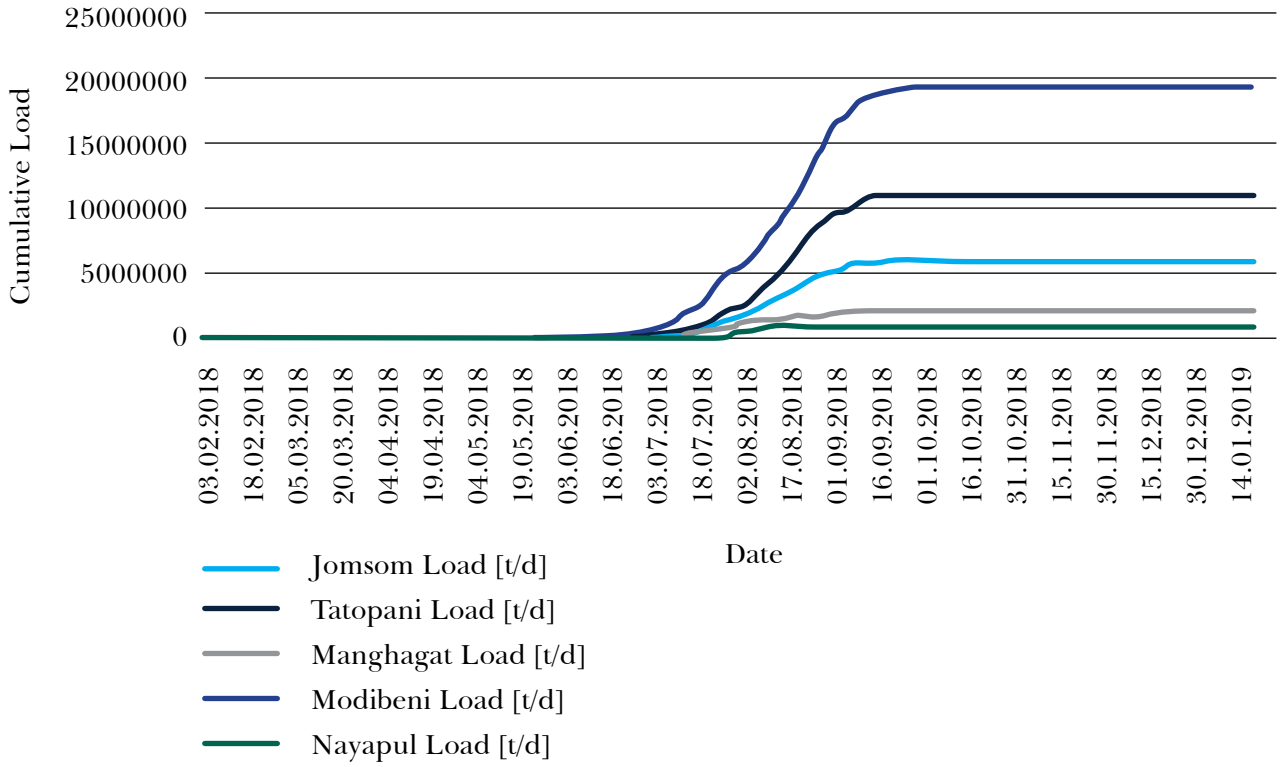

4.2. Sediment loads and sediment budgets for Kali Gandaki

4.2.1. 2018-2019 Sediment summary

Figure 3 shows the instantaneous daily load, as well cumulative load over the length of the sampling campaign in the five considered gauging stations. What is notable is the small sediment load of tributaries compared to the main stem of the Kali Gandaki, as visible for both the instantaneous observations and daily values for Manghalgat and Nayapul station. The contribution of each catchment, ΔQ_S can be calculated as follows

- Jomsom, Mustang Kali Gandaki: $\Delta Q_{S,Jomsom} = Q_{S,Jomsom}$
- Tatopani, Kali Gandaki Gorge: $\Delta Q_{S,Tatopani} = Q_{S,Tatopani} - Q_{S,Jomsom}$
- Manghalgat, Myagdi Khola: $\Delta Q_{S,Manghalgat} = Q_{S,Manghalgat}$
- Nayapul, Modi Khola: $\Delta Q_{S,Nayapul} = Q_{S,Nayapul}$
- Seti Beni, middle Kali Gandaki: $\Delta Q_{S,Seti\ Beni} = Q_{S,Seti\ Beni} - Q_{S,Tatopani} - Q_{S,Manghalgat}$
- Kali Gandaki A, Lower Kali Gandaki: $Q_{S,Kaligandaki\ A} = Q_{S,Kaligandaki\ A} - Q_{S,Seti\ Beni} - Q_{S,Nayapul}$ (keeping in mind that sediment load in Kali Gandaki A is calculated from a mixture of different sources of discharge and sediment concentration and cannot be calculated for the year 2018/ 2019).

In terms of relative contribution, most sediment originated from the Mustang Plateau and the middle Kali Gandaki (around 30 % from each catchment). In terms of sediment yield, i.e., tons produced per area of catchments, the Kali Gandaki Gorge and the middle Kali Gandaki provide most sediment. The sediment yield from the Mustang is comparably low (<2000 t/ km²/yr). It is notable, that the tributary catchments of the Myagdi Khola and Modi Khola have similarly low rates of sediment load, even though they receive nearly an order of magnitude more of rainfall. This indicates that the soils and hillslopes in these catchments are relatively harder to erode (low erodibility) while the opposite is true for the Mustang Plateau.

Figure - 4: Sediment contribution from each sub-catchments in terms of total load (top) and sediment yield (bottom) for 2018/2019, please refer to Figure 1 for the definition of the different sub-catchments

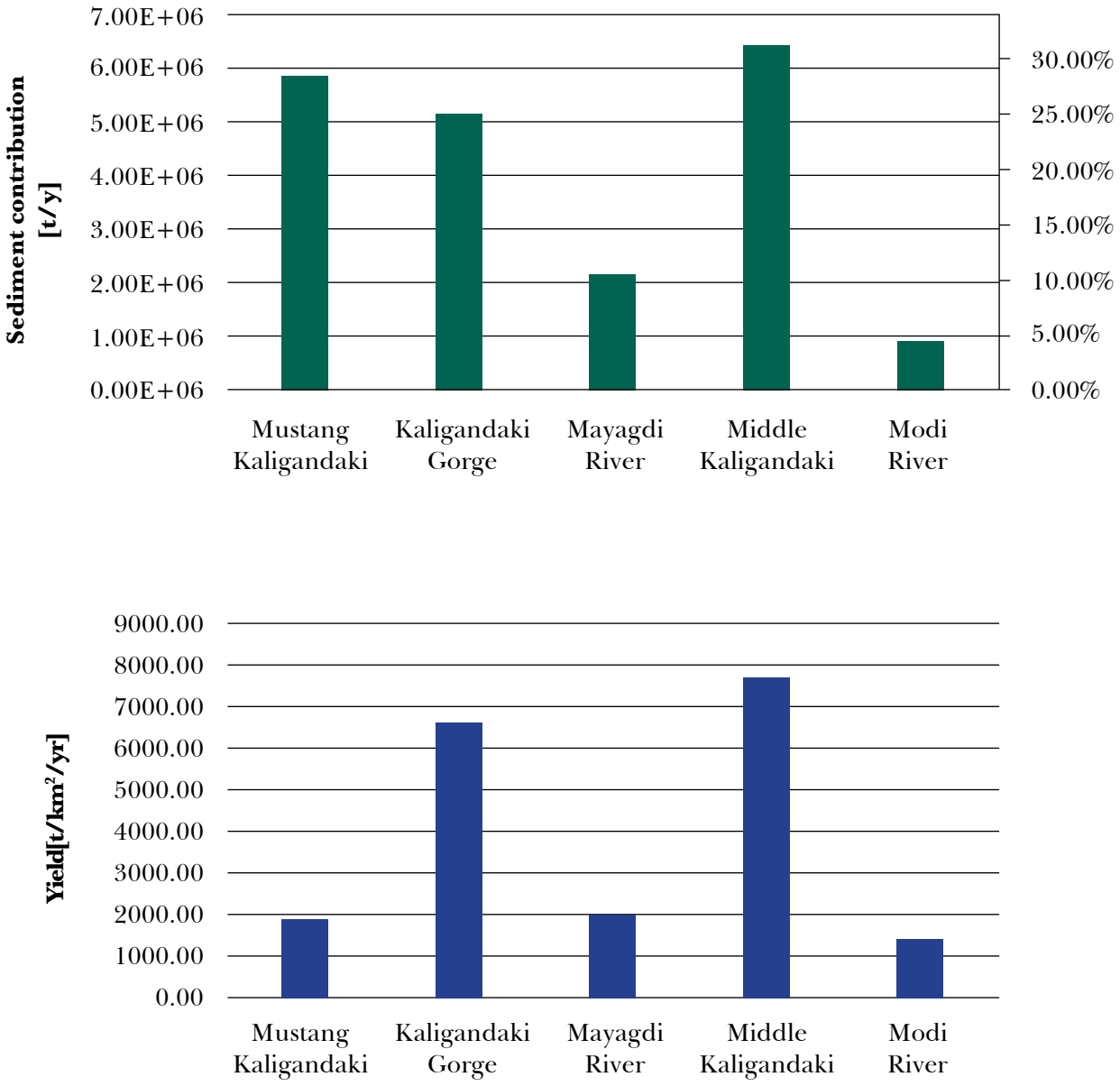

4.2.2. Longer-term averages

Figure 5). This analysis also includes the joint analysis of discharge and sediment concentration at KGA. The average annual load at Kali Gandaki A is 31± 4.9 Mt/yr of fine sediment. This is in a similar range than values reported elsewhere. For example, Struck et al. (2015) report 30 ± 3.2 Mt/yr for the 2011/2012, likely calculated from the same sediment concentration data but using observed rather than interpolated discharge data, as has been done in this study. In terms of sediment yield, these data emphasize the high variability in yield between sub-catchments and confirm the very high yields for the Kali Gandaki Gorge upstream of Tatopani and the middle Kali Gandaki.

Neither this study nor Struck et al. (2015) report values for bed load (i.e., gravels and coarser), which can likely make a major difference in a mountain river with high transport capacity. Assuming that bedload

Average sediment loads from different parts of the catchment and their variation over multiple years can be estimated using the rating curve approach

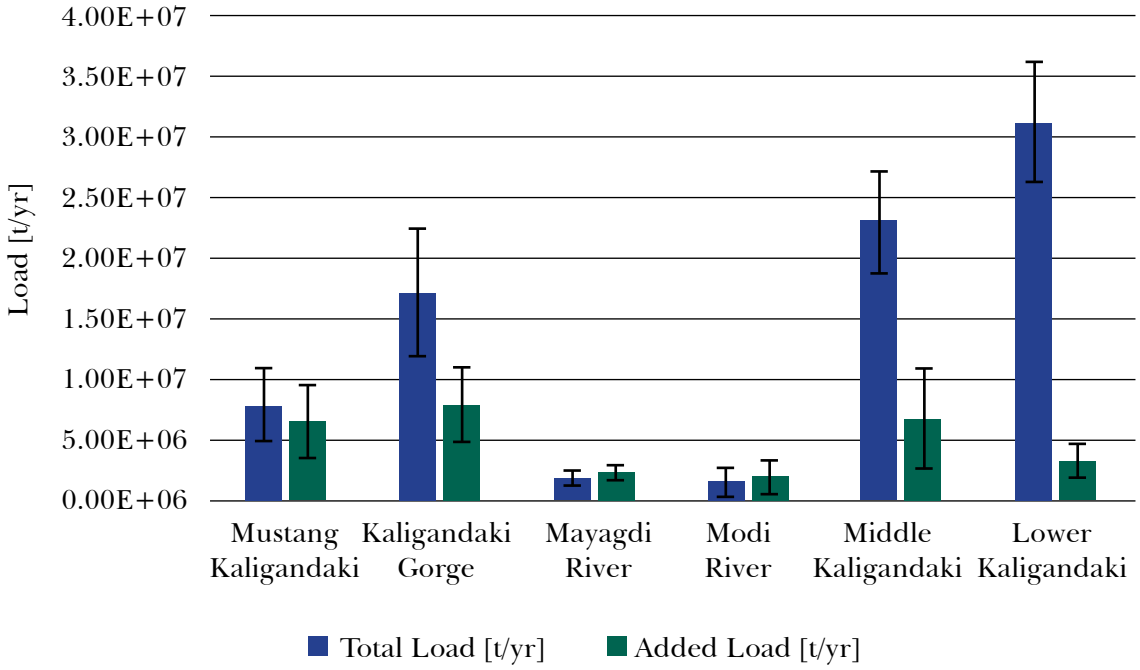

Figure - 5: Total load and contribution of sub-catchments as derived from past discharge data and rating curves for 2009 – 2015 (not all years covered for all stations, see Table 1)

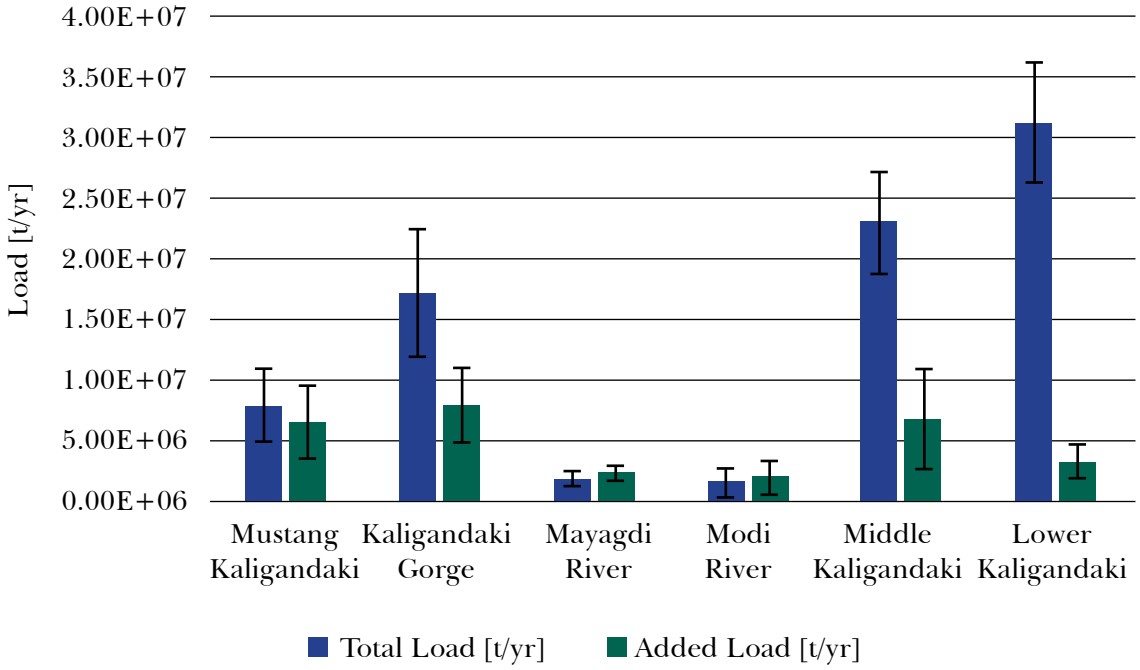

Figure - 6: Yield of sub-catchments as derived from past discharge data and rating curves for 2009 – 2015 (not all years covered for all stations, see Table 1)

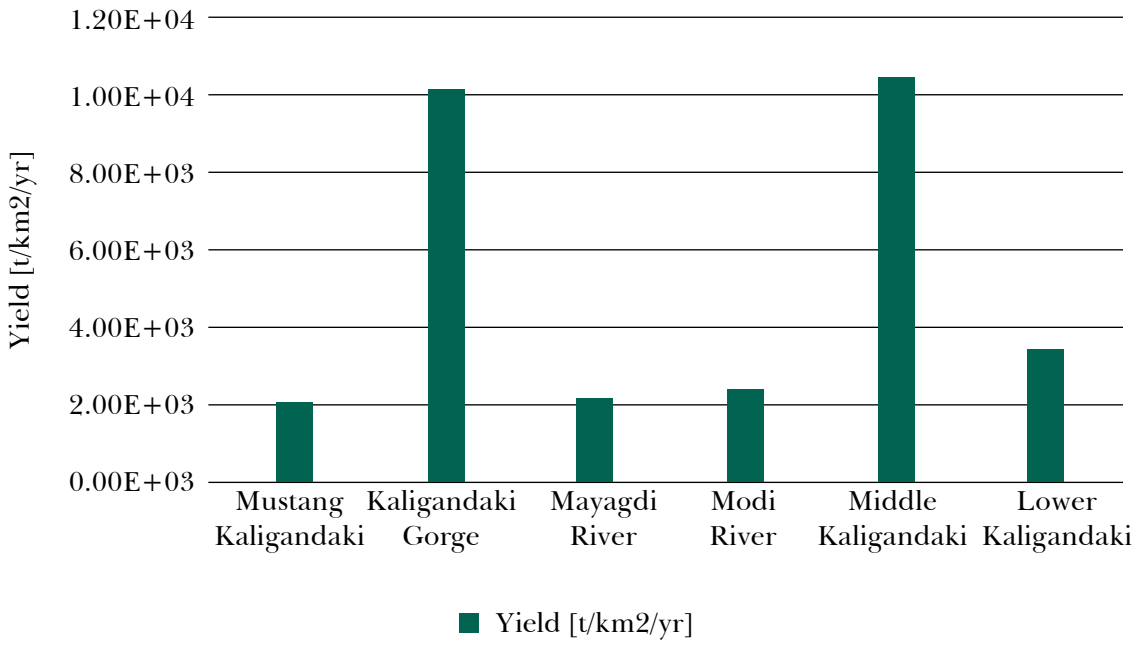

might constitute 10 to 20% of the total load, the total load can be estimated in the range of 33 – 36 Mt/yr. The longer-term interpolation indicates that there is a significant variability in load from the Mustang Plateau and the Kali Gandaki Gorge, as well as from the Middle and Lower Kali Gandaki sub-catchments. The Mustang area and the Kali Gandaki Gorge have a very similar sediment load, each contributing around 5 – 7Mt/yr. What is evident, too, is that the Myagdi and Modi rivers contributed relatively little to the overall sediment budget for all years on record.

APPENDIX 2: MODELING LANDSLIDE RISK AND VALUING BENEFITS

1. INTRODUCTION: STOCHASTIC MODELING OF CONNECTED HILLSLOPE STABILITY

Approaches for landslide hazard mapping on catchment scales are commonly based on evaluating the factor of safety equations on the scale of individual cells in a gridded model domain. Slope stability on the level of individual cells is potentially a causal factor in the creation of landslides. However, slope stability analysis on the scale of single cells does not consider for the spatial connectivity of hillslope processes. This is a major limitation both for estimating the spatial extent of potential landslides and their downslope runout zone and hence identifying structures at risk on the slide. Understanding connectivity of landslide prone cells is also crucial to estimate landslide magnitude in terms of sediment mobilization which information is important for analyzing landslide hazards and landslide contributions to catchment sediment budgets.

Herein, we propose Landslide Objects (LSOs) as the unit of analysis for catchment-scale landslide hazard screenings. LSOs are identified from an analysis of downslope connectivity amongst failure prone cells. LSOs provide the spatial template for evaluating landslide failure probability and downslope hazards. Finally, LSOs are integrated in a probabilistic hazard assessment driven by spatially generalized extreme-value distributions for precipitation. The resulting framework is demonstrated in the case study of the Kali Gandaki catchment in Nepal, where we model landslide occurrence probability as well as structures at risk, the possible economic loss, and benefits from landslide mitigation. Despite the great uncertainty in input parameters, we show how the framework can be used to identify locations and magnitudes of potential slope failures, assets at risk, and possible focal areas for landslide management, which makes the method one of interest fin the study of both catchment sediment dynamics as well as hazard mapping and mitigation.

2. METHODS

This section describes the method for the stochastic slope stability analysis, identification of LSOs and empirical estimation of downslope runout length. We describe first some basics of the factor of safety calculation and a statistical approach to determine threshold saturation conditions and failure probabilities of individual cells in the model domain. We then describe how we aggregate the derived information for groups of conditionally unstable cells that are connected in downslope direction, so called landslide objects (LSOs). We propose how LSOs can be used to aggregate certain properties (i.e., failure probabilities and threshold rainfall conditions) for all cells belonging to an LSO and enable analyzing properties of slope failure such as mobilized sediment volume and length of downslope runout which cannot be derived from commonly applied analyses of slope stability on the scale of single cells. The model resolution is identical to the resolution of the underlying DEM (30m for this study). It should be noted that coarser resolution will likely lead to a drastic underestimation of landslide probability, because local steep hillslope gradients would be increasingly smoothed out.

2.1. Current best practice: single cell deterministic slope stability

Catchment-scale landslide zonation are commonly based on evaluating slope stability using the Mohr Coulomb failure criterion for individual cells in a model domain, e.g., an individual cell in a digital elevation model (DEM), assuming an infinite slope and a relative shallow and surface-parallel failure mode. For a single cell i in a DEM, the factor of safety is defined as the balance between shear strength, $\tau_{i,}$ and shear stress, $\tau_{m,i}$ as

$$FS_i = \frac{\tau_i}{\tau_{mi}} \quad \mathbf{1}$$

With the assumption that cell i is prone to slope failure when $FS_i<1$. In its full form, FS_i is defined as

$$FS_i = \frac{c_i + \delta c_i + (\gamma_s - \gamma_w * m_i) * z_i * \cos^2 \alpha_i * \tan \phi_i}{\gamma_s * z_i * sin\alpha_i * cos\alpha_i} \quad \mathbf{2}$$

The equation is based on the following input variables:

c_i: soil cohesion [kPa]
δc_i: added cohesion because of plant roots [kPa]
γ_s: unit weight of soil [kN/m3]
γ_w: unit weight of water [kN/m3]
m: soil water saturation [-]
z_i: soil depth, assumed to be the depth of a potential failure plane [m]
α_i: slope angle [deg]
φ_i: soil internal angle of friction

It should be noted that the above notation distinguishes between global variables, e.g., physical constants, and variables that vary spatially within a watershed and are hence specific for a given cell (denoted by subscript i).

Table - 3: Data sources, typical values and references for key input variables for the landslide model.

Input	Typical values	Data Source - Nepal	Data source – Pakistan
c_i	Set to 10 kPa for all cells where soil is present (as an estimated average over values listed here: https://daac.ornl.gov/SOILS/guides/Global_Hydrologic_Soil_Group.html) and to infinity for all cells with no soil. Different soil types could be assigned different cohesion values if there was location specific evidence	Data on soil types and location of cells with no cells are derived from the ISRIC-SOTER database	
δc_i	Additional soil cohesion because of roots was set to 12 kPa (Vanacker et al. 2003), for all cells where land use landcover maps indicated presence of forest	Nepal-specific land use landcover map	Global data from remote sensing provided by the European Space Agency
γ_s	Set to 16 Kn/m^3 for all cells (Vanacker et al. 2003). Different soil types could have significantly different densities and weights but such information was not available	n/a	
γ_w	Set to 10 Kn/m^3 for all cells (physical constant)	n/a	
m	Calculated for each cell based on a spatial interpolation of observed rainfall data (see Figure 6)	35 rainfall gauges with 20 years of daily data (1995 - 2005). See Figure 6 for location	Global daily precipitation from remote sensing (TRMM) for 2000 – 2015
z_i	Derived from gridded global data	Derived from the ISRIC-SOTER database	
α_i	Derived from the digital elevation model	ASTER Digital Elevation Model (DEM), 30 m resolution	
φ_i	Set to 15° according to lower estimates (Vanacker et al. 2003) for all cells. Different soil types could be assigned different cohesion values if there was location specific evidence	n/a	

The soil saturation will undergo major temporal variations as a function of local infiltration and sub-surface water inflow from the area draining to , $A_{D,i}$, and the spatio-temporal variability in precipitation this area receives. To evaluate the soil saturation over a longer time period, the use of steady state hydraulic considerations is common practice (Montgomery David R. and Dietrich William E. 2010; Vanacker et al. 2003). According to O'Loughlin (1986), the local soil saturation can be derived from

$$m = \frac{q_i * A_{D,i}}{b_i * T_i} \quad 3$$

In this model, q_i is the average subsurface flow to i from upslope [m3/s]. $A_{D,i}$ is the upslope area [m], b_i is the downstream boundary length of cell i [m] and T_i is the transmissivity, which is calculated as

$$T_i = K * z_i * cos\alpha \quad 4$$

[m2/s], with K being the saturated hydraulic conductivity [m/s]. In simple terms, the numerator is the water supplied from the area draining to i and the denominator is the local soil transmissivity at the downstream boundary of cell i of length b_i, i.e., how much water can be conveyed by subsurface flow at the downstream boundary of i. Hence, if m_i>1, water inflow is larger than subsurface drainage and overland flow occurs.

q_i is the residual of precipitations minus losses to evapotranspiration $ET0$, direct runoff Q_R, and deep percolation Q_D. Hence

$$q_i = p - ET0 - Q_R - Q_D \quad 5$$

where each variable is in [m] and denotes the average over the upslope area of i. Alternative to such a spatial averaging, q_i can be calculated to consider explicitly for spatial variability in upslope conditions. Let $j \in AD_i$ be a cell located in the area draining to i. Then, the upstream contribution to subsurface flow is:

$$q_i * A_{D,i} = Q_i = \sum_{j \in AD_i} (p_j - ET_j - Q_{R,j} - Q_{D,j}) * b_j^2 \quad 6$$

It should be noted that i might also receive some percolation from the surface flow created upslope and flowing over i. However, we do not consider for this effect in here.

Most of the variables can be determined using standard procedure, specifically

$$ET_j = ET0_j * c_j \quad 7$$

$ET0_j$ is the reference evapotranspiration and c_j is the crop-coefficient in cell j. The surface runoff can be determined using a standard approach based on, e.g., the curve number method, i.e.,

$$Q_{R,j} = \begin{cases} \frac{(p_j - 0.2S_j)^2}{p_j + 0.8S_j} \; if \; I_{a,j} < p_j \; (initial \; abstraction \; \; less \; than \; precipitation) \\ 0 \end{cases} \quad 8$$

and

$$S_j = \frac{1000}{CN_j} - 10 \quad 9$$

and

$$I_{a,j} = 0.2 * S_j \quad 10$$

In which CN_j is the local curve number depending on land use type and soil characteristics, which is described in detail in standard engineering literature. Finally, we don't consider for deep percolation (i.e., $Q_{D,j}$=0), which will strongly depend on local geology and lithology. Thus, information which is not commonly available on catchment scales.

The factor of safety for an individual cell i for longer term average hydrologic conditions can be calculated from the above equations. However, this approach (which is the current state of the art for catchment scale hazard assessments) has two significant shortcomings:

1. Calculations are based on long-term averages of soil moisture (typically annual means), while it is evident from basic science and observations that most landslides occur for individual extreme rainfall events
2. Calculations are considering all cells in the model domain individually. Not considering for possible connections between these cells disables estimating landslide magnitude and spatial extent. Both parameters are crucial parameters for landslide risk assessments but not commonly available on catchment scales using standard FS-mapping approaches.

2.2. Probabilistic factor of safety calculations

Most parameters in the Factor of Safety equation

$$FS_i = \frac{c_i + \delta c_i + (\gamma_s - \gamma_w * m_i) * z_i * \cos^2 \alpha_i * \tan \phi_i}{\tau_{m,i}} \quad 11$$

vary in space but are constant for a single cell over a management-relevant time horizon (years to decades). Soil moisture conditions, however, vary on seasonal and daily timescales as a function of variability in precipitation. The factor of safety equation allows one to derive the saturation which relates in a specific value of FS_i as

$$m_i = \left[\frac{FS_i * \tau_{m,i} - (c_i + \delta c_i)}{z_i * \cos^2 \alpha_i * \tan \phi_i} - \gamma_{s,i}\right] \frac{1}{-\gamma_w} \quad 12$$

Assuming that slope failure occurs when $FS_i \leq 1$ allows to define m_i^* is the threshold saturation for slope failure at a value of $FS_i = 1$

$$m_i^* = \left[\frac{\tau_{m,i} - (c_i + \delta c_i)}{z_i * \cos^2 \alpha_i * \tan \phi_i} - \gamma_{s,i}\right] \frac{1}{-\gamma_w} \quad 13$$

Reaching the threshold saturation m_i^* is a function of threshold subsurface flow Q_i^* which can be derived from

$$m_i^* = \frac{Q_i^*}{b_i T_i} \quad 14$$

$$m_i^* b_i T_i = Q_i^* \quad 15$$

In tropical settings, failure of a slope will often occur when a rainfall event of a specific magnitude will add soil moisture to an already partially saturated slope during the rainy season (Dahal and Hasegawa 2008; Gabet et al 2004). Hence, we can define Q_i^* as

$$m_i^* b_i T_i = Q_i^* = \overline{Q_\iota} + Q_i(e)^* \quad 16$$

Respectively

$$m_i^* b_i T_i - \overline{Q_\iota} = Q_i(e)^* \quad 17$$

Where $\overline{Q_\iota}$ is a represents the average subsurface flow from the upstream area through cell i, e.g., during the rainy season, and $Q_i(e)^*$ is the critical moisture an event e will need to add to result in an exceedance of threshold conditions. Similar to equation 6, the average subsurface flow can be estimated from the water balance of the upslope area, assuming that cell i is at a seasonal equilibrium with regard to subsurface flow when event e occurs

$$\overline{Q_\iota} = \sum_{j \in AD_i} (\overline{p_J} - \overline{ET_J} - \overline{Q_{R,J}}) * b_j^2 \quad 18$$

With $\overline{p_J}, \overline{ET_J}, \overline{Q_{R,J}}$ being the average for precipitation, evapotranspiration and runoff over a period of interest, e.g., the rainy season or the entire year. The average runoff, $\overline{Q_{R,J}}$, can be estimated using a curve number approach.

The curve number approach and a water balance for cell i can also be a practical approach to determine which threshold rainfall would be required to add enough water to the seasonal soil wetness to reach the threshold soil moisture conditions during an event e.

Let the water balance for cell i during event e be

$$Q_i^*(e) = (p_i^*(e) - ET_i(e) - Q_{R,i}(e) - Q_{D,i}(e)) * b_i^2 \quad 19$$

Where $p_i^*(e)$ is the threshold rainfall, $ET(e)$ is the evapotranspiration, $Q_{R,i}(e)$ is the surface runoff, and $Q_{D,i}(e)$ (assumed to be 0) is the deep percolation (all in [m]). Then, the threshold rainfall to reach the sum of infiltration and evapotranspiration is

$$p_i^*(e) = \frac{Q_i^*(e)}{b_i^2} + ET_i(e) \quad 20$$

However, only a part of that rainfall would infiltrate locally, while

$$Q_{R,i}(e) = \begin{cases} \frac{(p_i^*(e) - 0.2S_i)^2}{p_i^*(e) + 0.8S_i}, if\ I_{a,i} = 0.2 * S_i < p_i^*(e) & (initial\ abstraction\ less\ than\ precipitation) \\ 0, \text{ else} \end{cases} \quad 21$$

will describe the runoff created by event e on cell i. The partial conversion of precipitation to runoff will increase the required rainfall to reach threshold conditions to:

$$p_i^*(e) = p_i^*(e) + Q_{R,i}(e) \quad 22$$

To conclude, $p_i^*(e)$ is the threshold precipitation for which the failure threshold will be exceeded for cell i under consideration of the hydrologic partitioning of rainfall in different components as well as for average antecedent moisture conditions. For management purposes it is now crucial to understand how likely $p_i^*(e)$ is exceeded, which is a function of the local precipitation regime.

Let us assume that the maximum annual precipitation values at cell i can be described by an extreme value distribution of the form

$$F_i^* = 1 - F\,(p < p_i^* \mid \mu_i, \sigma_i)$$

$$f(p_i \mid \mu_i, \sigma_i) = EV(p_i) = \frac{1}{\sigma_i}\, e^{\frac{p_i - \mu_i}{\sigma_i}}\, e^{-\exp\left(\left(\frac{p_i - \mu_i}{\sigma_i}\right)\right)} \qquad 23$$

Where $f(p_i \mid \mu_i, \sigma_i)$ is the probability for precipitation p to occur in cell i, and μ_i and σ_i are the empirical scale and location parameters of observed annual rainfall maxima in cell i. The cumulative distribution of p_i is then

$$F(p_i \mid \mu_i, \sigma_i) = \frac{1}{\sigma_i}\, e^{-\exp\left(\frac{\mu_i - p_i}{\sigma_i}\right)} \qquad 24$$

So that $F(p < p_i^* \mid \mu_i, \sigma_i)$ is the cumulative probability of not exceeding p_i and

$$F_i^* = 1 - F\,(p < p_i^* \mid \mu_i, \sigma_i) \qquad 25$$

is the failure probability of cell i.

With the above method, and specifically by combining equations 22 and 25, the probability of slope failure can be estimated for a specific cell.

Typically, rainfall is measured at specific locations in a catchment, only, while the proposed approach requires μ_i, σ_i for each cell in the model domain. To derive the required spatially distributed information, μ_i, σ_i can be derived from observed annual maximum rainfall values at available gauges and interpolated for the entire study area using krigging or a similar interpolation approach (see Figure 6 for an example from the Kali Gandaki catchment) .

To conclude, the above method considers for

- Natural spatial variability in static factors controlling slope stability, namely hillslope gradient, soil cohesion and friction angle
- Spatial variability in factors which could be linked to management decisions. Namely, the model considers for local root cohesion as well as for catchment scale changes in hydrology because of changing vegetation
- Changing seasonal as well as single event soil moisture conditions based on a curve number approach
- Spatial variability in extreme rainfall and the resulting spatial variability in probabilistic slope stability, i.e., how likely conditions at cell i result in a factor of safety smaller than one and hence possible slope failure.

Figure - 6: Spatially generalized parameters of an extreme value distribution (Equation 23) for annual maximum precipitation in the Kali Gandaki catchment. Shown are the scale parameter μ and location parameter σ derived from observed rainfall time series at precipitation gauges (white squares) and interpolated for the whole study area using krigging. The resulting information can be used to calculate the exceedance probability for any rainfall value for each cell in the model domain.

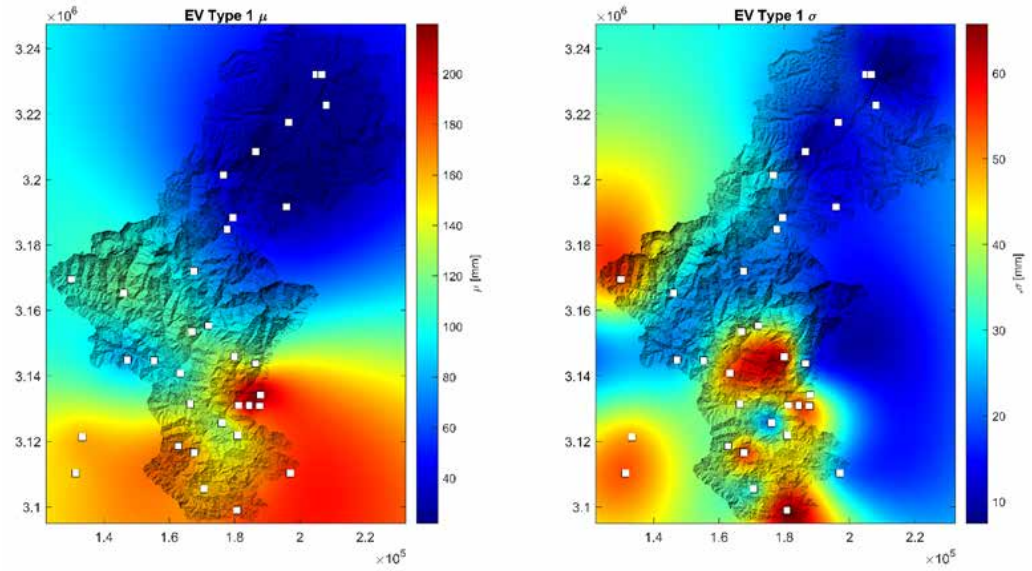

2.3. Connected landslide assessments

Normally, landslides will not occur on the scale of single cell. Rather, the failure of a single part of a slope within a wider area at near-threshold conditions might trigger the failure of the entire connected area of failure-prone slope. Quantifying this spatial relation is also key to understand landslide magnitude (slide extent and volume and mass of mobilized sediment). Determining landslide volume is relevant for catchment sediment and hazard management for three reasons. Firstly, because of the highly non-linear relation between landslide area and volume, it is crucial to determine the connected area of sliding pixels rather than considering single pixels. Secondly, landslide volume will affect run-out length, i.e., how far mobilized sediment will travel downslope of the landslide scar and which additional assets it might damage on that path and how well a zone of landslides is connected to the river network. Thirdly, calculating the mobilized volume is crucial to determine the contribution of landslides to overall sediment budget of a catchment. Common landslide hazard zonation approaches on the scale of single pixels fall short in providing that information in a consistent manner. In this section, approaches to group single pixels on a hillslope into larger, failure-prone connected areas based on concepts of downslope geomorphic connectivity are introduced. We then describe how landslide volume is derived and how downslope zones at risk in the run-out area are delineated.

Identifying connected landslide objects

To identify cells which might be possibly unstable and form failure-prone areas, we can analyze lowest and highest risk conditions of a watershed. According to the factor of safety calculations, the lowest risk of failure for a cell will occur if saturation is null, i.e.,

$$\min(FS_i) = FS(m_i = 0)$$

while the highest risk of failure occurs if soil is fully saturated

$$\max(FS_i) = FS(m_i = 1)$$

based on these considerations there are three possible conditions of a slope

1. $FS(m_i=0)<1$, unconditionally unstable area identifies slope pixels which are not stable even for completely dry conditions. This identifies areas without stable soil mantle
2. $FS(m_i=1)>1$, unconditionally stable areas identify slope pixels that will not fail even for completely wet conditions.
3. $FS(m_i^*) \leq 1$ conditionally unstable areas identify slope areas which can fail as a function of changing soil moisture conditions.

We filter all cells for which $FS(m=1)>1$ and with $FS(m=0)<1$, with the remaining cells identifying parts of a hillslope which are possibly prone to failure (Figure 7 a, red cells). We identify connected conditionally unstable areas following a downslope gradient (Figure 7 b). A set of connected conditionally unstable cells is from now on treated as a single object, referred to as Landslide Object or LSO. $i \in LSO_k$ is a cell belonging to the Landslide Object with identifier k, which includes n_k cells. We then assume that the Landslide Object has certain properties as a function of the cells it entails.

The challenge is now to identify the joint probability with which cells of LSO_k will fail. The probability of single cell failures is not independent, because (1) cells are physically connected to each other and (2) subject to same or similar rainfall conditions. Instead of using joint probabilities, we hence assume that the failure probability of LSO_k is can be described as

$$F(k) = \frac{\sum_{i \in k}(1 - F(p_i|\mu_i, \sigma_i))}{n_k} \quad 26$$

i.e., the mean failure probability of cells belonging to LSO_k. It should be noted that this assumption can be replaced with alternatives, e.g.,

$$F(k) = \min_{i \in k}\left(1 - F(p_i|\mu_i, \sigma_i)\right) \quad 27$$

Which would be a "weakest link" assumption, i.e., hillslope failure is triggered by the weakest element in that slope failing.

Estimating LSO volume

There is strong empirical evidence that the volume of a landslide increases non-linearly with its size. Based on a global analysis of landslide scars, Larsen et al. (2010) propose a power-law relationship between the surface area of a landslide and the volume of the mobilized sediment as

$$V_{LS} = \alpha * A_{LS}^{\gamma} \quad 28$$

Figure - 7: Derivation of connected landslide objects (LSOs) and failure probabilities. a: identification of conditionally unstable cells. b: grouping of conditionally unstable cells along downslope gradients. Different colors identify the resulting downslope-connected landslide objects (LSOs). c: identification of failure probability for single cells (blue fill colors) and aggregation of failure probability for each LSO scale (green to red outline colors).

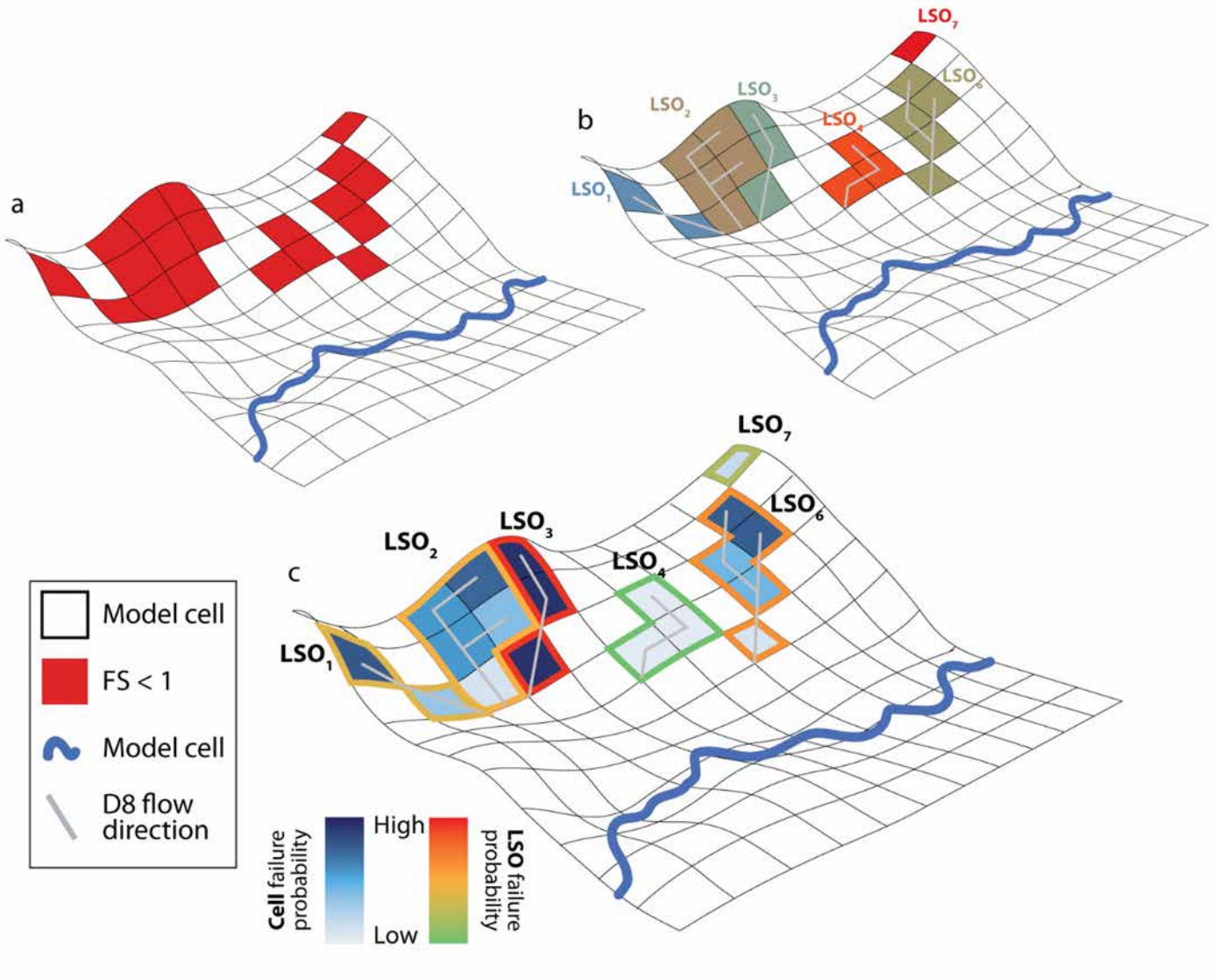

(with V_{LS} and A_{LS} being the volume and the area of a landslides). Based on a set of more than 4000 observations, they found a best fit between Equation 28 for $\log\alpha=0.86$ (i.e., $\alpha=10^{0.86}=7.24$) and $\gamma=1.322$ with an $R^2=0.95$.

Based on the above definitions, we can determine the area of a landslide object by summing the area of cells belonging to it as

$$A_{LSO,k} = \sum_{i \in k} b^2 \qquad 29$$

Where b is the side length of a cell in the DEM so that the volume of an LSO [m3] finally reads as

$$V_{LSO,k} = 7.24 * A_{LSO,k}^{1.322} \qquad 30$$

$V_{LSO,k}$ can be converted to a mass through the relation

$$M_{LSO,k} = V_{LSO,k} * \rho_S \quad 31$$

With $\rho_S = 1600 \frac{kg}{m^3}$.

Estimating runout length

Lastly, we can calculate the runout length as a function of mobilized sediment volume. How far sediment will run out from a landslide scar is depending on the volume of the landslide, which controls the energy mobilized during a landslide, but also on the downslope topography. Hence, a larger landslide on a steep slope will travel farther than a smaller landslide on a gentler slope. This effect has been studied empirically by Rickenmann (1999), see discussion in Rickenmann (2005), based on runout observations from the Alps. Despite the different geography, the wide range of considered landslide volumes, runout lengths and geomorphic conditions seem to make this model one of the most well-founded.

Runout length of an LSO can thus be calculated as

$$L_{LSO} = 1.9 V_{LSO}^{0.16} H_{LSO}^{0.83} \quad 32$$

Where L_{LSO} is the runout length and H_{LSO} is the vertical distance between the start point of runout (i.e., the lowest point on a landslide) and the downslope distance along the runout path (both in m). L_{LSO} and H_{LSO} are not independent as a longer runout length will also lead to a larger vertical distance. For computations in a gridded model domain, it is practical to calculate the condition in equation 32 for all cells along the possible runout pathway downslope of a runout pathway. For each cell, the travelled distance as well as the vertical distance will increase. We assume that the landslide runout stops as soon as the runout length from equation 32 is less than the total travel distance to the next downslope cell.

For the calculation, we can first define all cells between LSO_k ,and the channel network. This downslope runout path is denoted as γ_k. Let $h \in \gamma_k$ be a cell along γ_k. Then, δH_h is the elevation difference from LSO_k to h $\delta H_h = z_{LSOk} - z_h$. And δL_h is the runout length from LSO_k to h. Along γ, we can the continuously calculate the ratio between L and H.

Figure - 8: Conceptualization of runout modeling in a gridded domain, where individual cells can be on the runout path γ of multiple landslides. The longitudinal hillslope section A-B in the small pane indicates how runout length is calculated following an empirical relation developed by Rickenmann (2005).

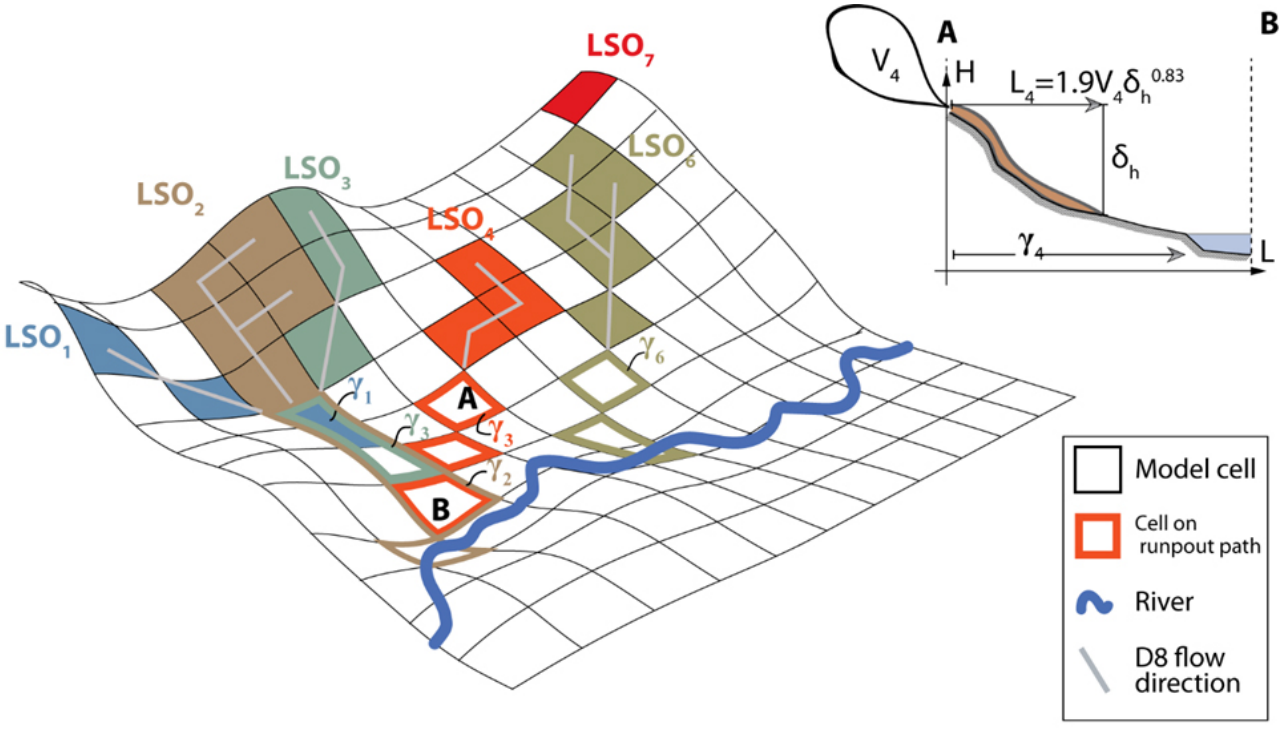

$$F(h) = \max_{F}(k, l, m)$$

There is an important distinction between the calculation of hazard for cells on an LSO and the calculation of hazard along a runout path. This is because each cell on an LSO is unequivocally assigned to a single LSO. In contrast, downslope cells can be on the runout paths of multiple landslides (see Figure 2). For example, let us assume that $h \in \gamma_{k,l,m}$ is a cell on the runout path of the three *LSO* denoted *k*,*l* and *m*. The risk of h *h* h hhh*hh* and any assets on h to be affected by upslope landslides is hence the joint probability of *k*,*l* and *m* failing. That joint failure hazard for h, i.e., could be defined in various ways. For example, the probability that either of the upslope slides fail is

$$F(h)=F(k) \cup F(l) \cup F(m) \quad 33$$

The probability of these independent but not mutually exclusive events can be calculated as

$$F(h)=F(k)+F(l)+ F(m) - (F(k)F(l) F(m)). \quad 34$$

Alternatively, we can also adopt a "worst case" approach

$$F(h) = \max_{F}(k, l, m) \quad 35$$

in which the runout hazard of a cell is defined by the maximum hazard from upslope landslides and which we adopt in this paper. Similarly, we can also calculate the volume of upslope slides as

$$V(h)= V_k+V_l+ V_m \quad 36$$

and the mean distance between cell *h* and each upslope LSO.

$$L_{LSO,h} = \frac{L_{LSO,k} + V_{LSO,l} + V_{LSO,m}}{3} \quad 37$$

2.4. Sediment mobilization from road induced landslides

Mountain roads can destabilize slopes through various interactions with hillslope hydrology and soil mechanics. Besides, seeping irrigation canals ("hill canals") and other infrastructure might increase landslide risks. However, the impacts of infrastructure, e.g., roads, on slope stability is not explicitly considered in this study. This is mainly due to the complexity of road impacts on hillslopes and the many different failure mechanisms through which roads can trigger slope failure. Most of the processes that link roads to slope failure also act on much smaller scales than the model resolution. This section also gives some outlook on how the landslide model and the derived information could be used to estimate links between roads and slope stability in the future and in cases where more data is available.

Road cuts on steep slopes destabilize slope toes, which can initiate slope failure. Infiltration from cut slope ditches can increase soil saturation under the road prism. Similarly, material dumped on the downslope (fill slope) increases the loading on slopes and can decrease slope stability leading to smaller landslides in the fill material as well as to deeper seated landslides. In the Himalayas, such road induced landslides can significantly impact sediment budgets (Leibundgut et al. 2016; Sidle and Ziegler 2012; Hearn 2011). The potential failure mechanisms and impacts of roads on landslides and vice versa are shown in Figure 9 and Figure 10.

It should also be noted that some landslide susceptibility mapping approaches consider the presence of roads as a predictor. In such susceptibility-based approaches, various factors (e.g., topography, antecedent rainfall, land use and, possibly, roads) are correlated to observed landslide occurrence via statistical methods. We did not adopt a susceptibility mapping approach for two main reasons. First, such approaches require landslide inventories to train the model. Such inventories are not commonly available. Second, a susceptibility mapping approach would not allow the representation of the different impacts that land use interventions have on landslides. However, synergies between the LSO model and susceptibility mapping approaches should be explored in the future.

Figure - 9: Links between road construction and road failure (Sidle and Ochiai 2006, p. 184)

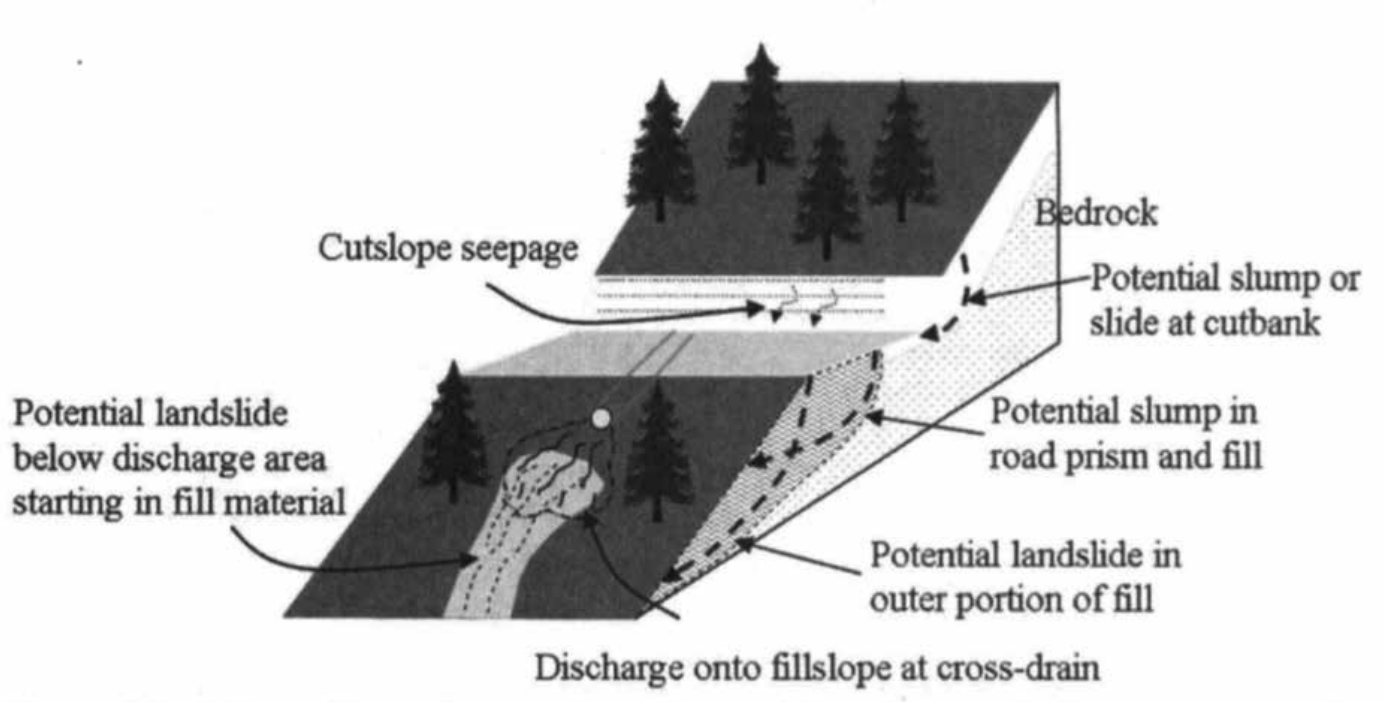

Figure - 10: Road induced slope failures and their link to infrastructure damage and connectivity to streams (Hearn 2011).

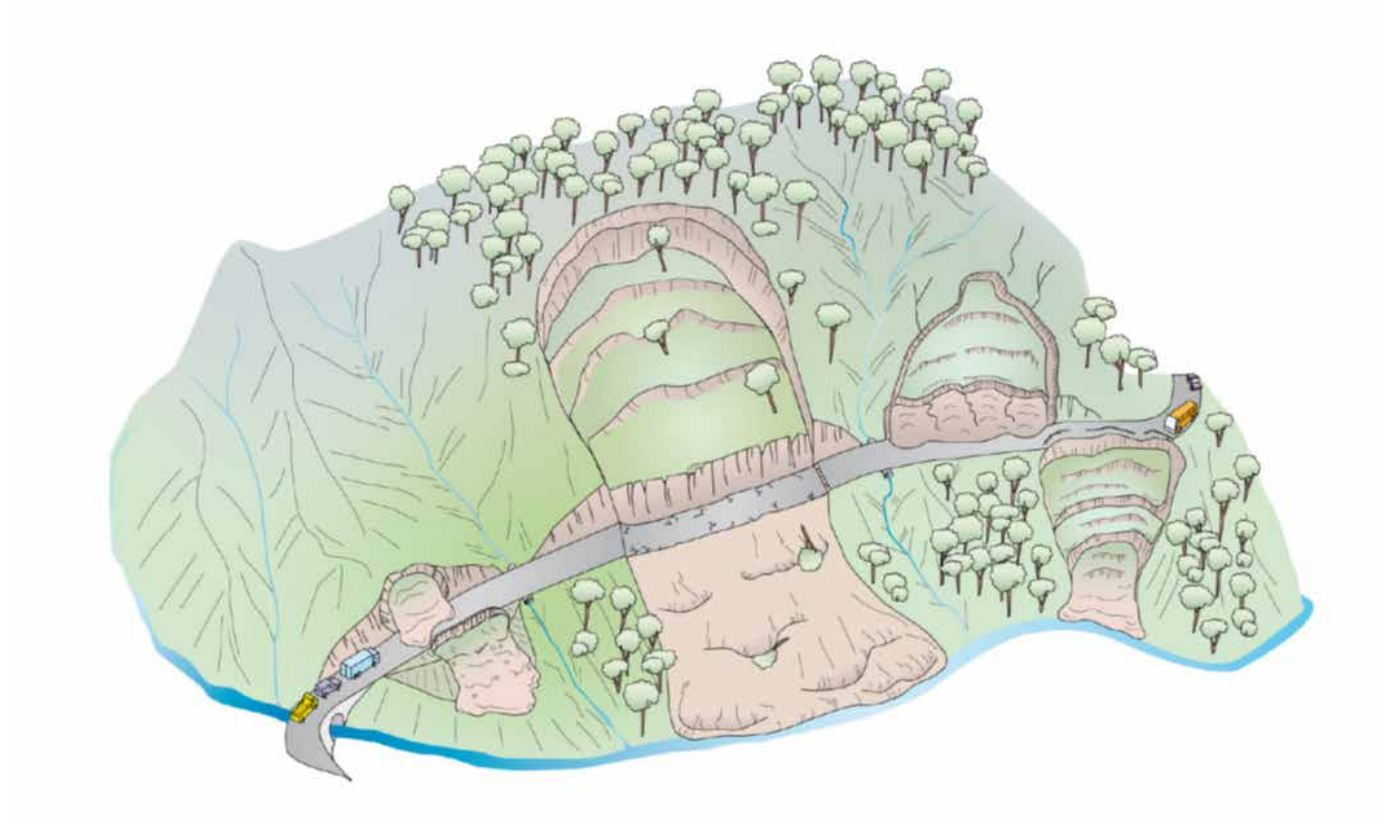

The variability of processes contributing to possible road induced slope failure would require detailed assessments of slope stability on the scale of single slopes and is hardly feasible on a landscape scale. We hence do not explicitly model road-related reductions in the slope stability/ landslide model.

2.5. Landslide hazards for infrastructure

Landslide hazards for buildings

Building footprints are derived from Open Street Maps. Footprints can possibly overlap with multiple cells. However, each footprint is assigned to the cell which is closest to its center. If that cell is part of a landslide, we assume that the entire structure is destroyed. As each building is located on a single cell, there is a one-to-one relationship between the landslide and runout hazard at the location of that cell each structure. Note that the error introduced by assigning each footprint to a single cell is likely rather small, as the size of cells (30 X 30 m, 900 m2) is very large compared to the typical building footprint. However, the spatial relation between buildings and cells would require more detailed analysis when using a DEM with a high resolution (e.g., 1 or 5 m), in which each footprint would cover many cells.

Landslide hazards for roads

Road segments are derived as lines from Open Street Maps. First, we identify all cells a road segment traverses. Because a road can traverse many cells, there is a many-to-one relationship between roads and landslide, i.e., a road can traverse multiple potential landslides and runout paths. Hence, we need to aggregate the values for all relevant LSO and runout paths for each of the road segments. The resulting fields and methods of aggregation for each road segment is shown below. Note that the methods of aggregation can be easily altered for specific analyses. Similar to buildings, we assume that a road is impacted by a landslide on a specific cell even if it traverses just a small fraction of that cell. However, we calculated the exact length of road that traverses the unstable cell(s).

2.6. Modelling management interventions

The intention of this study is to evaluate the cost-effectiveness of certain management measures. Hence, we need to derive information on three domains:

1. What management measures are available for landslides in the Himalayas, e.g., regarding required skills, materials and costs
2. Evaluate the costs to treat an LSO
3. Evaluate the resulting change in LSO failure probability.

For points 1 and 2, this study uses data reported by Dahal and Dahal (2017). From the methods reported therein, we focus on two types, tree and bamboo plantation, and installation of subsoil drains. This selection is because changes in root cohesion and soil moisture can be directly represented in the model by changing the wetness parameter m and the root cohesion parameter δ_c in the landslide model. Modeling hard engineering solutions is more challenging on catchment scales and, hence, is not part of this assessment.

We also acknowledge that such low-cost engineering measures are not suitable to address very large landslides with deep-seated failure planes. Hence, we classify landslides identified by the model into four groups with increasing magnitude and develop a "prototype portfolio" of measures that can be applied for the mitigation of the first three types.

Specifically, we propose the following classification:

1. Shallow landslide (<1.5m) in the topsoil (i.e., landslide depth < soil depth). The minimum depth of an LSO is given by the cell size and is around 1.4 m;hence, the 1.5 m threshold. Failure plane in the range of deeper rooting plants and trees.
2. Landslide depth > 1.5 m but still in the topsoil. Failure plane in the range of deep rooting trees.
3. Landslide depth > depth of the topsoil, but less than 3 m. Failure plane in the bedrock (i.e., cannot be reached quickly by roots) but still possibly in the range for soft/ grey-green engineering
4. Landslide depth > 3 m. Deep seated landslides which would require massive engineering for mitigation. Not considered for mitigation measures but useful information for hazard mapping and disaster awareness.

To model the impact of different mitigation strategies, we design a prototype mitigation strategy for landslide classes 1 – 3. It is challenging to quantify the impact of specific strategies on the parameters of the model and the herein presented values are a first, expert-based attempt on the parameter estimation. We change the model parameters for all considered landslides according to Table 5 below (e.g., for all landslides of

type 1, we apply the appropriate mitigation measure), which then results in a change in probability of slope failure. This probability is then used to evaluate the change in value of roads and structures at risk and to quantify the changed sediment mobilization.

Table - 5: Details of landslide interventions and impacted model parameters.

Landslide class	Interventions	Impacted parameters
C1: Shallow top soil	I_1: Plantation of grass and coir netting on the entire landslide surface Reforestation	• Soil cohesion: Increase soil cohesion by 15 KPa (Vanacker et al. 2003)
C2: Deep top soil	I_2: Reforestation Excavation of sub-soil drains	• Soil cohesion: Increase by 10 KPa (Vanacker et al. 2003) • Saturation: decrease m by 20 % [1]
C3: Shallow bed rock	I_3: Excavation of deep drains	• Saturation: decrease m by 20 %

We simulate the following intervention scenarios:

Scenarios	Interventions	Target landslide class
A	I_1	C1
B	I_1 and I_2	C1 and C2
C	I_3	C3 only
D	I_1, I_2, I_3	C1, C2, C3

For all interventions, we assume that they are only feasible on hillslopes not more than 1 km away from a road, as they might require transport of large equipment and material. We also consider all agricultural land, assuming that there will always be some sort of access there, even if it does not show up in the road dataset.

Figure 12: Drainage system for failure prone roadside slopes (Dahal et al, 2006)

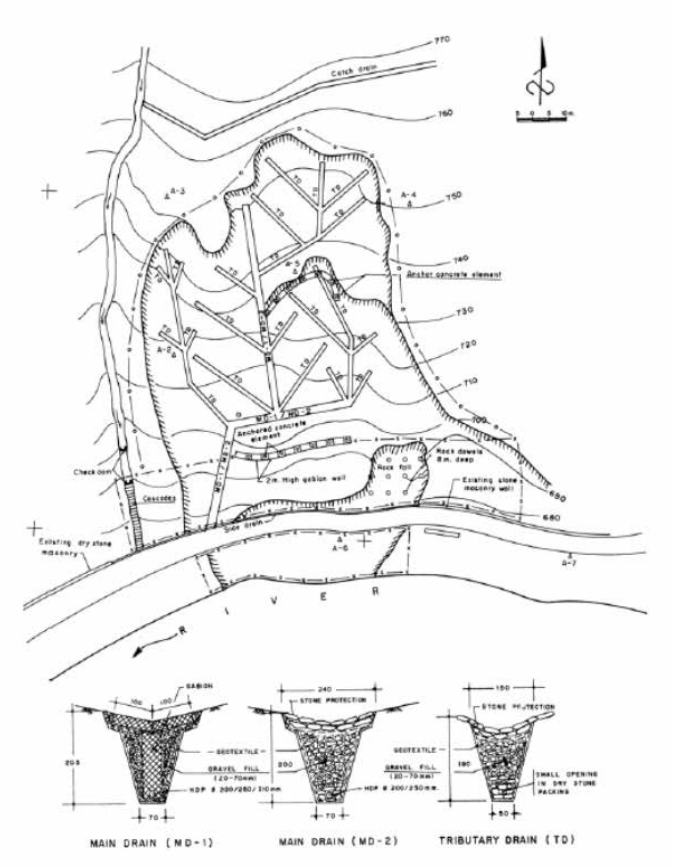

3. RESULTS

3.1. Modelled and empirical rainfall thresholds

Landslide inventories for the study area are absent. Hence, we need to resort to some broader evidence to test if the results produced by the proposed method are reasonable. Dahal and Hasegawa (2008) found a good empirical relationship between hourly rainfall over a certain period *D* and the occurrence of landslides (Figure 12).

[1] The reduction in soil saturation will depend on many local factors, such as soil type, slope, quality of the drainage works, etc., hence, we assume the 0.2 value. However, the effectiveness of drainage for landslide prevention and its modeling on catchment scales would merit more detailed study.

Based on their findings, landslides are unlikely to occur for rainfall intensities below

$$I = 73.9D^{-0.79} \quad 38$$

I [mm/hr] is the rainfall intensity and D in [h] is the length of an event. I can be interpreted as lowr boundary for p_i*. As we are bound to daily data, we find that the threshold intensity should be

$$I = 73.9 * 24^{-0.79} = 6.0017 \frac{mm}{h} \quad 39$$

To make results compatible with our daily timescale, I would become

$$\begin{aligned} I_D &= 73.9 * 24^{-0.79} * 24 \\ &= 73.9 * 24^{0.21} \\ &= 144 \frac{mm}{d} \end{aligned} \quad 40$$

which gives us at least some estimation on the rainfall intensity that triggers landslides in Nepal. The range of rainfall conditions under which landslides were observed in the data of Dahal and Hasegawa (2008) is between around $I_{D,min} = 144 \frac{mm}{d}$ and $I_{D,max} = 264 \frac{mm}{d}$. This range is, obviously, a result of the landslide and rainfall data used therein, but can provide an initial estimation of the threshold of rainfall magnitude we should expect.

Figure 12: Threshold duration vs. intensity relationship for landslides in Nepal (modified from Dahal and Hasegawa, 2008)

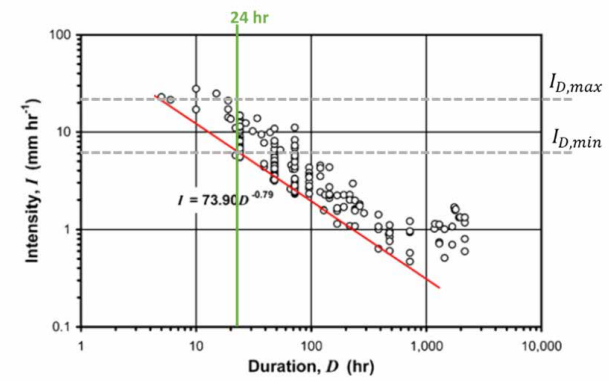

These general findings can now be compared to results for Kali Gandaki (Figure 13). The mean precipitation threshold for LSOs in the study area is 264 mm and hence in the range expected from Dahal and Hasegawa's results. Only 9.5 % of modeled LSOs fall below the threshold defined by 40. Based on the observed rainfall, we can translate these values in failure probabilities (middle panel). It should be noted that there are also a significant number of LSOs for which threshold conditions are not reached (i.e., F(k)=0). The distribution of failure probabilities for all LSOs with F(k)>0 is shown in the right panel, indicating that the mean failure probability is around 0.16.

Figure 13: Distribution of LSO threshold rainfall compared to the threshold proposed by Dahal and Hasegawa (2008) (right). Distribution of LSO failure probability (center) and failure probability for LSOs with a non-zero failure probability.

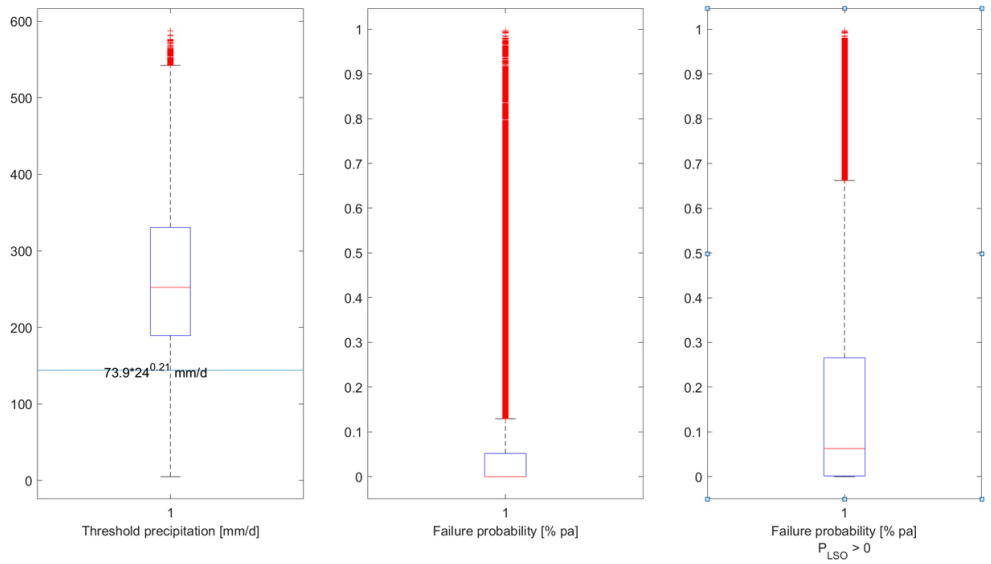

3.2. Road and building exposure

Key findings:

- Roads and buildings show a greatly different exposure to landslides (Figure 14 and Figure 15). These figures report how many buildings and road segments fall in probability classes (x axis). The y axis reports to how much percent of the total buildings and roads respectively are located on potential landslides or runout paths shown on the x axis.
- Less than 10% of all buildings are on landslides or on downstream runout pathways (Figure 14, yellow line). Of all buildings at risk, most fall in a low risk category (<10 %) and even in this category, much more structure are at risk because they are located on runout pathways, rather than directly on an LSO.
- Across all risk classes, more than 40% of roads are at risk (Figure 15, yellow line). Again, most of the segments at risk (~25 % of all segments) are in the lowest (< 5% pa) category. However, compared to houses, a much greater percentage falls into higher risk classes (10 – 50 % pa). Similar to houses, there are much more segments at risk because of a runout path, rather than because of direct crossing of an LSO.
- Some visualization of landslide and runout risk for the middle Kali Gandaki are shown in Figure 16 and Figure 17. This shows that most buildings are located outside of the most prominent zone of landslide mobilization, but many more buildings and roads are located in downslope areas that could be subject to runout from upstream landslides. Figure 17 shows that the most prominent zone of landslide probability in the upper right corner corresponds to an active steep escarpment (no vegetation).

Figure 14: Buildings at risk, binned by the failure probability of the landslide/runout they are located on. Lines show cumulative values

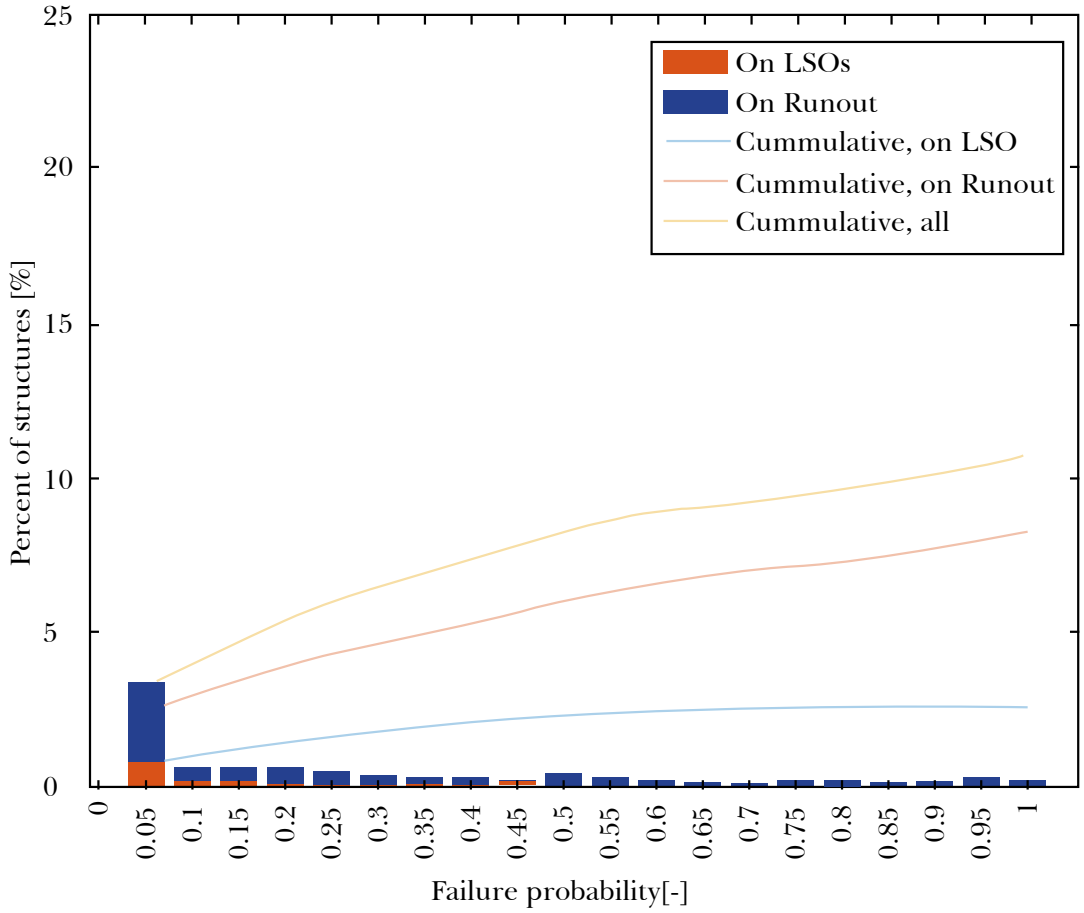

Figure 15: Road segments at risk, binned by the failure probability of the landslide/runout they are located on. Lines show cumulative values

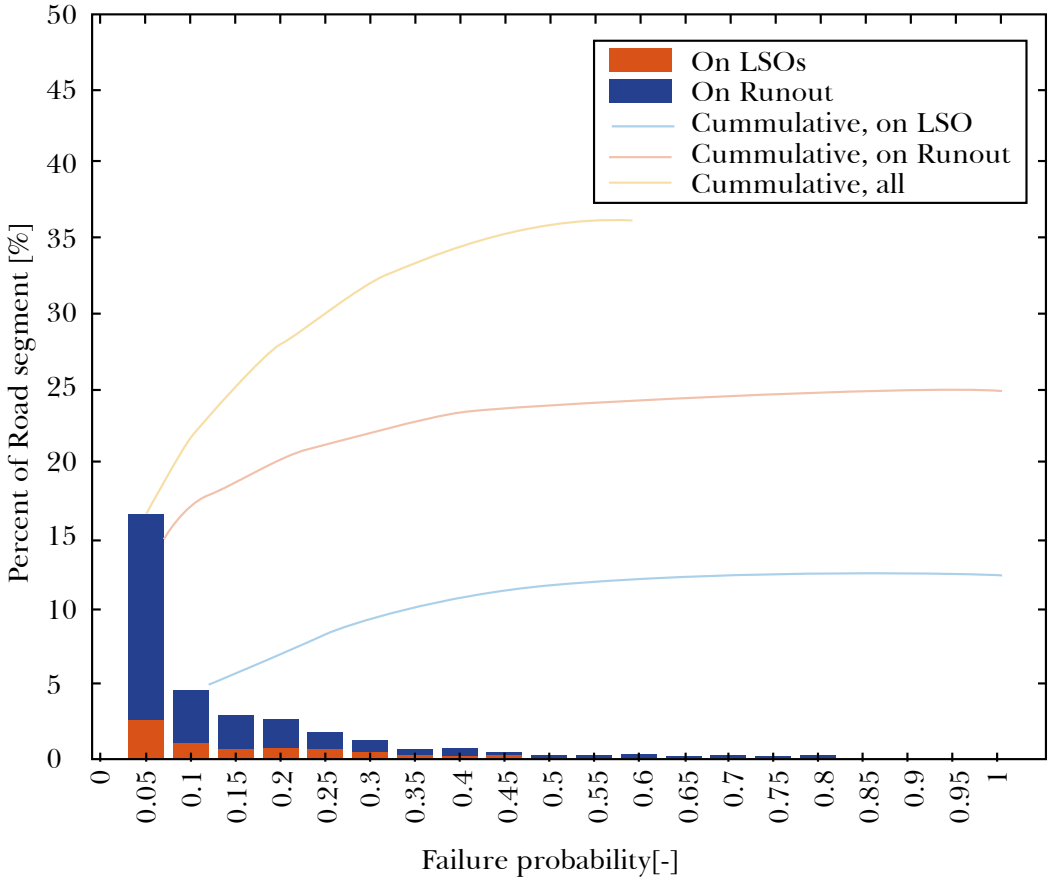

3.3. Calibrating landslide contributions to sediment budgets

The sediment budget for 5 sub-catchments in of the Kali Gandaki can be determined from sediment measurements performed by Kathmandu University. These measurements allow us to determine the contributions of the Mustang Plateau, the Kali Gandaki Gorge, the middle and lower Kali Gandaki, the Modi Khola and Myagdi Khola tributaries. A key finding is the great diversity in sediment load and yield, which is not aligned with the spatial distribution of rainfall, in the sense that the tributary catchments receiving most of the basin's precipitation do not contribute most to the basin's sediment budget.

A comparison of observed sediment load to our multi-model approach with separate models for hillslope erosion (SDR), landslides, roads, and glaciers shows that the models over-predict sediment load from the tributaries and under-predict load from the Mustang and the Kali Gandaki Gorge and makes some calibration of the multiple models necessary.

Because landslides make up the largest part of the sediment budget of each sub-catchment, which is in line with the understanding that landslides and other mass movements are most important factors in the sediment budget of Kali Gandaki (Struck et al. 2015), we focus calibration on the landslide model. Specifically, we modify the soil cohesion by a calibration factor in each sub-catchment. This assumption means that each sub-catchment is a homogeneous unit with regard to the geomorphic processes impacting landslides. While this is a simplification, it should be noted that the sub-catchments are indeed distinct with regard to their topography, climate and geology (lithology, uplift, fracturing) and, hence, with some key factors influencing landslides. It is, therefore, likely that each sub-catchment has a specific susceptibility to landslides, though we cannot yet provide a mechanistic model to explicitly reproduce the differences between the sub-catchments. To modify soil cohesion, the original uniform value of 10 KPa was changed according to the values tabulated in Table 6.

Figure 16: Results of the stochastic connectivity of landslides and runout tool for an area on the middle Kali Gandaki River. Red colors indicate landslide probability and brown colors indicate runout probability

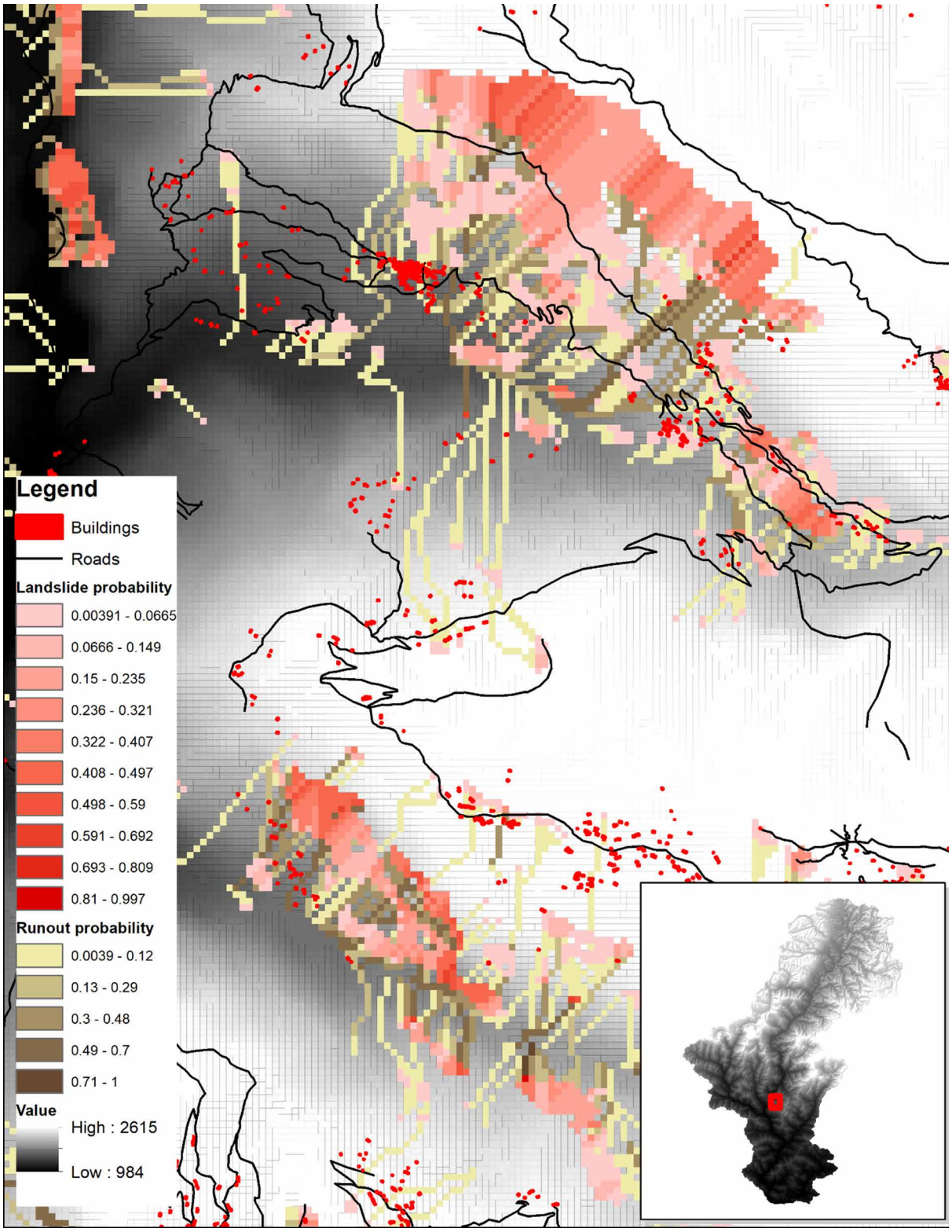

Figure 17: Results of the stochastic connectivity of landslides and runout tool for an area on the middle Kali Gandaki River. Transparent landslide and runout data overlaid over satellite imagery, showing the origins of the major landslides from an escarpment in the top right area.

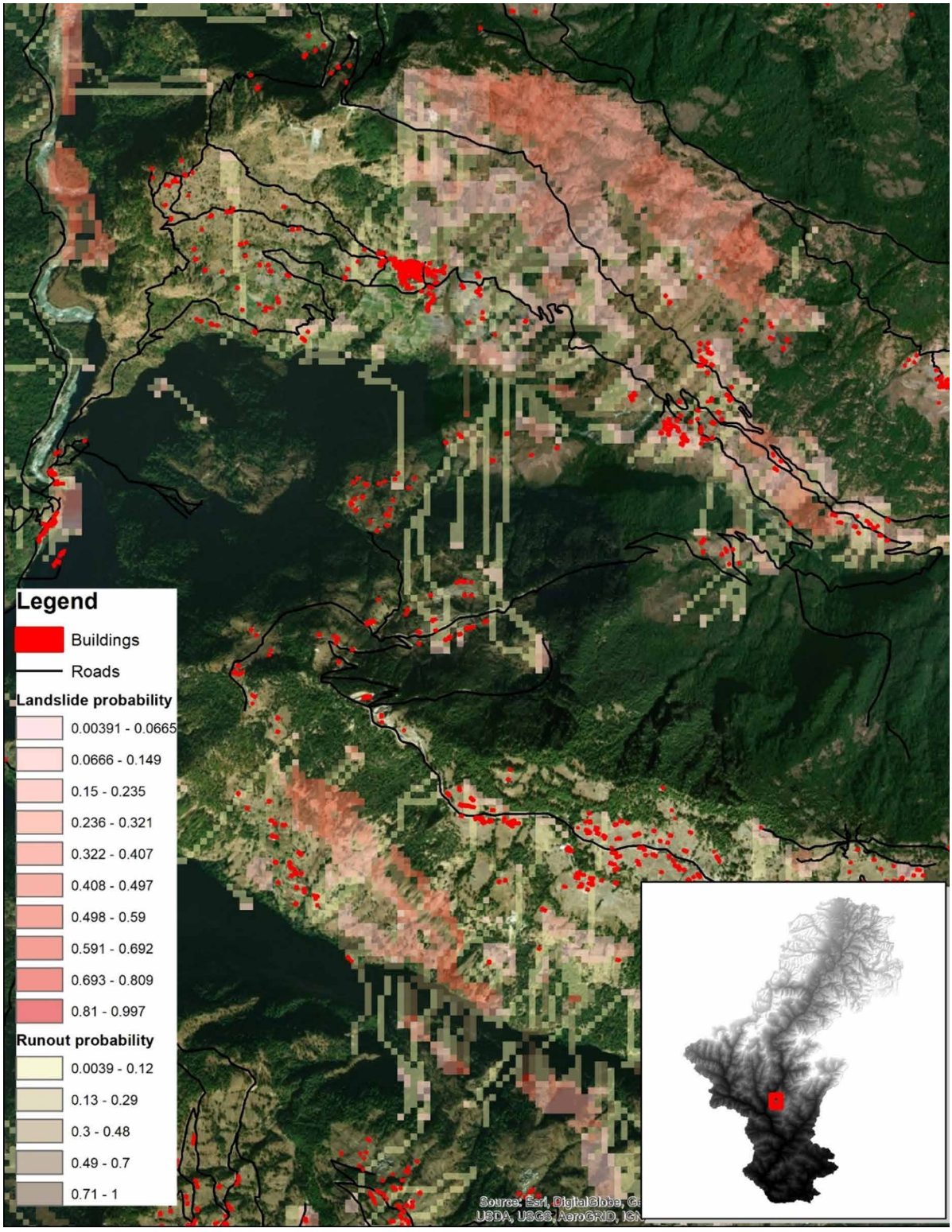

Figure 18: Total sediment load at different gauging stations (orange) and the contribution of the respective sub-catchments (blue) Error indicators show ± 1 standard deviation

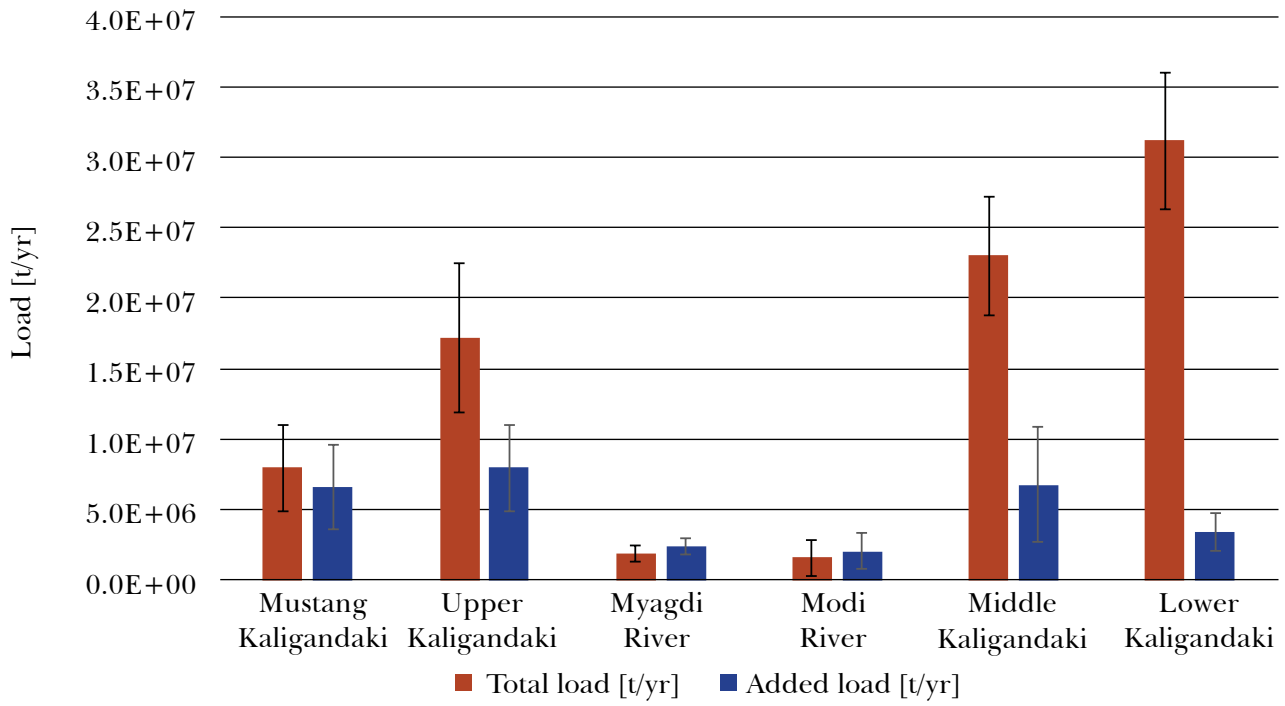

Figure 19: Comparison of modelled and observed load from the uncalibrated multi-model package. Observed load is the same as in Figure 18, error bars indicate ± 1 standard deviation in observed loads

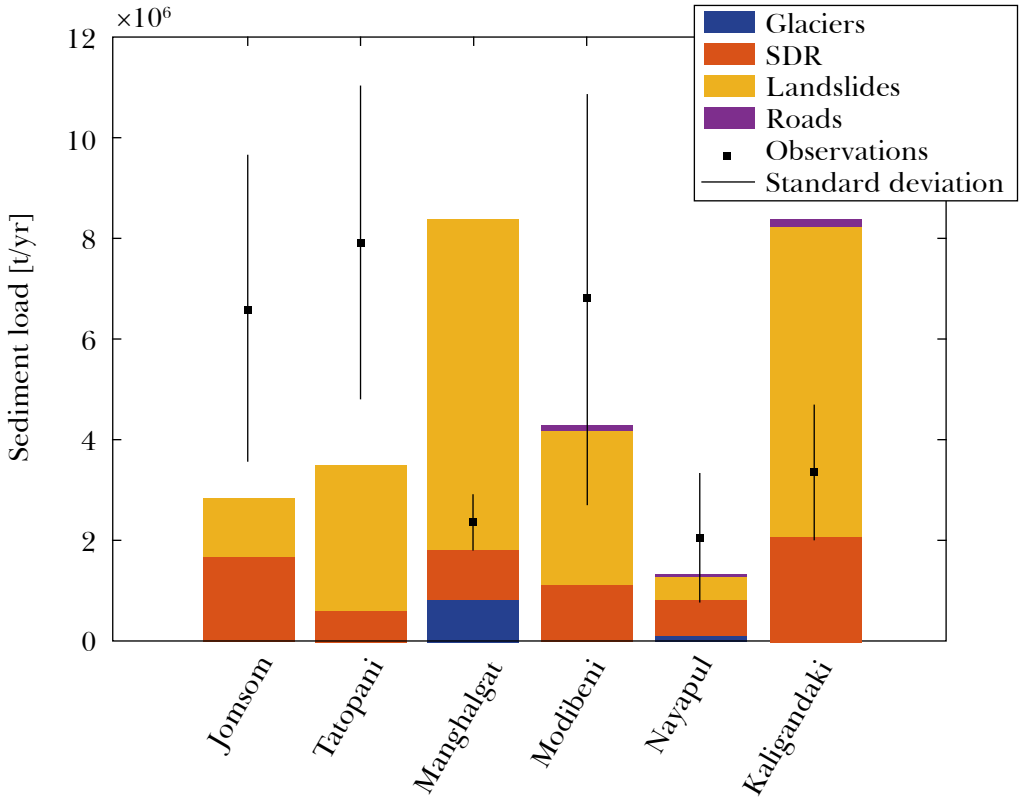

Figure 20: Comparison of modelled and observed load from the multi-model package with a calibrated mass-movement/landslide model (yellow)) . Observed load is the same as in Figure 18, error bars indicate ± 1 standard deviation in observed load.

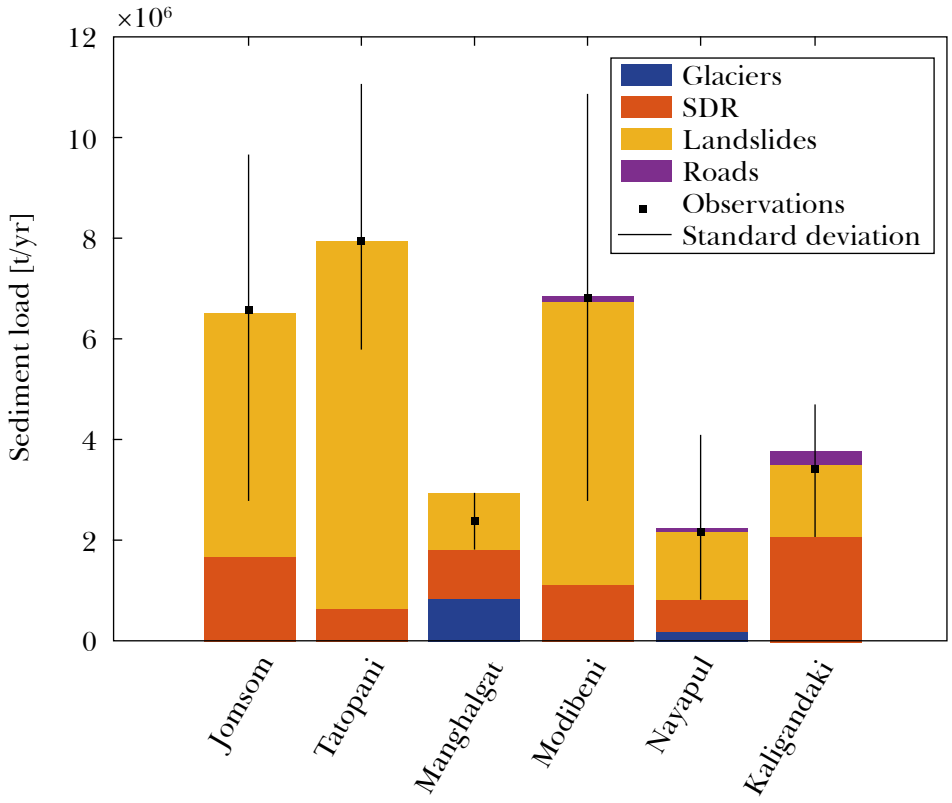

Table 6 gives the change cohesion in the different catchments, assuming that they have different soil types and are under the influence of different tectonic conditions, fractures, etc.

Table - 6: Sub-catchment modifiers for soil cohesion, which were used to calibrate the landslide mode. The baseline cohesion factor was derived from Vanacker et al. (2003). Note that no calibration was performed for the Mangla catchment as sediment data were not available and the baseline value was thus used for the whole catchment

Catchment	Soil cohesion (baseline) [kPa]	Soil cohesion calibration factor
Mustang	10 kP	0.85
KG Gorge		0.7
Myagdi River		1.2
Middle KG		0.725
Modi River		0.9
Lower KG		1.15

4. REFERENCES

Dahal, B.K., Dahal, R.K., 2017. Landslide hazard map: tool for optimization of low-cost mitigation. Geoenvironmental Disasters 4, 8. https://doi.org/10.1186/s40677-017-0071-3

Dahal, R.K., Hasegawa, S., 2008. Representative rainfall thresholds for landslides in the Nepal Himalaya. Geomorphology 100, 429–443. https://doi.org/10.1016/j.geomorph.2008.01.014

Dahal, R.K., Hasegawa, S., Masuseda, T., Yamanaka, M., 2006. Roadside Slope Failures in Nepal during Torrential Rainfall and their Mitigation, in: Disaster Mitigation of Debris Flows, Slope Failures and Landslides. Universal Academy Press, Inc. Tokyo, Japan.

Gabet, E.J., Burbank, D.W., Putkonen, J.K., Pratt-Sitaula, B.A., Ojha, T., 2004. Rainfall thresholds for landsliding in the Himalayas of Nepal. Geomorphology 63, 131–143. https://doi.org/10.1016/j.geomorph.2004.03.011

Larsen, I.J., Montgomery, D.R., Korup, O., 2010. Landslide erosion controlled by hillslope material. Nature Geosci 3, 247–251. https://doi.org/10.1038/ngeo776

Montgomery David R., Dietrich William E., 2010. A physically based model for the topographic control on shallow landsliding. Water Resources Research 30, 1153–1171. https://doi.org/10.1029/93WR02979

O'Loughlin, E.M., 1986. Prediction of Surface Saturation Zones in Natural Catchments by Topographic Analysis. Water Resources Research 22, 794–804. https://doi.org/10.1029/WR022i005p00794

Rickenmann, D., 2005. Runout prediction methods, in: Debris-Flow Hazards and Related Phenomena. Springer, pp. 305–324.

Rickenmann, Dieter. 1999. "Empirical Relationships for Debris Flows." Natural Hazards 19 (1): 47–77. https://doi.org/10.1023/A:1008064220727.

Struck, M., Andermann, C., Hovius, N., Korup, O., Turowski, J.M., Bista, R., Pandit, H.P., Dahal, R.K., 2015. Monsoonal hillslope processes determine grain size-specific suspended sediment fluxes in a trans-Himalayan river. Geophys. Res. Lett. 42, 2015GL063360. https://doi.org/10.1002/2015GL063360

Vanacker, V., Vanderschaeghe, M., Govers, G., Willems, E., Poesen, J., Deckers, J., De Bievre, B., 2003. Linking hydrological, infinite slope stability and land-use change models through GIS for assessing the impact of deforestation on slope stability in high Andean watersheds. Geomorphology 52, 299–315. https://doi.org/10.1016/S0169-555X(02)00263-5

APPENDIX 3: MODELING SEDIMENT GENERATION FROM ROADS

There is an important feedback loop between roads, infrastructure and livelihoods. On the one hand, roads enable access of rural population to markets, healthcare and education. On the other hand, poorly constructed and non- strategically planned roads can increase the risk of natural hazards such as landslides, and mobilize sediment that impacts downslope agriculture, aquatic ecosystems, and water infrastructures. Roads are possibly a major source of sediment in many Himalayan catchments, where topography is very steep and precipitation is high. Here, we describe the development of a model to estimate erosion from roads to (1) quantify the contribution of roads to basin sediment budgets, and (2) identify hotspots of road-related erosion and sediment generation, so as to (3) propose areas where better road management could have the greatest benefit for catchment management. Herein, we describe the different components of the road model and present some results.

1. METHODS

We quantify two main mechanisms for road sediment generation based on a review of pertinent literature and consider a third mechanism quantitatively. Specifically, these mechanisms are

1. Erosion of road surfaces and cut-slopes through runoff. Heavy precipitation on unpaved but compacted road surfaces can create significant surface runoff, which, in turn, erodes the road surface. Similarly, precipitation falling on a road cut-slope which are typically steeper and less vegetated than natural slopes will cause erosion. Roads also intersect natural flow lines and can capture surface run-off from upslope, increasing the runoff and erosion on the road surface. There is often a good connection between roads and the channel network, because roads often run along the slopes and frequently intersect the channel network (Sidle et al. 2006).
2. Mobilization of sediment during road construction. Roads in the Himalayas are commonly built by cutting slopes and using the cut material as fill on the downslope side (fill slope). The remaining material is commonly dumped on hillslopes below the roads. Both cut slopes and dumped sediment is typically poorly compacted and, hence, prone to erosion.
3. Sediment generation from road-induced landslides. Road interfere with slope stability via three common mechanisms (Hearn 2011; Sidle and Ochiai 2006).
    - Reduction of support by undercutting unstable slopes
    - Increasing the load on fill slopes
    - Changing flow-paths of sub-surface flow and concentrating flows on unstable areas of hillslopes

Because of the complexity of interactions between roads and sub-surface hydrology which eventually leads to an increased landslide risk, this process is not considered explicitly, but via a spatial analysis of roads and landslide objects.

1.1. Modeling erosion from road surfaces and cut slopes

Water running off an unpaved road surface creates shear stress on the particles of the road surface, causing sediment mobilization of sediment. Often, flow is not diffuse over the road surface but concentrates in ruts, which increases the erosive forces. Flow on roads is derived from two distinct processes, direct runoff from the road surface and intercepted runoff from uphill slopes. First, surfaces of unpaved roads are often compacted, which reduces infiltration capacity and increases the runoff per area of road surface. Second, roads typically run in parallel to hillslope contours and hence interrupt downslope flow path, which run perpendicular to hillslopes. As a result, surface runoff from upslope is intercepted by a road. Ideally, roads are equipped with ditches on their upslope side. These ditches collect upslope runoff, and route it downslope and discharge the runoff in a controlled way (e.g., via a culvert to the next stream). Ditches should be protected against erosion and/

or equipped with sediment traps. However, many mountain roads in Asia are not equipped with such ditches-;, the upslope runoff is routed over the road surface, where it increases erosive forces (Sidle et al., 2006). Roads will also intercept sediment travelling from upslope areas and can introduce preferential pathways of sediment connectivity.

Herein, we focus on the effect of erosion from unpaved roads, assuming that the sediment volume mobilized from a road segment r can be defined as

$$V_{R,r}=(V_{RS,r}+V_{CS,r})*SDR_r \quad 41$$

(Fu et al. 2010), where V_R is the total erosion, V_{RS} is the erosion from a road surface, and V_{CS} is the erosion from the cut slopes. SDR is the sediment delivery ratio between the drainage point of a road and the stream network.

There are no specific studies for road-induced erosion in the study area and no physically-based models which could be applied for the case study to calculate V_R and V_{CS}. Hence, the road model mentioned herein relies on empirical models formulated for different geographies (often the Pacific North West of the United States, e.g., Luce and Black [1999]), which significantly increases uncertainty. However, we aim to select a model that explicitly considers as many location-specific parameters as possible, so as to make calculations specific for the study area. With the absence of location-specific data, we use the equation proposed by Ramos-Scharròn et al (2007; 2005) to calculate

$$V_{R,r}=(-0.432+f_g\,(S^{1.5}\,P))*L_r*W_r \quad 42$$

Where f_g is a grading factor and is set to 4.73 for freshly graded roads and to 1.88 for ungraded roads. As we have no information about the grading of roads, we use the mean of the two values in this study.

Cut slope erosion is calculated as:

$$V_{CS,k}=0.09*V_{R,r} \quad 43$$

Indicating that sediment yield from cut slopes is around one order of magnitude lower than erosion from the road surfaces, which is in line with findings by Luce and Black (Luce and Black, 1999). It should be noted that some studies indicate that cut-slope erosion is the most relevant source of sediment from roads (Arnáez et al. 2004), pointing to a need for more local studies. Parameters in equation 42 are the slope of a road segment *(S)* [-], the area (*Lr*) [m] and width (W_R)[m] of a road segment and P is the annual rainfall in [cm/yr].

1.2. Modeling sediment mobilization from road cuts

The second important mechanism of sediment mobilization from roads is the displacement of hillslope soil and bedrock to create the road cut. Often, the cut material is disposed of on the downslope side of the road, a practice which is common in Nepal. The unconsolidated sediment disposed on steep slopes is then likely to become easily eroded and eventually transported to the stream network. The amount of material that will be disposed of will depend on the road design, and specifically how much of the cut material will be used to construct the embankment (Figure 21). In here, we assume that roads are constructed in full benching design, i.e., that all displaced cut material is disposed of. It should be noted that those designs with reuse of cut material for embankment construction often suffer from a failure and sediment mobilization from these embankments.

The amount of cut material can be determined knowing the gradient of a hillslope on which a road is constructed (α), the angle of the cut slope β, and the width of the road (W_R). The cut area of the road prism is then

$$A_{c,r} = h_a \frac{a}{2} \quad 44$$

(see Figure 22) for a definition sketch of triangle geometry) with

$$h_a = b \sin(\gamma) \quad 45$$

$$b = W_r \frac{\sin(\beta)}{\sin(\gamma)} \quad 46$$

$$a = W_R * \frac{\sin(\alpha)}{\sin(\gamma)} \quad 47$$

and

$$\gamma = 180 - a - \beta \quad 48$$

These functions can be solved assuming that α is equal to the local terrain slope derived from the DEM, and, using the road width from OSM data, and assuming a utslope angle, β*, which can be used to calculate β via

Figure 21: Road construction practices with various degrees of reuse of cut material (dark grey) (Sidle and Ochiai 2006).

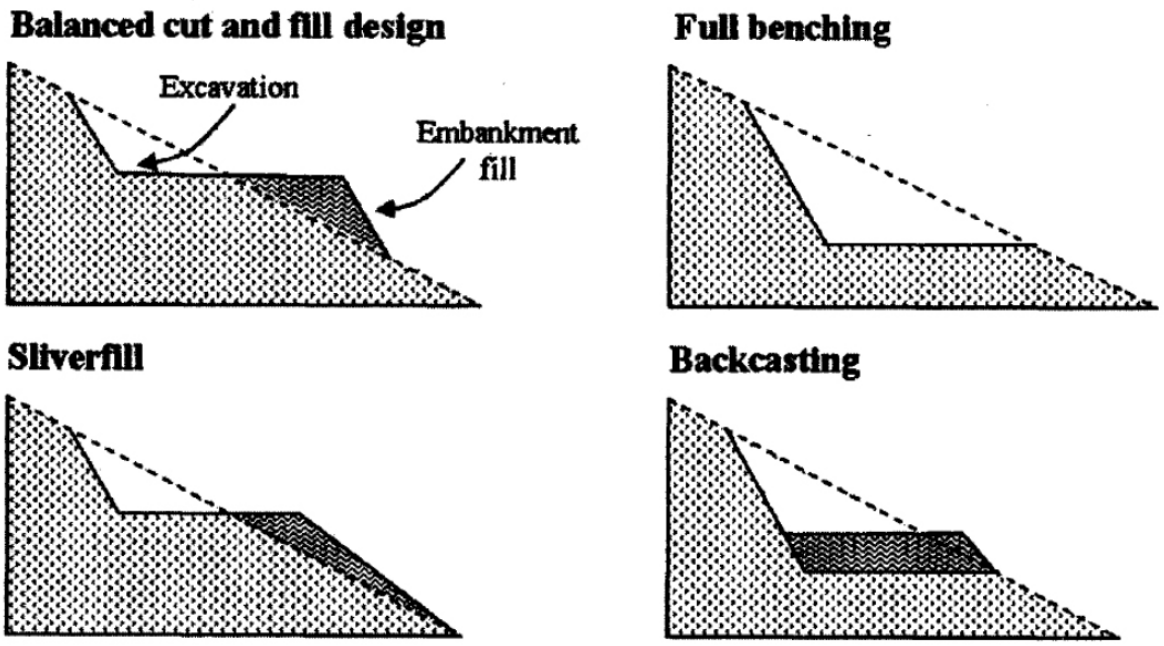

$$\beta = 180 - \beta^* \quad (49)$$

Without details on the design of each road it is challenging to determine cut slope angles for all roads. We use of $\beta^* = 45°$ as default value. This value is chosen based on field observations made during a field trip to the Kali Gandaki catchment (Figure 24). It should be noted that these observed cut slope angles exceed proposed values for mountain roads (Hearn 2011, p. 150) without additional stabilization. Also, many roads are built on hillslopes with gradients larger than 45°. From Figure 22, it is obvious that in these cases β^* must be larger than 45°, as otherwise sides *a* and *b* of the road prism would not intersect. For a road segment *r* where α is larger than 40°, we define

$$\beta^* = a * 1.1 \quad (50)$$

This condition is met for approximately 2% of all roads, as roads are built on slopes with as much as 60% gradient.

We can now calculate the volume of sediment mobilized by a road cut, assuming that the local slope of the terrain is equal to α. The assumptions of steeper cut slope angles on steeper hillslopes might even link to actual conditions, as steeper hillslopes might consist of more competent soil and rock material and hence allow for steeper cut slope angles. The resulting relationship between hillslope angle and cut material from the road prism is shown in Figure 23.

Figure 22: Calculating cut area of a full benched road (small panel) and the geometric definitions (large panel)

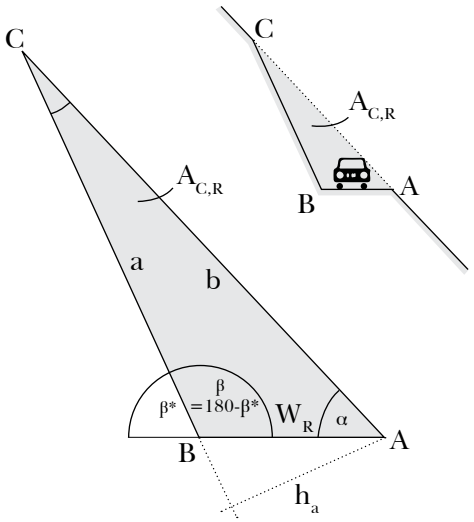

Figure 23: Relationship between hillslope angle and the cut material from the road prism when applying equations 44-50

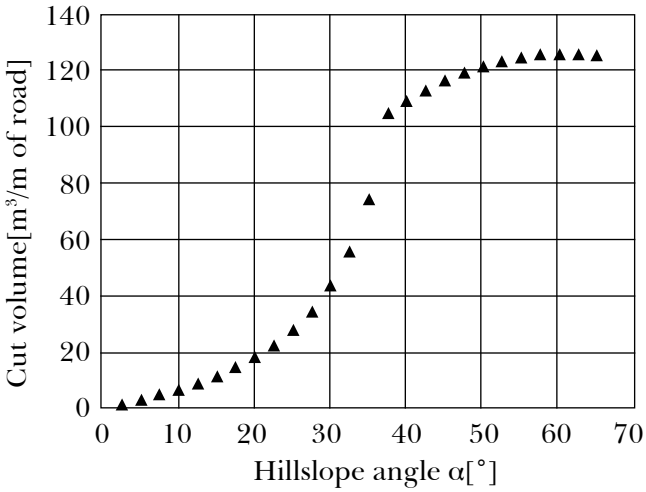

The volume of sediment that needs to be disposed of after the construction of a road ($V_{C,r}$ [m3]) can be calculated as

$$V_{C,r}=A_{C,r}*L_r \quad 51$$

and

$$M_{C,r}=V_{C,r}*\rho_S \quad 52$$

With L_r being the length of a road segment and ρ_S being the sediment density. It should also be noted that $M_{C,r}$[t] does not have a time dimension. Equation 52 yields the sediment that needs to be disposed of once, during the construction of the road. To calculate the annual contribution of the displaced material to the sediment budget of a basin, we would need to make assumptions about how many new roads are constructed per year, and how fast the sediment displaced during previous road constructions is

Figure 24: Observed road construction practices in the Kali Gandaki catchment (pictures by D. Cutler). Cut slope toe angles, β, are measured in Adobe Illustrator. All pictures show that relatively steep cut slopes (45° to 60°) are realized in soil or fractured rock, contributing to visibly high erosion (e.g., top right and bottom left panel). The top left and bottom right panels indicate how road-cut material is often only partially stabilized on the fill slope (bottom right) or disposed of in downslope channels (top left)

being eroded on the hillslopes. Most likely, erosion of dumped cut material will be fastest in the first years after the road construction. However, here we select a somewhat arbitrary time span of δ_(t,E) = 25 years, after which we assume that dumped cut material has either been eroded or stabilized by vegetation, and assume that erosion rates are similar each year, so that

$$M_{C,r} = \frac{\mathrm{M}_{C,r}}{\delta_{t,E}} \qquad 53$$

with $M_{C,r}$ in [t/yr].

2. ROAD DATA

Spatial data on road locations are derived from Open Street maps. This information is crucial, as it allows us not only to locate roads, but also contains some information on road types and building material. Table 7 shows the road type information available for the Kali Gandaki catchment. Most road segments don't have any information on their surface material. We assigned information regarding the surface material, and specifically if a road is black-topped or not, as a function of the road type for all road segments without information on surface material (Table 7, Black top). For roads with black top, erosion from the road surface is set to 0 in Equation 41 and only erosion from the cut slope is considered, but it should be noted that only a few road segments have information on surface material available. Our observations from satellite imagery is that very few roads in Kali Gandaki have blacktop or concrete cover (mostly roads classified as "primary") and even roads classified as "highway" or "secondary" mostly do not have blacktop.

Similarly, information on road width is not available from the Open Street Maps data, and we assigned information on road width based on the presumed number of lanes and assuming that lanes are 4 m wide. Footpaths and road types used mainly by humans and pack animals are assigned a smaller width. It should be noted that even such small paths can produce significant amounts of sediment (Sidle et al. 2006). Some of these footpath segments display very steep slopes of 100% plus, which is not realistic; this is likely because of inaccurate mapping of the exact course of these paths on steep hillslopes. Hence, we set the maximum slope of all roads to 1 [m / m].

Table - 7: Road type table defining road parameters such as blacktop cover (1: blacktop, 0: no blacktop) and width

Road Type ID	Type	Count	Total length [m]	Blacktop	Width
1	Bridleway	6	2565	0	2
2	Construction	4	630	0	2
3	Footway	316	90959	0	1
4	Living_street	5	883	0	4
5	Path	5400	2288972	0	1
6	Primary	16	34878	1	16
7	Residential	470	146279	0	4
8	Road	248	90574	0	4
9	Secondary	107	149593	0	8
10	Service	52	10251	0	4
11	Steps	25	2487	0	0.5
12	Tertiary	177	431202	0	4
13	Track	1294	770209	0	1
14	Trunk	31	66596	0	8
15	Unclassified	1404	1871361	0	4
16	Highway	10	5952	0	12

A brief analysis of the 7000 km of road network in Kali Gandaki reveals that small tracks and paths dominate the road network (around 3500 km), and that the road type is not specified for a large part (around 2250 km) (Figure 25, top panel). A brief visual analysis of satellite imagery of roads falling into that category reveals that "unclassified" roads entail small and hardly visible footpaths, as well as major roads.

Major road types with possible blacktop cover (highways, primary and secondary roads, trunk roads) make up only a small part of the road network by length; however, they are more relevant in terms of total road area because of their larger width (Figure 25, bottom panel). Small tracks and paths make up less of the road area because of their small width. Similar to the length statistics, most of the road area falls in the "unclassified" category. It should be noted that the area of "unclassified" roads is dependent on their assumed width (4 m).

Figure 25: Summary statistics in terms of length and surface area of different road types present in the OSM data-base for Kali Gandaki

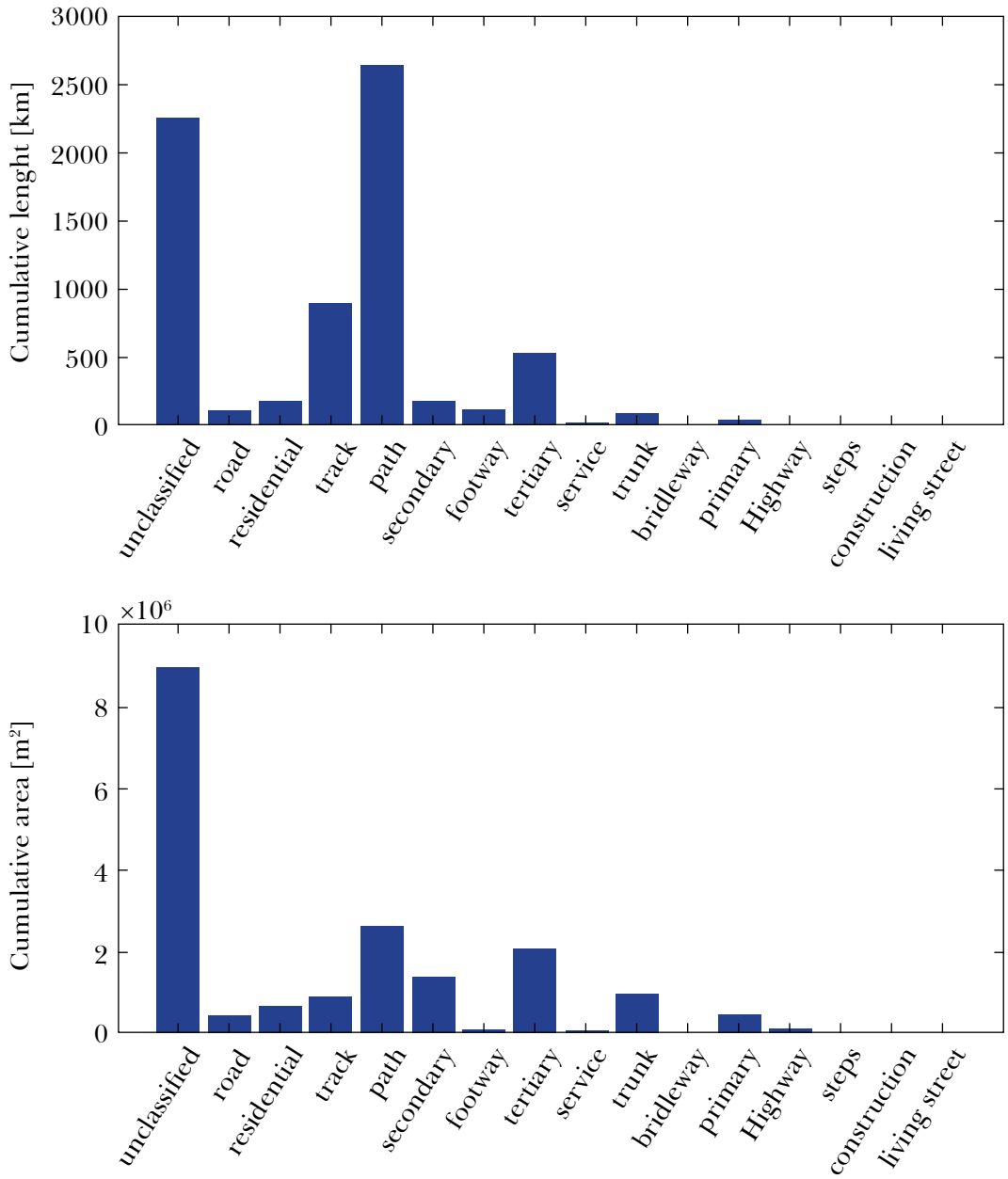

3. RESULTS

3.1. Erosion from road surfaces

Total erosion from road surfaces is between 0.5 and 4 Mt/yr, as a function of the road grading factor, when the mean value of the grading factor is used, the result is around 1.1 Mt/yr. Analyzing road surface erosion by road class shows which road types dominate road contributions to the sediment budget. Unclassified roads contribute the largest part (around 0.6 Mt/yr). Paths and tracks contribute a significant amount of sediment (see increase in cumulative curve in Figure 26, top panel), not only because they have a relatively large cumulative area (Figure 25, bottom), but also because of their steep slope. Highways have the highest erosion rates per segment; however, because of their relatively small number (Figure 25), highways do not contribute much to the cumulative sediment budget.

Figure 26: Summary statistics in terms of surface erosion from members of different road classes (boxplots, top panel) and the cumulative erosion over all road classes (green line, top panel). The bottom panel shows the relative erosion per road length for different road classes

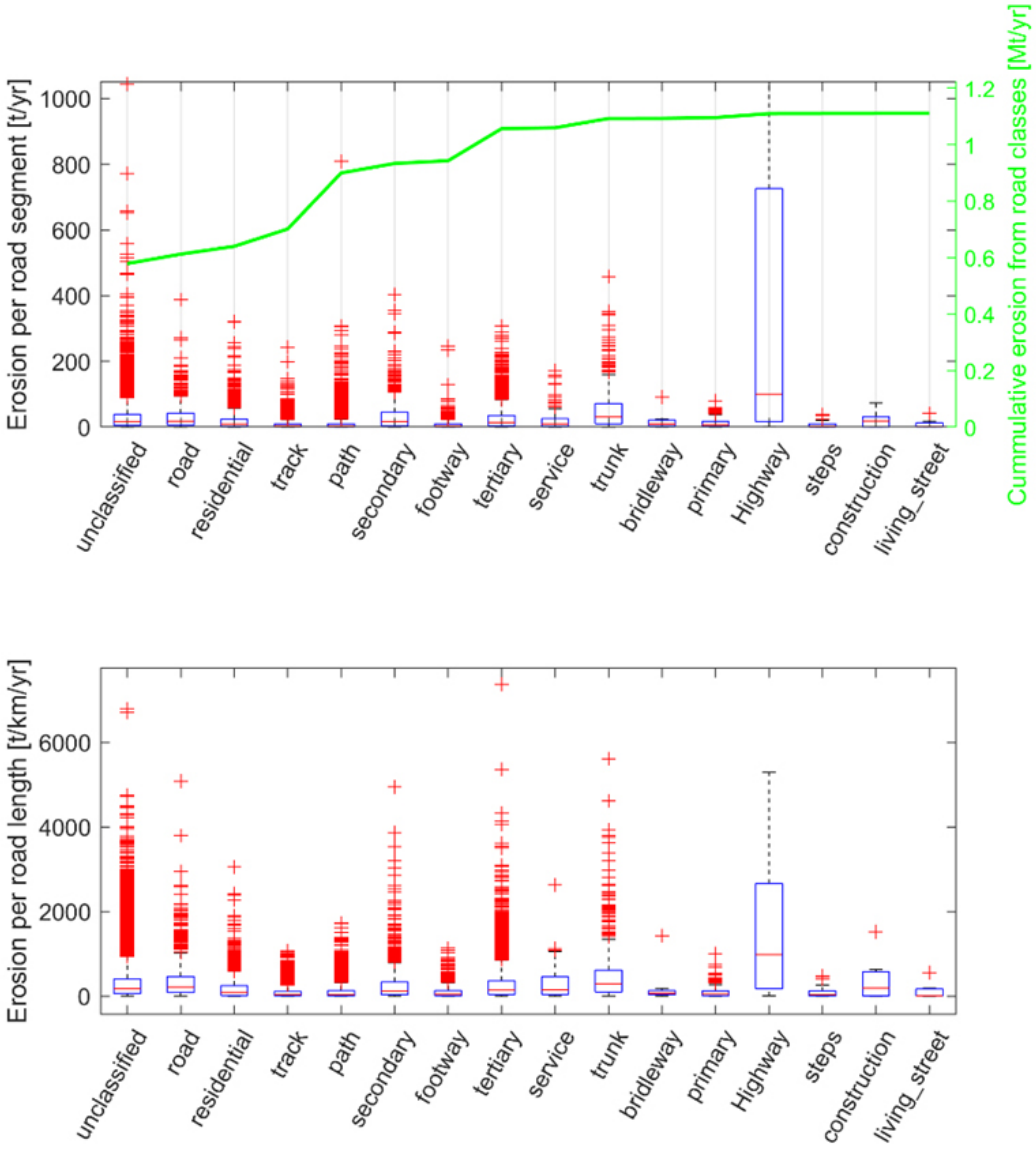

Figure 27: Modelled erosion from road surfaces in Kali Gandaki. The color code indicates the sediment load from road surface erosion aggregated over smaller sub-watersheds. Red points indicate the 500 road segments with the highest surface erosion

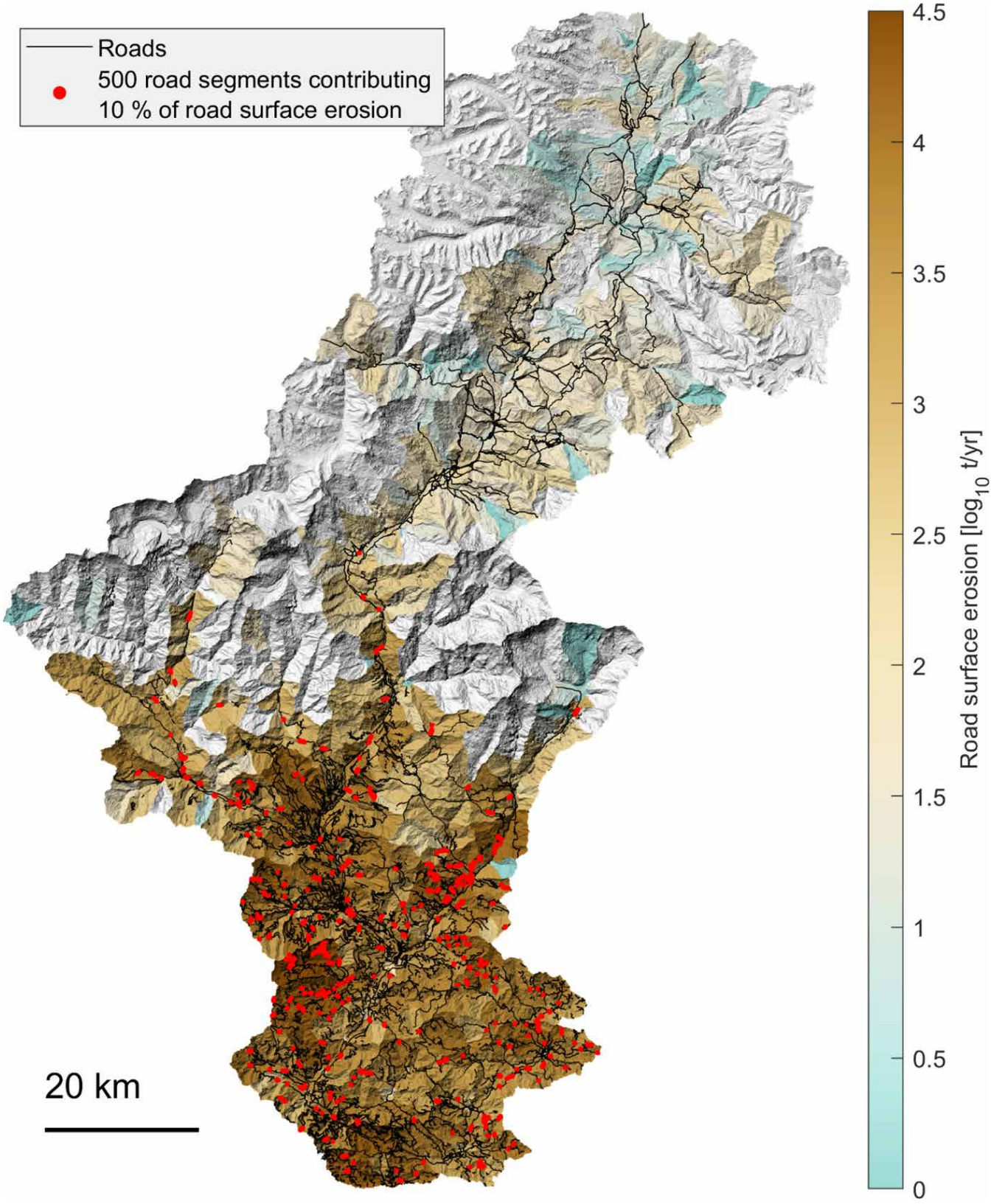

With the absence of measurements, modelled road erosion should be judged carefully, especially as the calculation of erosion rates is based on an empirical model for a different geography. However, modelled erosion rates per length of road (Figure 26, bottom) are in the range of value reported by Leibundgut et al. (2016) for the earthen roads in the Phewa watershed in eastern Nepal, who report values of up to 8000 m3/km/yr, or 12800 t/km/yr (though these data sets possibly include landslides as well as erosion from the road surfaces).

The spatial distribution of road surface erosions shows a clear pattern following slope and precipitation gradients in the catchment. Erosion from road surfaces is several orders of magnitude higher in steep catchments in the lower Kali Gandaki, where most of the precipitation occurs, and where road density is highest (Figure 27). Figure 27 also shows the 500 road segments with the highest surface erosion, which are all located in the lower Kali Gandaki valley. It should be noted that these 500 road segments (out of more than 60,000) make up for more than 10% of the total road surface erosion.

3.2. Erosion from roads

According to our calculations, the total removed material to build all roads in the Kali Gandaki watershed accounts to 90 Mt (around 0.5 t/m of road). Assuming that this cut sediment contributes to the sediment budget over a time span of 25 years, this translates to around 3.5 Mt/yr (Figure 28). Large roads have the highest mobilization of cut materials (primary, secondary, and highways), because of their assumed larger width. For surface erosion, highways display the highest rates of erosion, but do not contribute a lot to the cumulative sediment budget. This is different for cut material mobilization, for which primary and secondary roads and highways make up for a significant part of the cumulative mass (see "steps" in the green cumulative mass curve in Figure 28).

Figure 28: Summary statistics in terms of surface erosion from members of different road classes (boxplots, top panel) and the cumulative erosion over all road classes (green line, top panel). The bottom panel shows the relative erosion per road length for different road classes

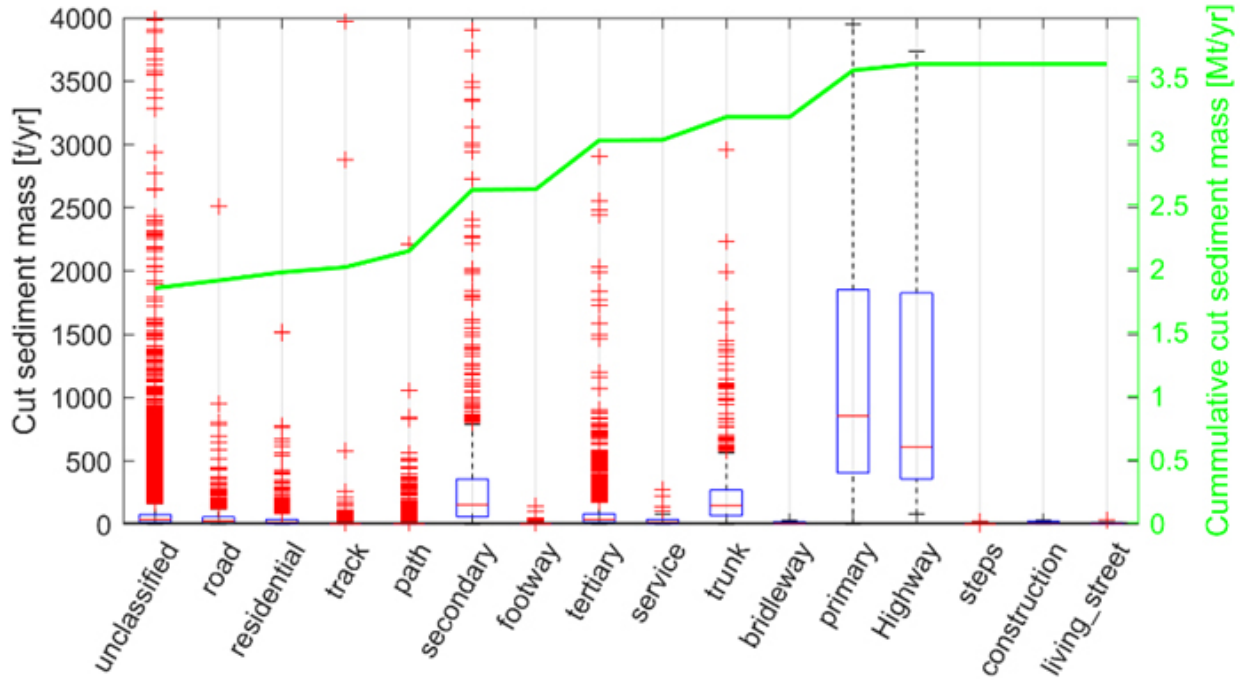

Figure 29: Modelled mobilization of cut material from roads in Kali Gandaki. The color code indicates the sediment load from road surface erosion aggregated over smaller sub-watersheds. Red points indicate the 500 road segments with the most mobilized cut material

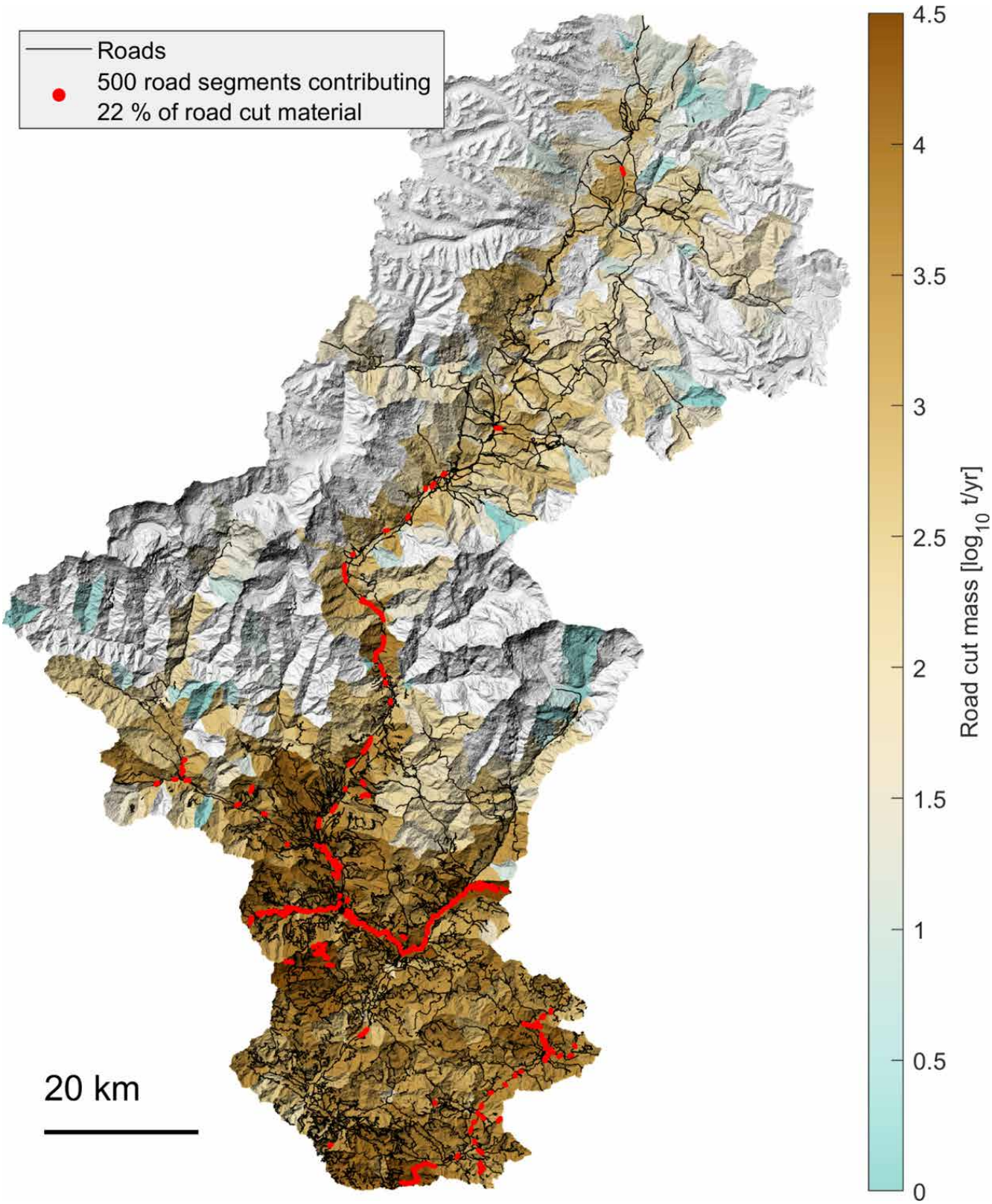

Figure 30: Modelled sediment mobilization from landslides intersected by roads. All points indicate where a landslide object (LSO) is intersected by a road. Colors of markers indicate in which risk category this intersections falls [following the modified categorization from (McAdoo et al. 2018)]

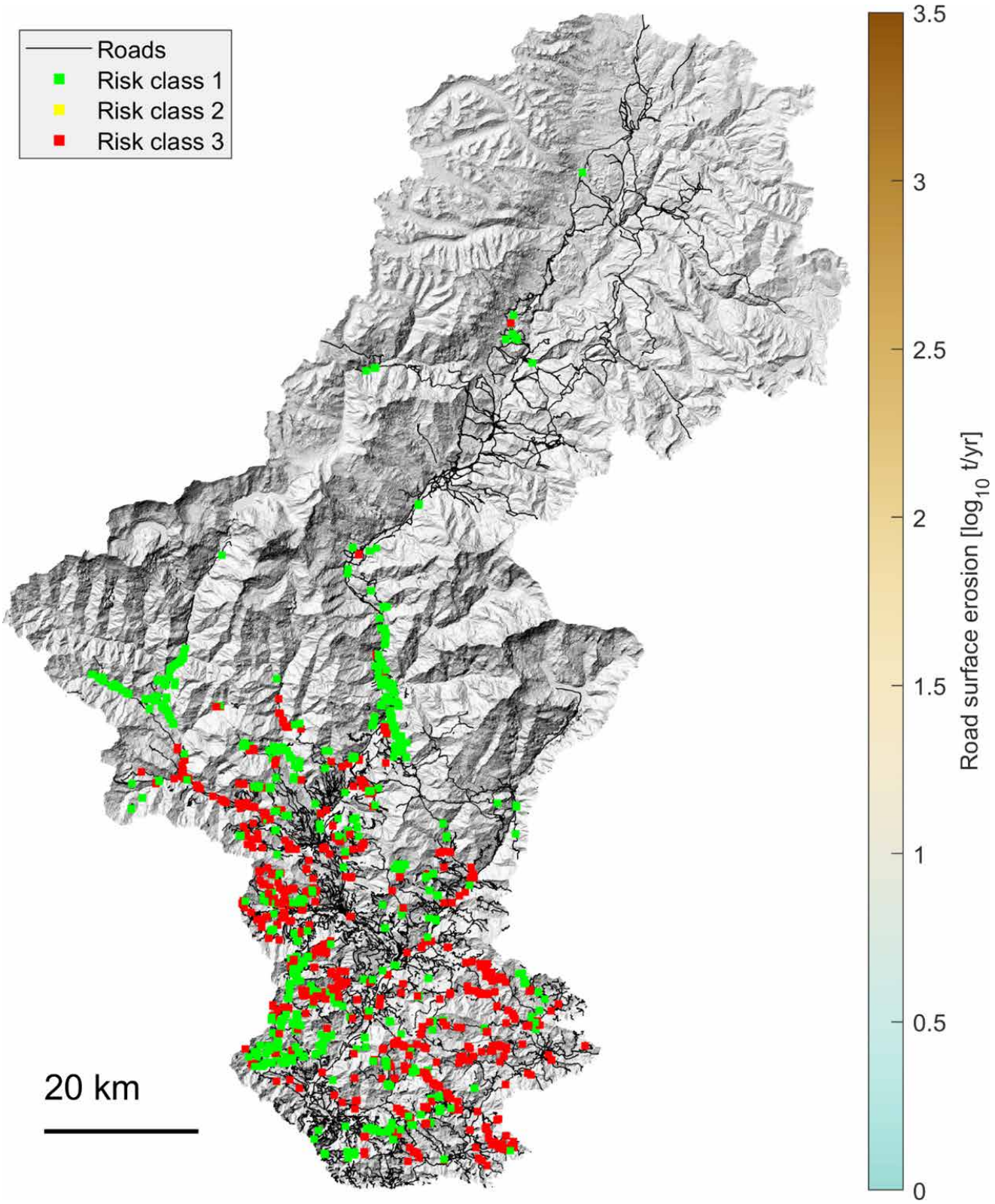

Cut sediment is a function of road width and the local slope angle. Hence, the spatial distribution of cut material mobilization does not follow the spatial gradient of precipitation (Figure 29). Roads with the major mobilization of cut material are, instead, wide roads constructed in steep terrain. Notably, road erosion is most emphasized along the major east-west and north-south corridors, the Pokhara-Baglung and Mid-Hill Highway (east-west) and the Beni-Jomsom Highway (north-south). Similar to surface erosion, a small fraction of road segments mobilizes a major part of sediment (500 road segments with highest cut material mobilization contribute 22 % of total cut material (Figure 29, red dots

3.3. Sediment generation from possibly road related landslides

In total, 2700 road segments intersect with LSOs. The possible sediment generation from these LSOs is more than 4 Mt. The distribution of risk classes amongst these road segments is nearly equal between category 1 and category 3; category 2 does not occur. This implies that landslide road intersections are either such that the road cuts above the potential failure plane and is in the topsoil, so that roots might be used to stabilize the slope (class 1), or the road cut intersects with the potential failure plane and reaches into the bedrock, which would make it hard to stabilize failure plane and bed rock – road cut intersections with plants (class 3). With regard to sediment mobilization, however, more sediment is derived from category 1 rather than from category 3 (3.1 vs. 1.2 Mt). The spatial distribution of landslides mirrors the geomorphic and meteorological drivers of landslides. Roads most commonly intersect landslides in the lower part of the Kali Gandaki catchment, and along the road corridor in the Kali Gandaki Gorge. In the Mustang area, landslides are less common and the road network has a much smaller extension, resulting in fewer intersections between landslides and roads.

Figure 31: Enlarged view of the central Kali Gandaki Gorge, roads intersecting LSOs, and the risk class of the intersecting rod segments

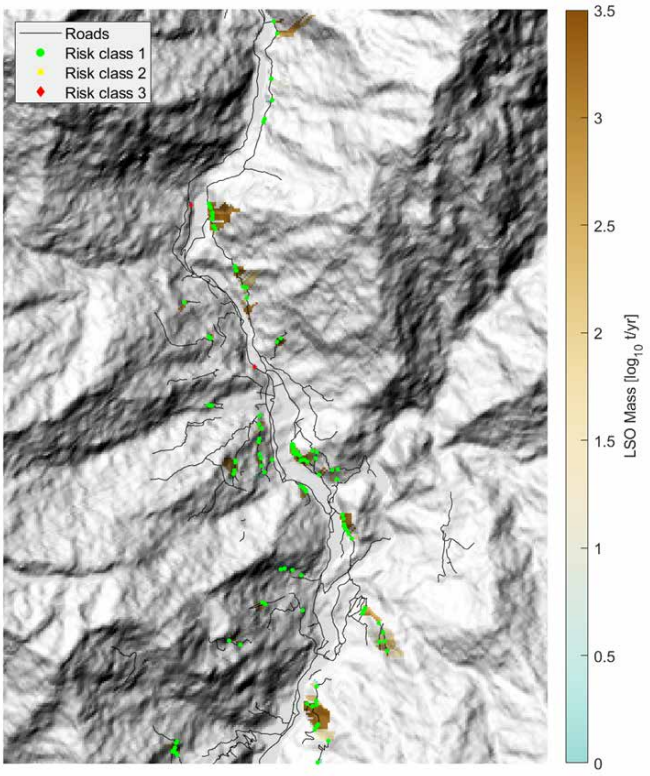

4. REFERENCES

Arnáez, J., Larrea, V., Ortigosa, L., 2004. Surface runoff and soil erosion on unpaved forest roads from rainfall simulation tests in northeastern Spain. CATENA 57, 1–14. https://doi.org/10.1016/j.catena.2003.09.002

Fu, B., Newham, L.T.H., Ramos-Scharrón, C.E., 2010. A review of surface erosion and sediment delivery models for unsealed roads. Environmental Modelling & Software 25, 1–14. https://doi.org/10.1016/j.envsoft.2009.07.013 Hearn, G.J., 2011. Slope Engineering for Mountain Roads. Geological Society of London.

Leibundgut, G., Sudmeier-Rieux, K., Devkota, S., Jaboyedoff, M., Derron, M.-H., Penna, I., Nguyen, L., 2016. Rural earthen roads impact assessment in Phewa watershed, Western region, Nepal. Geoenviron Disasters 3, 13. https://doi.org/10.1186/s40677-016-0047-8

Luce, C.H., Black, T.A., 1999. Sediment production from forest roads in western Oregon. Water Resources Research 35, 2561–2570. https://doi.org/10.1029/1999WR900135

McAdoo, B.G., Quak, M., Gnyawali, K.R., Adhikari, B.R., Devkota, S., Rajbhandari, P.L., Sudmeier-Rieux, K., 2018. Roads and landslides in Nepal: how development affects environmental risk. Natural Hazards and Earth System Sciences 18, 3203–3210. https://doi.org/10.5194/nhess-18-3203-2018

Pelletier, J.D., Broxton, P.D., Hazenberg, P., Zeng, X., Troch, P.A., Niu, G.-Y., Williams, Z., Brunke, M.A., Gochis, D., 2016. A gridded global data set of soil, intact regolith, and sedimentary deposit thicknesses for regional and global land surface modeling. Journal of Advances in Modeling Earth Systems 8, 41–65. https://doi.org/10.1002/2015MS000526

Ramos-Scharrón, C.E., MacDonald, L.H., 2007. Development and application of a GIS-based sediment budget model. Journal of Environmental Management 84, 157–172. https://doi.org/10.1016/j.jenvman.2006.05.019

Ramos–Scharrón, C.E., MacDonald, L.H., 2005. Measurement and prediction of sediment production from unpaved roads, St John, US Virgin Islands. Earth Surface Processes and Landforms 30, 1283–1304. https://doi.org/10.1002/esp.1201

Sidle, R.C., Ochiai, H., 2006. Landslides: processes, prediction and land use. American Geophysical Union, Washington, D.C.

Sidle, R.C., Ziegler, A.D., 2012. The dilemma of mountain roads. Nature Geosci 5, 437–438. https://doi.org/10.1038/ngeo1512

Sidle, R.C., Ziegler, A.D., Negishi, J.N., Nik, A.R., Siew, R., Turkelboom, F., 2006. Erosion processes in steep terrain—Truths, myths, and uncertainties related to forest management in Southeast Asia. Forest Ecology and Management, Catchment Processes in Southeast Asia 224, 199–225. https://doi.org/10.1016/j.foreco.2005.12.019

APPENDIX 4: METHODS FOR VALUING IMPACTS OF SEDIMENT ON KALI GANDAKI A

1. INTRODUCTION

Interest in catchment area treatment in the Kali Gandaki basin was largely spurred by concerns for the effects of sediment on operations at the Kali Gandaki "A" Hydroelectric Plant (KGA). In the section below, we consider three benefits that would accrue from reduced sediment loading in the watershed: reduced costs of flushing the desanding basins; reduced costs of equipment maintenance; and preservation of pondage capacity, which enhances the Plant's ability to supply power during periods of peak demand.

We presented summary results and the basic intuitions underlying them in the main text. In this Appendix we present formal analyses and details. In the section below, we will treat each category of benefits in turn: avoided damage to equipment; avoided costs of desanding; and preservation of peaking capacity.

Before turning to these categories, however, we will quickly review some overarching issues in economic valuation and some common themes in valuing sediment reductions in hydropower generation in Nepal. We follow generally accepted principles of economic valuation e. g., (Freeman, Herriges, and Kling 2014):

- Economic values are defined in the context of *incremental* (in the limit, *marginal*) *changes*; when we discuss a value of sediment reduction, we tie it to a particular quantum of sediment reduction.
- Economic values always reflect *willingness to pay;* what it might cost to do something is relevant only to the extent that someone is actually willing to bear the cost.

Economists rely on prices to determine willingness to pay when they are available. However, environmental economists must often work in contexts in which prices are not observed because of externalities (Kolstad 2011). Part of our challenge, then, is to infer what the price of sediment *should* be. This challenge is complicated by another market imperfection. Power production in Nepal has frequently failed to meet market demand at the prices NEA is charging at the time. Figure 32 illustrates a typical situation. For much of the day, NEA's own, largely hydroelectric generation assets, in combination with its purchases from independent power producers (IPPs), were sufficient to meet demand. Nepal imports power at all times, but imports are particularly important in meeting daily peak demand from about 5:00 pm to 11:00 pm. At such times, however, the combination of NEA generation, IPPs, and imports are insufficient to meet demand, resulting in the phenomenon illustrated by the dark-shaded, sharp peak in Figure 32: System load curve for annual peak load day. Source: NEA (2018): load shedding.

The prospect of load shedding affects our analysis in several ways:

- Scarcity determines economic value, and so values will vary by time of day and season of year as the availability of water for generation and of power for purchase from other sources varies
- Because the availability of power and water for generating it vary, maintenance will be planned to occur at times at which the opportunity costs of forgone generation are lowest
- During periods of load shedding, the economic value of power must be inferred in the absence of meaningful prices. A shortage is defined, in economic terms, as a situation in which the quantity demanded exceeds that available at the price being charged. Under such circumstances, the price being charged is less than consumers' willingness to pay, and therefore does not reveal economic value. Researchers have estimated actual willingness to pay from prices paid to purchase electricity from alternative sources – usually private diesel generation; see e. g, (R. S. Shrestha 2011; J. P. Shrestha and Shrestha 2016; Timilsina and Toman 2016), or from surveys of users' willingness to pay for expanded supply (see, e. g., Karki, Mishra, and Shrestha 2010).

Figure 32: System load curve for annual peak load day. Source: NEA (2018)

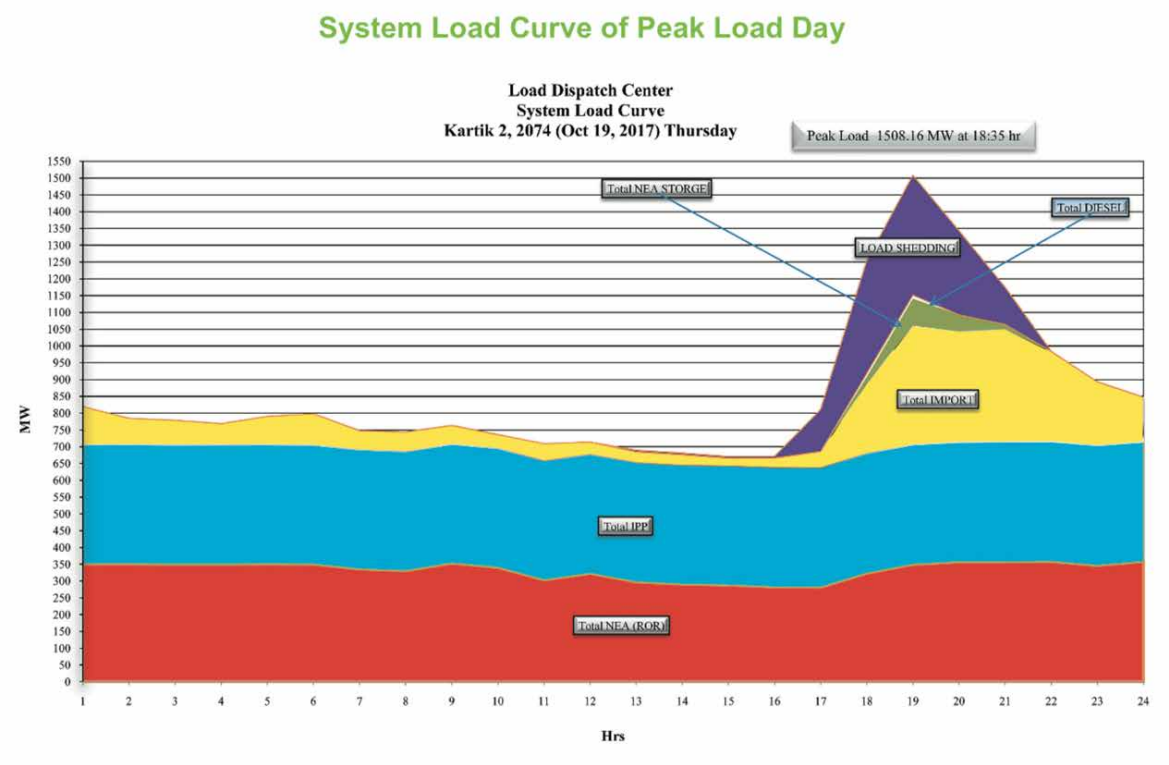

- Nepal is experiencing rapid growth in both domestic generation capacity and demand for power, as well as in power imports from India (see Figure 33). Even more explosive growth will likely occur in coming decades. The growth in supply has enabled NEA to more effectively deploy its generation resources; it has recently been reported that, for the first time in recent memory, load shedding is not occurring in Nepal (Shrestha, et al., 2018; NEA Annual Report 2018). Whether this continues to be the case will depend on developments in supply and demand that cannot now be forecast with precision.

With these considerations by way of context, we turn now to the value of sediment reduction in reducing desanding costs, avoiding damages, and preserving reservoir capacity.

Figure 33: Expansion in electricity provision 2009 – 2018. Source: NEA 2018

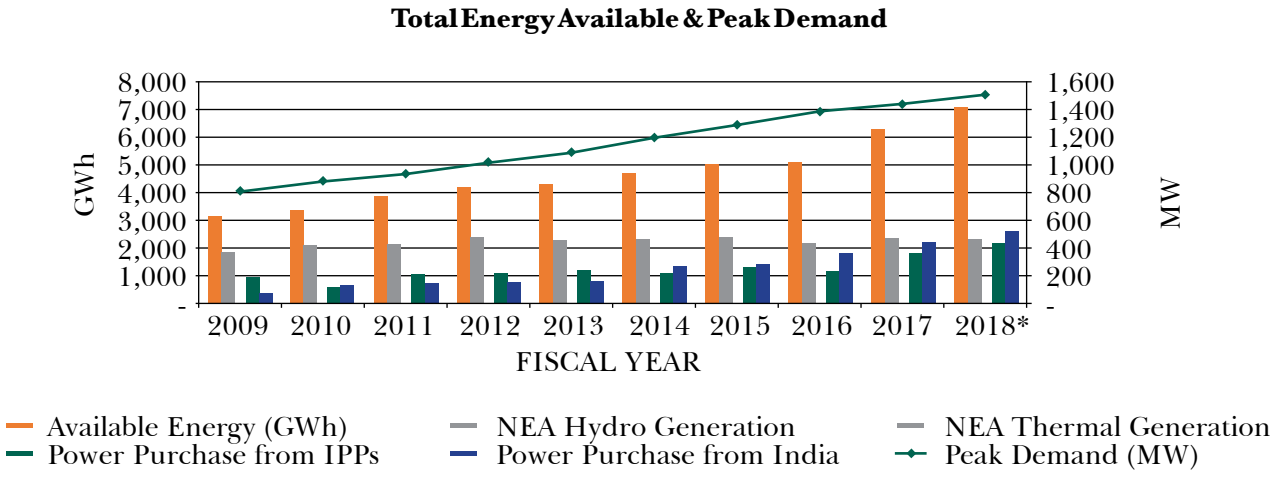

2. DESANDER FLUSHING

The designers of the Kali Gandaki "A" Plant were well aware that sediment control would be a challenge, and planned the facility accordingly (ADB, 2004). Several subsequent modifications to the plant have also been devoted to better handling of sediment.

Sand that passes through the generating equipment causes damage by abrading turbines, valves, vanes, and other parts (see, e. g., NEA 2018 for a comprehensive list of repairs performed during a major overhaul).[2] To reduce the volume of sand passing through the generating equipment, the Kali Gandaki plant is equipped with twin desanding basins. Each basin measures 14 meters in depth, 40 in width, and 187 in length (Bishwakarma 2012). With the twin-basin design, it is possible to run the plant at half-power while one basin is being flushed. It takes between four and five hours to flush each basin; as the basins only collect sediment when water flow (and hence, sediment load) in the river is high, this means that even when one basin is flushed, there is still sufficient flow in the other to operate the plant at half- power.

Sediment suspended and transported in the river varies dramatically and non-linearly with the volume of flow (see Figure 34). Sediment accumulation and damage is a negligible concern during the dry season. However, when flow is high, active steps for sediment management are required to be carried out. . NEA estimates that, under current conditions, the basins are flushed about 22 times per season. The two basins are emptied sequentially each time they are flushed. The general rule of thumb is to flush a basin when sediment has accumulated to a depth of three meters. The accumulation is not so rapid, however, that it cannot be deferred until an off-peak period.

We suppose, then, that each flush takes nine hours, and that it occurs during off-peak hours at times when the plant would otherwise operate at full capacity. While there may be some other costs involved in flushing the desanding basins, they appear to be *de minimis*, and we will ignore them. Plant capacity is 144 MW, and so 9 hours · 144 MW = 1,296 MWh of power would be generated with the plant operating at full capacity. If half of this power is lost while one and then the other desanding basin is flushed, the power loss would be 648 MWh.

Assigning a price to power is difficult, even during the off-peak hours when NEA has generally been able to meet demand. NEA's tariff schedule lists literally hundreds of different rates depending on class of customer (domestic, industrial, municipal, etc.), amount of consumption, current, voltage of transmission, time of day, and season of year. Moreover, customers are generally charged a two- or more part tariff: a service or demand charge for connection, plus an energy charge per kWh consumed. Finally, there is a block-rate structure under which prices increase with level of consumption.

If determining a price per marginal kWh of power produced is difficult, an alternative might be to estimate the cost to NEA of acquiring marginal power. NEA imports power from India, and purchases power from independent power producers. A figure of about NPR 6 per kWh (US$ 0.054) might be a reasonable estimate of cost of supply from such sources. This is the average (across voltage transmission categories) rate agreed for purchases from India's Central Electricity Authority. NEA recently agreed to purchase solar power at a rate of 6.60 NPR per kWh, it has set a long-run average price of 5.30 NPR per kWh for power purchase from the new Upper Tamakoshi Plant and has paid about 5.50 NPR per kWh for power purchases from PTC India, Ltd. (NEA 2018).

However, NEA has paid a higher average price, 7.12 NPR (US$ 0.063) per kWh of electricity purchased, on an annual basis (NEA 2018). However, NEA reports do not break down payments for purchased power by season or time of day. As Figure 32 shows, however, reliance on imports increases markedly during periods of peak demand. Thus, it might be reasonable to infer that power purchases are more expensive during peak hours.

Returning to the NEA's tariff schedule, there is variation between peak and off-peak prices, at least for larger customers. Time-of-day pricing is only instituted for industrial and other large consumers

[2] A variety of sediments are transported in the Kali Gandaki. Landslides and major floods can mobilize boulders which, while they may reduce reservoir capacity, are too heavy to be borne through the generating equipment. At the other extreme, very fine particles are easily transported, but they lack the mass to do severe damage. It is the sand-sized particles that are small enough to be suspended but large enough to damage equipment that are most problematic.

served by high-voltage lines. For such consumers, however, there is typically a one to three Rupee per kWh difference between prices charged during "peak" (5:00 pm to 11:00 pm) and "normal" times during the dry months between roughly November and April. Between roughly May and October, when water is more plentiful, an additional "off peak" period between 11:00 pm and 5:00 am is added, when, prices are roughly half their peak value, a difference of about four to six Rupees per kWh, depending on service class.

Finally, while it is difficult to say what combination of meeting societal objectives and cost recovery any particular power price is intended to achieve, it seems reasonable to suppose that the marginal price charged to the largest industrial customers might be most representative of the value attached to power on the margin. These rates are, during the high-flow months during which desander flushing occurs, 4.15 and 5.25 NPR/kWh "off peak" and 7.50 and 8.40 NPR/kWh "normal" for industrial customers with the highest (66 kV) and second-highest (33 kV) voltage service. Taking averages of these figures, assuming that six of the nine hours required for desander flushing occur off-peak and the remaining three in the normal period, gives a figure of 5.8 NPR (US$ 0.052)/kWh.

All of the above considerations, in combination with an appreciation of the imprecisions inherent in the assignation of such a figure, lead us to adopt an estimate of 6 NPR (US$ 0.054) per kWh of power generation forgone for desander flushing.

Priced at 6 Rupees per kWh of off-peak power lost, the total opportunity cost of a single flushing event would be 3.89 million Rupees (US$ 34,730).[3]

Figure 34: Suspended sand concentration in the Kali Gandaki. Source: Morris (2014)

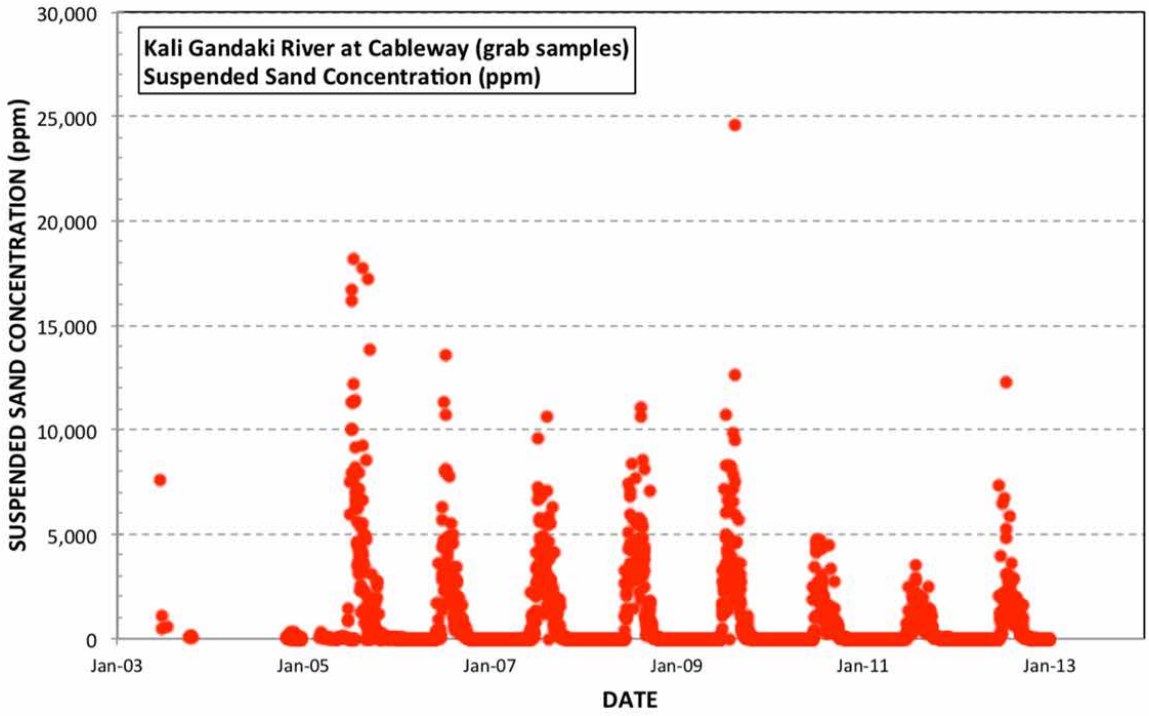

3. While desander flushing is a discrete event, we are assuming that the accumulation of sediment is sufficient to generate the need for at least slightly more frequent flushes.

Expressing these figures in NPR per cubic meter of sediment deposited, the volume of the desanding basins is 3 m deep · 2 ·40 m wide ·187 m long = 44,880 m^3. Dividing NPR 3.89 million by 44,880 m^3 we have about NPR 86.7 (US$ 0.77) per cubic meter of material deposited in the desanding basins. This would be cost savings per season. At a discount rate of 10%, the net present value of a one cubic meter reduction in the amount of sand that settles in the basins every year would come to about NPR 867 (US$ 7.74) m^{-3}.

It would be important to bear in mind that this figure is the value of a one cubic meter reduction in the volume of sand deposited in, and subsequently flushed from, the desanding basins. To apply this figure in the valuation of a cubic meter of erosion prevention at any point in the watershed, we would have to multiply the figure we have just derived, 867 (US$ 7.74) NPR m^{-3}, by the fraction of sediment originating at that location that is deposited in the desanding basins.

3. DAMAGE TO EQUIPMENT

The purpose of the desanding basins is to prevent sand from passing through the generating equipment, where it damages the turbines, vanes, valves, and other parts. The desanding basins do not remove all sediments, however; some 1.7 million tons, of which some 700,000 tons are sand, pass through the turbines every year (Morris, 2014). Damage is seasonal. Sediment transport varies greatly with flow. During the dry season, it is virtually nil. Sand transport then spikes with the Monsoon. Morris finds that sand concentration varies as the fourth power of river flow (Morris 2014; see also, Chhetry and Rana 2015a). Virtually the entire year's load is delivered over a few months in the summer, as illustrated in Figure 35. Note that the vertical scale is logarithmic; the intervals between dashed horizontal lines denote multiples of ten.

Figure 35: Sand concentration by month. Source: Morris (2014)

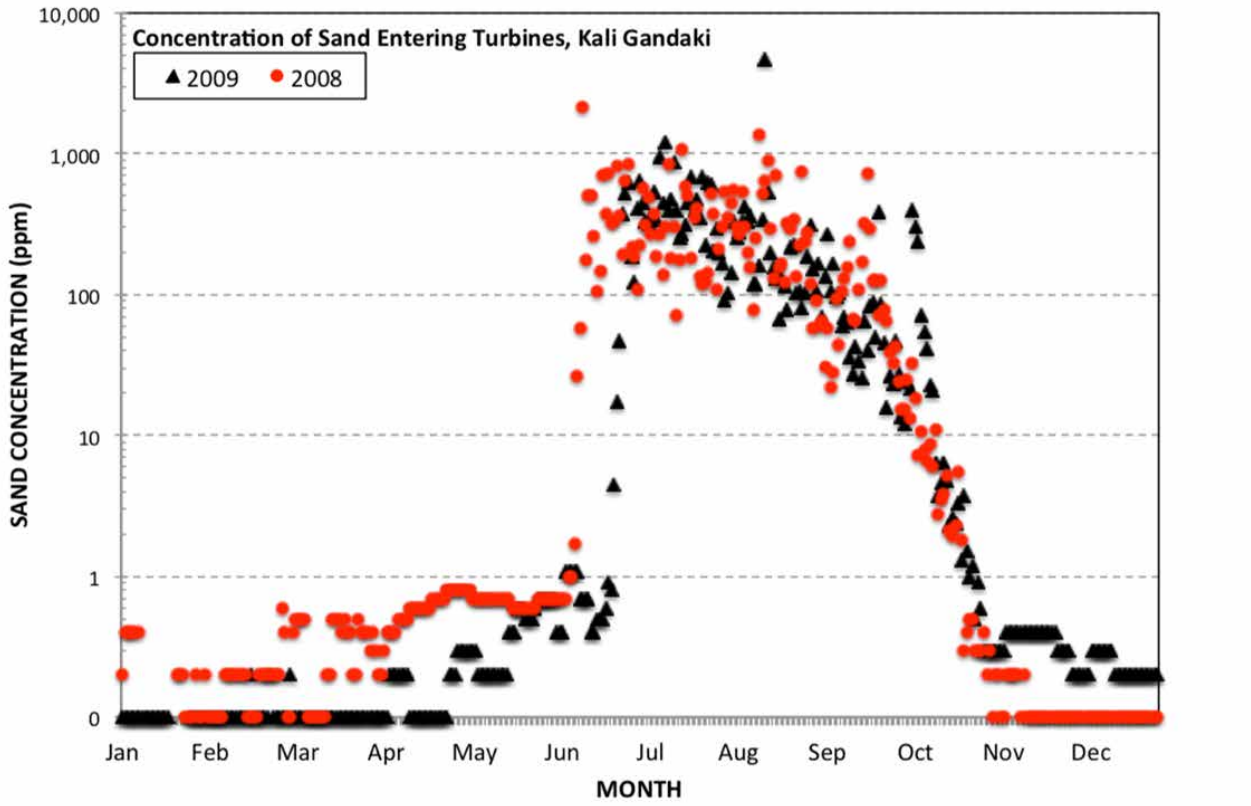

Sand causes damage which may result in reduced operating efficiency of the generating equipment while it is in use, the need to conduct more frequent repairs, and, possibly, its failure in use, which would lead to a need for immediate repairs. Unexpected breakdowns might prove to be particularly costly if they necessitated repairs during periods of peak demand; repairs are generally scheduled for the dry season when water flow in the river is not sufficient to support continuous generation at full capacity (NEA 2015; Chhetry and Rana 2014).

Figure 36 gives an indication of maintenance practices at the Kali Gandaki "A" Plant. It shows daily generation for a six-and-a-half-year period from the summer of 2011 through the end of calendar year 2017. Generation totals are color-coded by the unit producing the power. Generally speaking, when water flow is high, all three generating units are operated simultaneously. When flow is low, one of the units is often taken out of service.

Unit 1 was taken out of service for extended periods in 2012, 2014, and 2017; Unit 2 in 2013 and 2016; Unit 3 in 2015. Generally, each unit is overhauled every third year, on a staggered basis. While major overhauls are generally recorded in NEA's Annual Reports, Figure 36 shows that each unit was also occasionally withdrawn from service for shorter periods.[4] In the absence of more detailed maintenance records, it is difficult to infer what motivated these temporary suspensions – if they were to perform necessary repairs, or simply because the unit was not needed at a particular time. It is worth noting, though, that save for an anomalous episode in the summer of 2016, all three units were almost always used simultaneously during the summer and fall months when water flow, and hence, generation potential, was greatest.

It is difficult to characterize the effects of sediment damage on operating efficiency. Physical measurements reveal that parts are eroded while they are in service, with consequences that must surely compromise performance and reliability (Chhetry and Rana 2015b). While it seems intuitively obvious that damaged equipment will be less efficient, the data do not reveal an obvious pattern to this efficiency loss. We have evaluated the data depicted in Figure 36 to see if a unit produced less power than did the other two in the months before its overhaul (when presumably, it would have been in service longer, and so its efficiency would be reduced relative to the other two), or if a unit produced more power than did the other two in the months after its overhaul (when presumably, the other two would have been in service longer, and so their efficiency would be reduced relative to the one that had just been overhauled). However, we have not been able to find any consistent pattern documenting such phenomena. Moreover, it does not seem reasonable to ascribe all damage to sediment. Normal wear and tear may account for some of the need for maintenance.

Given these many uncertainties, our efforts to estimate the benefits that would result from a reduction in sediment delivery are necessarily speculative and have relied on indirect approaches. We have developed two methods for conducting this estimation. In the first, we took as a datum the observation that maintenance was scheduled every third year. We then asked "Given such information as is available on the financial and opportunity costs of performing this maintenance, how much effect must abrasion have on the efficiency and reliability of the generating units so as to motivate the observed every-third-year overhaul pattern?" Several factors made this calculation very imprecise:

- We had no data on the relationship between sediment delivery, equipment damage, and efficiency loss,
- NEA data on Kali Gandaki maintenance expenditures were not broken down by particular procedures, and did not record opportunity costs of units being withdrawn from service,
- Calibration of the model required identifying a rate of efficiency loss such that maintenance would be performed in every third, rather than every second, or every fourth, year. This admitted a wide range of possible rates of damage that would be consistent with the data.

4. There were also short intervals during 2013 and 2016 during which generation was completely suspended.

Figure 36: Daily power generation at the Kali Gandaki "A" Plant, July 2011 - January 2018. Source: data provided by NEA

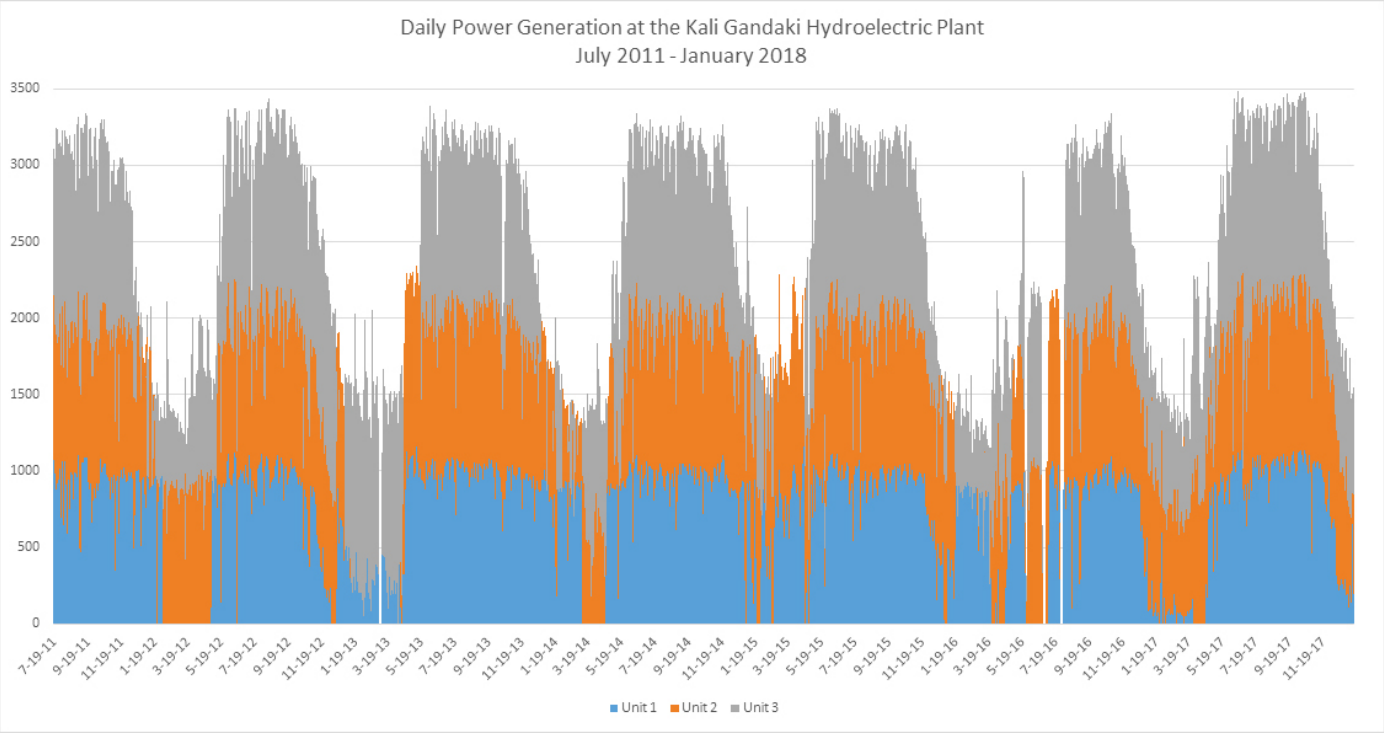

Given these concerns, we developed a second method and, in the interest of space, we will focus on it here. While the mathematical details underlying the approach are somewhat tedious, the basic economic idea is simple. It is that the plant operator faces a tradeoff in operating the desanding basins. We noted above that the basins are flushed about 22 times every year. This rate of flushing is determined by a sort of rule-of-thumb: the basins are flushed when the sediment accumulated in them reaches a depth of three meters. The basins themselves, however, are much deeper than this. More sediment could be allowed to accumulate between flushes. Alternatively, the basins could be flushed more frequently. There would be some cost savings from allowing more sediment to accumulate between flushes; the plant would have to reduce to half power less frequently. But the more sediment accumulates in the basins, the less effective they are in removing sediment; balanced against these cost savings from reduced flushing would be increased damages from more sediment going through the turbines. Conversely, more frequent flushing would spare the turbines from damage, but increase the time during which generation of power is curtailed.

We do not have a reliable direct way to measure the damage that sediment causes to equipment, but we do have a relatively good way to measure the costs of flushing, as we demonstrated in the previous section. What we are about to show is that if the operator trades off flushing costs against equipment damage to minimize their sum, we can use the marginal cost of flushing sediment to estimate the marginal damage sediment causes. By the "equimarginal principle" of economic optimization, the operator will equate the cost of disposing of the marginal cubic meter of sediment via the desanding basins to the marginal damage expected to arise from *not* disposing of it, and instead letting it pass through the generating equipment.

The formal analysis proceeds as follows. Suppose the total volume of sand that is borne in water diverted for generation during year t is S_t. A fraction $f(V)$ of this sand will be settled out in the desanding basins. This fraction depends on V, which we define as the volume of accumulation reached before the basins are flushed. V is a variable under the control of the operator; the operator decides the rule-ofthumb to follow in basin

flushing. We will suppose that $\partial f/\partial V<0$; if the operator allows more sand to accumulate before flushing, the residence time of water in the basins will be shortened, and less sand will settle in them.

When the operator adopts a practice of flushing the basins when the volume of sediment accumulated has reached V, she will flush the basins

$$N_t=f(V)\ S_t/V$$

times per year. If each flush cost c, the total cost of flushing per year would then be

$$C(V,S_t)=c\cdot(f(V)\ S_t)/V$$

Sand that is not detained in the desanding basins and flushed away causes damage to the generating equipment. A fraction $1-f(V)$ of the total volume of sand in water diverted for generation passes through the turbines. Let the monetary value of damage done by this sand be $D(V,S_t)=D([1-f(V)]\ S_t)$. The dam operator should, then, adopt a flushing rule to minimize

$$C(V,S_t)+D(V,S_t)=c\cdot(f(V)\ S_t)/V+D([1-f(V)]\ S_t) \qquad (A4.1)$$

A couple of clarifications may be helpful here. First, by "adopting a flushing rule," we mean setting a level of V such that, when the volume of sand deposited in the basins reaches V, they will be flushed. Second, c is assumed to be a constant that is multiplied by $f(V)\ S_t/V$, while D is assumed to be a function of $[1-f(V)]\ S_t$.]

Differentiating the sum in (A4.1) with respect to V and setting the result to zero to find the flushing rule that would minimize the sum of costs and damages,

$$cS_t\ \frac{V(\partial f/\partial V)-f}{V^2}-\frac{\partial D}{\partial S_t^G}\ \frac{\partial f}{\partial V}S_t=0, \qquad (A4.2)$$

Where $S_t^G=[1-f(V)]S_t$, the amount of sand that is *not* trapped in the desanding basins and, hence, that passes through the turbines.

Now to find the value of a reduction in sand in the water diverted for generation, differentiate the sum of costs and damages, (A4.1) with respect to S_t, finding

$$\frac{\partial(C+D)}{\partial S_t}=\frac{c}{V}f+\frac{\partial D}{\partial S_t^G}\ (1-f) \qquad (A4.3)$$

Simplifying and rearranging the optimization condition for the flushing criterion, (A4.2)

$$\frac{c}{V}\left(1-\frac{1}{\varepsilon}\right)=\frac{\partial D}{\partial S_t^G} \qquad (A4.4)$$

where ε is defined at the logarithmic derivative of trapping efficiency with respect to the flushing rule

$$\varepsilon=\frac{\partial f/\partial V}{f/V}.$$

Expression (A4.4) encapsulates the "equimarginal condition" we are exploiting to estimate equipment damage. We do not know the marginal damage caused by sediment passing through the turbines, $\partial D/(\partial S_t^G)$, but if we can estimate ε, we can relate it to a quantity we do know, the cost per desander flush, c/V.

So using (A4.4) in (A4.3)

$$\frac{\partial(C+D)}{\partial S_t}=\frac{c}{V}\left[1-\left(\frac{1-f}{\varepsilon}\right)\right] \qquad (A4.5)$$

To evaluate ε, we will suppose that the fraction of sand that settles in the desanding basins depends on the residence time of sand-laden water in the basins. Suppose the fraction remaining suspended in the water in the desanding basins after water has been in the basins for a time τ will be

$$\phi(\tau)=e^{-\kappa\tau}$$

Suppose water is entering the desanding basins at a flow rate of r cubic meters per second. We will treat the two desanding basins as if they were a rectangular prism of width W, length L, and height H. We will suppose also that sediment settles uniformly along the length of the basins and designate by h the depth of sediment in the basin. This depth increases with deposition, of course. Note that width and length are fixed by the dimensions of the basin, and so only the depth of the sediment deposited in the basins can vary. If length is measured in the direction of water flow, then the rate at which water traverses the basins will be $dL=r/W(H-h)$, where units are now meters per second. Thus, the residence time of water in the desanding basins will be

$$\tau=L/dL=(\overline{V}-V)/r$$

Where $\overline{V}=WLH$, the maximum volume of water that could be held in the desanding basins when they are empty, and $V=WLh$, the volume occupied by sand at the time the basins are flushed. Thus, the fraction that goes through the turbines will be

$$\phi(\tau) = e^{-\kappa(\overline{V}-V)/r}$$

and the fraction settling in the desanding basins will be

$$f(V) = 1 - \phi(\tau) = 1 - e^{-\kappa\tau} = 1 - e^{-\kappa(\overline{V}-V)/r}$$

Differentiating with respect to V,

$$\frac{\partial f}{\partial V} = -\frac{\kappa}{r} e^{-\kappa(\overline{V}-V)/r}$$

Thus

$$\frac{\partial f/\partial V}{f/V} = -\frac{\kappa V}{r} \frac{e^{-\kappa(\overline{V}-V)/r}}{1 - e^{-\kappa(\overline{V}-V)/r}} = -\frac{\kappa V}{r} \frac{1-f}{f}$$

We can write

$$e^{-\kappa(\overline{V}-V)/r} = 1 - f$$

or

$$\kappa/r = -\frac{\ln(1-f)}{\overline{V}-V}$$

Thus, we have

$$\varepsilon = \frac{\partial f/\partial V}{f/V} = \frac{V}{\overline{V}-V} \frac{\ln(1-f)\,(1-f)}{f}$$

Substituting in (A4.5),

$$\frac{\partial(C+D)}{\partial S_t} = \frac{c}{V}\left[1 - \frac{\overline{V}-V}{V} \frac{f}{\ln(1-f)}\right] \qquad \text{(A4.6)}$$

Above, we have estimated the cost per cubic meter of sediment flushed, c / V, as 86.7 NPR/m^3. An International Hydropower Association study reports that of the 15% of sediment that is suspended in water diverted for generation at the Kali Gandaki Plant, 11% is removed by the desanding basins (IHA, n.d.), and so 4% is passed through the turbines. Thus, we suppose trapping efficiency, f, is 11/15 = 73%, and so $-f / \ln(1-f) = 0.56$. While the depth of the desanding basins is 14 meters, the partition between them only rises to 11 meters. The basins are flushed when sand reaches a depth of 3 meters. Since the width and length of the basins are invariant with respect to sand deposition, $(\overline{V}-V)/V = (11-3)/3 = 2.33$. $2.33 \cdot 0.56 = 1.30$. So

$$\frac{\partial(C+D)}{\partial S_t} = 86.7\ NPR/m^3 \cdot (1 + 1.30) = 199.8\ NPR/m^3$$

or \$1.78/m^3. At a discount rate of 10%, this would translate into a net present value for a one cubic meter reduction in sediment delivery per year in perpetuity of almost 2000 NPR, or US\$ 17.84.

Let us make two final comments on this analysis:

- This figure of 2000 NPR or US\$ 17.84 per cubic meter is the *sum* of the value of avoided desander operating cost and avoided equipment damage. The figure of 867 NPR or US\$ 7.41 per cubic meter for avoided desander cost is already included in this sum; *it should not be added to it.*
- This figure is an estimate of the value of a cubic meter of sediment in water diverted for power generation. While it applies to sediment that either is retained by, and flushed from, the desanding basins, or passes through the generating equipment, it applies only to the roughly 15% of the annual sediment load (as estimated by (IHA) in water diverted for generation. To use this figure for estimating the value of sediment reduced at the source of the reduction, one would need to know what fraction of such sediment would eventually be found in water diverted for generation.

4. PEAKING CAPACITY

One of the most obvious reasons for concern over sediment transport in rivers used for hydroelectric generation is that sediment fills reservoirs. The more sediment accumulates in a reservoir, the lower is its storage volume.

For several months of the year, storage capacity does not matter. Flow in the Kali Gandaki varies from more than 1,000 cubic meters per second during the Monsoon to as little as 50 during the winter (Figure 37).

The turbines in the plant are designed to operate at a maximum flow rate of 47 $m^3 \cdot s^{-1}$ through each of the three units, or 141 $m^3 \cdot s^{-1}$. When flow in the river is greater than this rate, some water is released over the spillway. When flow is lower, the plant may either be run at less-than-full capacity, or water may be stored, and, consequently, less electricity generated, during parts of the day when demand is lower so that more may be provided during the peak demand period of the evening hours.

We are interested in assigning an economic value to storage in the reservoir. The Kali Gandaki plant was

Figure 37: Power generation and river flow at the Kali Gandaki "A" Plant 2011 - 2013. Source: Chhetry and Rana 2015

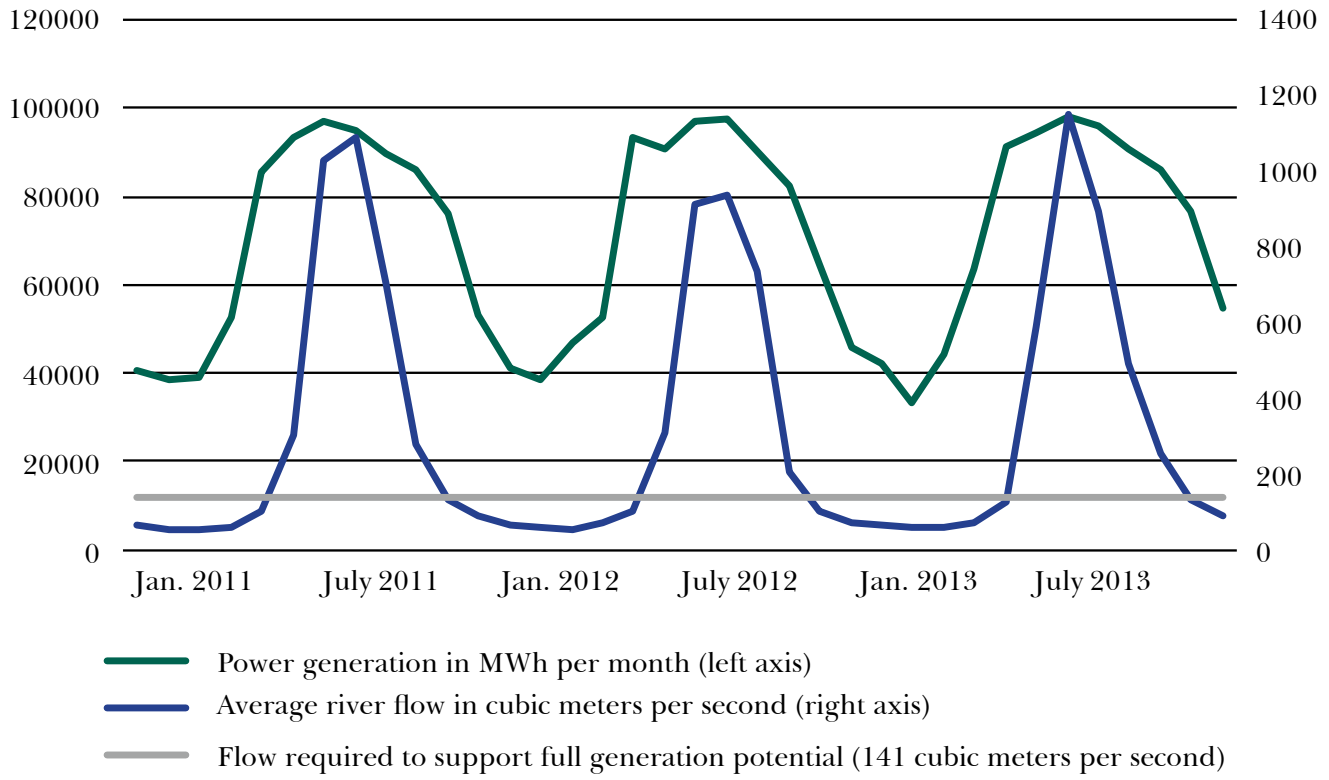

designed with pondage capacity of a little more than 3 million cubic meters. This is sometimes characterized as a six-hour peaking capacity, as a flow rate of 141 $m^3 \cdot s^{-1}$ is equivalent to 507,600 $m^3 \cdot h^{-1}$. As there is generally some inflow, however, the actual period of peak operation could extend longer. Over the course of its operation, however, the capacity of the reservoir has declined as sediment has accumulated in it. In the remainder of this appendix, we develop an estimate of the economic value of reservoir capacity.

We begin by supposing that the plant operator allocates water so as to provide consumers with benefits we will denote as $v(x_\theta,\theta)$. These benefits are realized at a particular instant in time indexed by θ. They depend on the amount of electricity generated, which is proportional to the volume of water the operator discharges, x_θ. The value of electricity also depends on the time of day, θ. We suppose the operator's objective is to maximize the sum (in the limit, the integral) of benefits over the course of a 24-hour daily cycle:

$$\max_{\{x_\theta\}} \int_0^{24} v(x_\theta, \theta) d\theta. \qquad \text{(A4.7)}$$

This objective is to be maximized over repeating 24-hour daily cycles. If S_θ is the amount of water stored in the reservoir at time θ and we can assume the flow of water in the river is approximately constant at rate f at any time of day,[5] then

$$\dot{S} = f - x_\theta. \qquad \text{(A4.8)}$$

A dot over a variable indicates its total derivative with respect to time. Expression (A4.8) just says the change in reservoir volume at any point in time is the difference between inflow and discharge at that time.

There is, of course, also a limit as to how much can be stored in the reservoir. It cannot be drained below some zero point, nor filled in excess of its capacity, which we will denote as K,

5. Precipitation during a day might affect flow, but such variations may not be large and, of course, the "dry season" is characterized by a general dearth of rain. Evaporation may be accommodated as a reduction in inflows.

$$0 \leq S \leq K \quad \text{(A4.9)}$$

The limits in (A4.9) then imply that

$$x_\theta = f \text{ if } S_\theta = 0 \text{ or } S_\theta = K; \quad \text{(A4.10)}$$

if the reservoir were completely full, or if it were completely empty over any interval of time, the discharge rate would have to be the same as the inflow rate over that interval.

Finally, as the plant is operated on a 24-hour cycle, suppose that $S_0 = S_{24}$: at the end of a 24- hour period there must be as much water in the reservoir as there was at the beginning, so the cycle can be repeated again.

Consider now the solution to the problem just described. It is instructive first to consider the case in which the constraints in (A4.10) do *not* bind, and hence that the operator's choice of discharge rate is never constrained to equal river flow. This would mean the reservoir was never completely filled nor completely emptied. To solve this problem, introduce a costate variable, λ, to append (A4.8) to the integrand of (A4.7) (in the language of optimal control theory, forming the Hamiltonian). A solution must satisfy

$$\frac{\partial v}{\partial x} = \lambda \quad \text{(A4.11)}$$

and

$$\dot{\lambda} = 0 \quad \text{(A4.12)}$$

Heuristically, the economic interpretation of the costate variable, λ, is as the implied price of the state variable, which is, in this case, the volume of water held in the reservoir, S. Equation (A4.6) says that the value of another liter of water in the reservoir is just the marginal value of the power that could be generated by releasing that liter. Equation (A4.6) says that, because the liter of water could be released at any time of day, the operator should allocate water in storage so as to keep its marginal value the same during every minute of the day. If it were not, the operator should allocate more discharges when they are more valuable and fewer when they are less valuable.

Denote by *V(K)* the value of the objective function, (A4.7), when the optimal sequence of discharges, $\{x_\theta\}$, is chosen. We are interested in the marginal value of capacity, *K*; by how much does the value of the objective, *V(K)*, increase with an incremental increase in *K*? Differentiating *V(K)* we find:

$$\frac{dV}{dK} = \int_0^{24} \frac{\partial v}{\partial x}\frac{dx}{dK} d\theta = \lambda \frac{d}{dK}\int_0^{24} x d\theta = \lambda \frac{d}{dK}(24f) = 0 \quad \text{(A4.13)}$$

The second equality comes from the maximization conditions that $\partial_v / \partial_x = \lambda$ and λ is constant; the third equality comes about because over a 24-hour repeating cycle, the total amount of water discharged must equal the total flow available; and the final equality results because river flow is independent of reservoir capacity.

While expression (A4.13) is, in a sense, trivial, it is worth underscoring that the mathematical argument substantiates the fundamental economic proposition. The value of an asset depends on how scarce it is. If the reservoir were never fully filled and drained in a 24-hour cycle – that is, if, as assumed in deriving (A4.7), the constraints in (A4.3) and their implication in (A4.4) never arose – then there would be no economic loss associated with lost capacity.

Expression (A4.13) does not say that discharges never vary over the daily cycle, nor does it say that there is no value in having the ability to store water at some point so as to be able to discharge more at another. If demand varies over the course of the day, discharges would certainly vary so as to better serve demand. Expression (A4.13) says, rather, that if discharges do not vary by enough to invoke capacity constraints, then capacity (again, as distinguished from the ability to vary discharges) will have no marginal value.

This begs the question of the conditions under which the capacity constraint binds. At the Kali Gandaki "A" Plant, the maximum flow of water each generating turbine is designed to handle is 47 cubic meters per second, so the overall limit for all three of its turbines operating simultaneously would be 141 meters $m^3 \cdot s^{-1}$. Designate the maximum rate of discharge at which power can be generated as $\overline{x}$. When the rate of flow in the river, *f*, exceeds $\overline{x}$ there is obviously no need for storage capacity. When flow is less than $\overline{x}$ the need for storage capacity depends on the difference between actual flow, *f*, and the maximum that can be used, $\overline{x}$.

This can be illustrated by considering an extreme example. Recall from expression (A4.13) above that the marginal value of capacity would be zero if

the reservoir were never fully filled and emptied within the same 24-hour operating cycle. It may be instructive to ask, then, under what conditions of actual and maximum flow it would be *physically possible* to fully fill and drain the reservoir in the same 24-hour cycle. It cannot be economically optimal to do what is physically impossible.[6]

Recall that K is the capacity of the reservoir. Let us introduce one additional quantity: define x_0 as the minimum allowable flow. At the Kali Gandaki Plant, a minimum flow of 4 $m^3 \cdot s^{-1}$ should be maintained to sustain aquatic life in the river. If we take it as given that the plant operates on a 24-hour peaking cycle, a necessary condition for reservoir capacity to bind would be that

$$K/(f - x_0) + K/(\overline{x} - f) = \frac{K(\overline{x} - x_0)}{(f - x_0)(\overline{x} - f)} \leq 24. \quad \text{(A4.14)}$$

The quickest possible option for filling the reservoir is to let water accumulate at the rate of f-x_0, releasing only the minimum amount required, x_0, while the reservoir is filling. This would take $K/(f\text{-}x_0)$ hours to accomplish. Then, when it is full, the quickest way to empty the reservoir would be to discharge water at rate $\overline{x}$. As more water is flowing in all the time, though, the net rate of discharge would be $\overline{x}$-f. It would, then, take $K/(\overline{x}\text{-}f)$ hours to empty at this rate. Note that discharging at a gross rate faster than $\overline{x}$ is ruled out on the argument that there would be no point in discharging water that could later be used for generation.

The *shortest possible* duration for an empty-to-full-to-empty cycle results when the denominator of the middle expression in (A4.14), $(f\text{-}x_0)(\overline{x}\text{-}f)$ is maximized. Differentiating this expression and setting the result to zero to find a maximum,

$$(\overline{x} - f) - (f - x_0) = 0 \Rightarrow f = (\overline{x} + x_0)/2$$

Substituting into (A4.14), if reservoir capacity comprises a binding constraint, we would need to have

$$K \leq 6(\overline{x}\text{-}x_0) \quad \text{(A4.15)}$$

The maximum designed flow at the Kali Gandaki Plant is 141 $m^3 \cdot s^{-1}$, or 507,600 $m^3 \cdot h^{-1}$. Minimum environmental flow is 4 $m^3 \cdot s^{-1}$, or 14,400 $m^3 \cdot s^{-1}$. So

$$K \leq 6 \cdot (507{,}600\text{-}14{,}400) = 2{,}959{,}200 \text{ m}^3.$$

Reservoir capacity would have to be less than about 3 million cubic meters to be *binding under any circumstances*. The rate of flow that minimizes the refill cycle length is about 72.5 $m^3 \cdot s^{-1}$. The minimum average flow in the Kali Gandaki River at the dam site is about 55 $m^3 \cdot s^{-1}$. At this flow, capacity would have to be less than about 2.77 million cubic meters to be binding.

While the original live storage capacity of the reservoir was more than 3 million cubic meters, that capacity declined over time as sediment accumulated. Interviews with NEA personnel indicated that capacity might have fallen below 2 million cubic meters in some recent years. It seems, then, that capacity may have declined enough to be scarce.

However, this is not to say that that capacity was always used. The dry season in Nepal typically runs from the winter through early spring. When generating power, the level of water in the reservoir can be drawn down as low at 518 meters. Yet, this level was never reached during many periods of generation (Figure 38). In fact, during some entire seasons (as shown by the yellow arrows in Figure 38), the level of water in the reservoir was never drawn below 520 meters. There was excess capacity. In earlier years Nepal was highly dependent on the Kali Gandaki "A" plant for baseload electrical generation. While the demand for power during peak periods was high, deferring generation in off-peak periods to provide peak power was not an option. In more recent years, however, increased availability of baseload power from other sources (particularly power purchases from India) have increased operating flexibility at the Kali Gandaki Plant. As a result, NEA's 2016/17 *Annual Report* indicates that in that fiscal year, the Kali Gandaki and Nepal's other hydroelectric plants were "operated in their full capacity during peak time in dry season using their pondage capacity *[for the]* first time in the plants' history". While reservoir

6. We might note in passing that if the marginal willingness to pay for power is determined by factors exogenous to the operation of the plant, such as the cost of supply from alternative sources, a so-called "bang-bang" operating rule could be optimal. The reservoir should first be filled as rapidly as possible, then emptied as rapidly as possible, as we describe here.

Figure 38: Hourly reservoir water level, 2003 – 13.

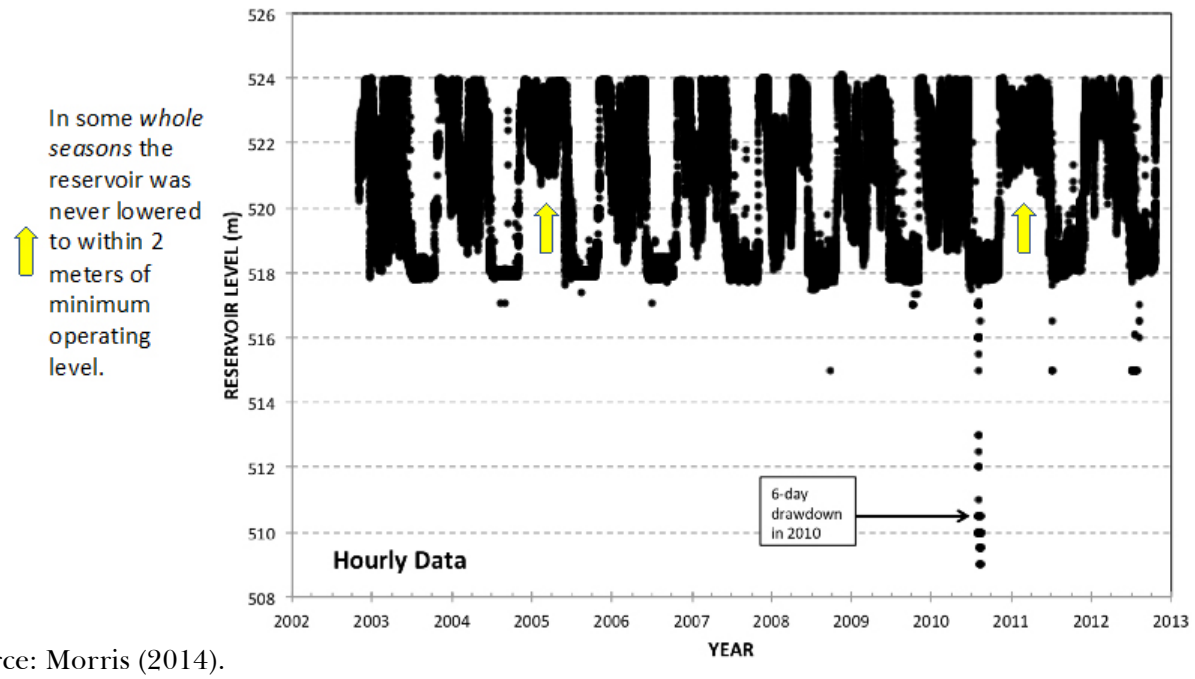

Source: Morris (2014).

capacity may not have been fully employed in the past, it is likely to be so going forward.

Let us return to the constrained optimization problem defined by (A4.7) – (A4.10), and suppose now that each constraint in (A4.10) binds at some point in the day. That is, at some point the reservoir is empty, and at some later point, it is full. Over any interval during which the reservoir is either full or empty, the rate of discharge is necessarily constrained to be equal to the rate of flow in the river, f.

Suppose for simplicity, but not unrealistically, that daily demand is a single-peaked function. Assume, then, that the operator adopts the following pattern:

- Starting at time 0, when the reservoir is empty, until some later time θ_1, when it is full, she discharges less water than flows in: $x_\theta < f$ for $0 \leq \theta < \theta_1$.
- Between θ_1 and some later time, θ_2, the reservoir is maintained at full capacity. Whenever the reservoir is full, discharge must equal flow in the river: $x_\theta = f$ for $\theta_1 \leq \theta < \theta_2$.
- Between θ_2 and θ_3 the operator discharges more water than flows in, meeting peak demand, and emptying the reservoir: $x_\theta > f$ for $\theta_2 \leq \theta < \theta_3$.
- Between θ_3 and 24 hours, the operator is again constrained to discharge as much water as flows in, as she cannot maintain less than zero volume in the reservoir: $x_\theta = f$ for $\theta_3 \leq \theta < 24$.
- At time 24 the cycle begins again, with discharges held to less than flow to begin to refill the reservoir.[7]

These assumptions lead to a multipart elaboration of the objective, (A4.7):

$$V(K) = \max_{\{x_\theta\}} \left[\int_0^{\theta_1} v(x_\theta, \theta) d\theta + \int_{\theta_1}^{\theta_2} v(f, \theta) d\theta + \int_{\theta_2}^{\theta_3} v(x_\theta, \theta) d\theta + \int_{\theta_3}^{24} v(f, \theta) d\theta \right] \quad \text{(A4.16)}$$

Now note that the intervals $[0,\theta_1)$ and $[\theta_2, \theta_3)$ are "free" in the sense that the operator can choose x's on these intervals without being constrained by the capacity of the reservoir. This means that expressions (A4.11) and (A4.12) above hold on these intervals, *but, importantly, for different values of the costate variable* λ *on the different intervals.* So

$$\frac{\partial v}{\partial x} = \lambda_1 \quad \text{(A4.17)}$$

and

$$\dot{\lambda}_1 = 0 \quad \text{(A4.18)}$$

7. The amount of power that can be generated by a cubic meter of water varies linearly with *hydraulic head*: the vertical distance between the surface of the reservoir and the turbines below. There is, then, the possibility that what we have described as the fourth part of cycle might be dispensed with, in order to more rapidly build up head so that more power can be generated more quickly. As variation in head tends to be relatively small – on the order of 5 meters in roughly 110 – we abstract from this consideration.

on the interval $[0,\theta_1)$, while

$$\frac{\partial v}{\partial x} = \lambda_3 \tag{A4.19}$$

and

$$\dot{\lambda}_3 = 0 \tag{A4.20}$$

on the interval $[\theta_2, \theta_3)$.

Equations (A4.17) – (A4.20) describe a sort of "complementary slackness" condition; when the operator is free to choose the flow rate, x_θ, the corresponding marginal value of capacity, λ_θ remains constant. Heuristically, the operator should allocate flow so that there are no "arbitrage opportunities" to increase overall value on the time interval over which choice is unconstrained. Conversely, constraints on flow would arise when the marginal value of capacity is rising (or falling) and it is impossible to generate any more (or less) power, given the limits of reservoir capacity.

As in the case in which the reservoir capacity constraint did not bind, we find the marginal value of capacity by differentiating (A4.16) with respect to K. Doing so,

$$\begin{aligned}\frac{dV}{dK} = \int_0^{\theta_1} \frac{\partial v}{\partial x}\frac{dx}{dK}d\theta + \int_{\theta_2}^{\theta_3} \frac{\partial v}{\partial x}\frac{dx}{dK}d\theta + [v(x_1,\theta_1) \\ - v(f,\theta_1)]\frac{d\theta_1}{dK} + [v(f,\theta_2) - v(x_2,\theta_2)]\frac{d\theta_2}{dK} \\ + [v(x_3,\theta_3) - v(f,\theta_3)]\frac{d\theta_3}{dK}\end{aligned} \tag{A4.21}$$

Note that we are condensing notation, avoiding subscripting subscripts by writing x_i for $x_{\theta i}$.

Consider the two integrals on the right-hand side of the equal sign in (A4.21) first. The choice of x is only free when the reservoir is neither full nor empty. From (A4.17) – (A4.20), optimization over intervals in which the choice of discharge is not constrained implies that the marginal value of discharges is constant over such intervals. So

$$\int_0^{\theta_1} \frac{\partial v}{\partial x}\frac{dx}{dK}d\theta = \lambda_1 \int_0^{\theta_1} \frac{dx}{dK}d\theta = \lambda_1 \frac{d}{dK}\int_0^{\theta_1} x_\theta d\theta \tag{A4.22}$$

Time θ_1 is defined implicitly as the duration required to fill the reservoir, starting from time zero. So, by definition,

$$\int_0^{\theta_1} (f - x_\theta)d\theta = K \tag{A4.23}$$

Differentiating (A4.23) with respect to *K*, and rearranging

$$(f - x_1)\frac{d\theta_1}{dK} - 1 = \int_0^{\theta_1} \frac{dx}{dK}d\theta \tag{A4.24}$$

Using (A4.24) in (A4.22),

$$\int_0^{\theta_1} \frac{\partial v}{\partial x}\frac{dx}{dK}d\theta = \lambda_1\left[(f - x_1)\frac{d\theta_1}{dK} - 1\right] \tag{A2.25}$$

A similar set of machinations, invoking the implicit definition of θ_2 and θ_3 by

$$\int_{\theta_2}^{\theta_3} (x_\theta - f)d\theta = K$$

gives

$$\int_{\theta_2}^{\theta_3} \frac{\partial v}{\partial x}\frac{dx}{dK}d\theta = \lambda_3\left[1 + (f - x_3)\frac{d\theta_3}{dK} - (f - x_2)\frac{d\theta_2}{dK}\right] \tag{A4.26}$$

Using (A4.26) and (A4.25) in (A4.21)

$$\begin{aligned}\frac{dV}{dK} = \lambda_3 - \lambda_1 \\ +[v(x_1,\theta_1) + \lambda_1 \cdot (f - x_1) - v(f,\theta_1)]\frac{d\theta_1}{dK} \\ +[v(f,\theta_2) - v(x_2,\theta_2) - \lambda_3 \cdot (f - x_2)]\frac{d\theta_2}{dK} \\ +[v(x_3,\theta_3) + \lambda_3 \cdot (f - x_3) - v(f,\theta_3)]\frac{d\theta_3}{dK}\end{aligned}$$

This expression can be greatly condensed, as each of the quantities in square brackets must be zero. The reason for this conclusion can be found in texts on dynamic optimization (see, e.g., Kamien and Schwartz 1981), but the heuristic argument is straightforward. Each of the terms in square brackets compares the instantaneous value of discharging a cubic meter of water immediately before and immediately after

the capacity constraint starts to bind. Consider, for example, the quantity in the first set of square brackets. Its first term, $v(x_1, \theta_1)$, is the instantaneous contribution to the operator's objective at time θ_1. The second term, $\lambda_1 \cdot (f - x_1)$, is the implicit value of the additional water stored in the reservoir at the last moment before it reaches full capacity. Balanced against the sum of these two terms is the third, $v(f, \theta_1)$, the value realized at time θ_1 when discharges are constrained to the flow rate, f, by having reached full. Since the operator has the ability to choose a strategy yielding a different "switch time," θ_1, if she has chosen that switch time optimally, a small variation in it should not yield a higher overall value.[8]

Thus, the entire expression reduces to simply

$$\frac{dV}{dK} = \lambda_3 - \lambda_1. \qquad \text{(A4.27)}$$

While the mathematics underlying the derivation of (A4.27) may have been tedious, the intuition underlying the result is straightforward. If reservoir capacity constrains the operator's choices, it is not because it forces her to produce less power over the course of a day than she would have liked to. Her ability to generate power is constrained, but the source of the constraint is the flow of the river, not the capacity of the reservoir. What the capacity of the reservoir constrains is the operator's choice of when she can produce the power the river's flow rate allows. A marginal cubic meter of storage means that the operator can produce the corresponding amount of additional power when its value is high (λ_3), but by choosing to produce more power when it is most valuable, she necessarily forgoes the option of using that cubic meter of water to produce the same amount of power when its value is lower (λ_1).

Putting values to expression (A4.27) is difficult, as it is hard to predict how long the current conditions under which supply may generally meet demand at posted prices will continue. We adopted above a figure of 6 NPR per kWh for the off-peak price of power. During the dry season, however, NEA only distinguishes between "normal" and "peak" power, eliminating the deeply discounted "off-peak" category. In the discussion of opportunity costs of forgone generation, we supposed that off-peak power might be valued at 6 NPR (US$ 0.054) per kWh. This was based on both prices charged to large industrial users and the cost of power purchase from India and IPPs. During the dry season, prices to large industrial users during the "normal" hours outside the 5:00 – 11:00 pm peak period climb to about 8 NPR (US$ 0.071) per kWH (7.5 NPR per kWh to those supplied at the highest voltages, 8.4 NPR per kWh to those at the next-highest). The cost of purchases from India and IPPs appear to remain at approximately 6 NPR (US$ 0.054) per kWh during the dry season.

Again, however, it is the *difference* between the peak price and that at the time of alternative generation is forgone that determines the value of capacity. While tariff schedules indicate peak prices on the order of 10 NPR (US$ 0.089) per kWh for large industrial users, it may be too optimistic to assume that demand will consistently be met at these prices. Hence, we will suppose that the marginal willingness to pay for power may be expected to differ by 6 NPR (US$ 0.054) per kWh between peak demand and other times.

We need to do a few more calculations to assign a net present value to the marginal meter of additional capacity. Let r denote the amount of power that can be generated by discharging a cubic meter of water. The rated capacity of the Kali Gandaki plant is 144 MW at a flow rate of 141 $m^3 \cdot s^{-1}$ = 507,600 $m^3 \cdot h^{-1}$. The plant would then produce 144,000/507,600 = 0.284 kWh per cubic meter of water discharged. Thus, the value of the marginal cubic meter of capacity is 6 NPR per kWh · 0.284 kwh per cubic meter = 1.70 NPR (US$ 0.015) per cubic meter for each day during which that cubic meter of capacity is needed to serve peak demand.

Next, let D represent the number of days in the dry season, when reservoir capacity constrains operations. Capacity is only valuable when water flow in the river is below that which is required to maintain full generation. We will suppose this is the case for six months, or 180 days, of the year.

Finally, a cubic meter of sediment that is not deposited in the reservoir this year should not constrain capacity in any subsequent year. Hence, although we are only now analyzing the benefit of a one-time reduction

8. Note also that the terms in square brackets in (A2.25) also provide formulae that could be used in conjunction with (A2.14) – (A2.17), (A2.18), and (A2.20) to calculate the optimal allocation of discharges.

in sediment deposition to the reservoir, we should calculate the net present value of the flexibility the extra storage capacity affords all future operations. To do this, we divide the seasonal benefit of capacity by the discount rate, δ, which we will take to be 10% per annum.

The calculations may be summarized by writing that the marginal value of reservoir capacity is

$$\frac{dV}{dK} = \frac{D}{\delta} r(\lambda_P - \lambda_0)$$

Using our figures above of D = 180 days, δ = 10%, r = 0.284 kWh/m3, and λ_p - λ_0 = 6 NPR (US$ 0.054) per kWh, this marginal value would be 3064 NPR, or US$ 27.36.

This figure is the value of reducing one cubic meter of sediment deposition at *present*, as the storage space it occupies would also be lost in all subsequent years. If that cubic meter of storage space were lost and another cubic meter were deposited next year, however, another cubic meter of storage lost would also not be available in all subsequent years, beginning next year. Thus, in order to calculate the net present value of a one-cubic meter reduction in storage loss in each and every subsequent year, we would need to take the net present value of *each year's storage loss's net present value*. This would mean dividing the figure above a second time by the discount rate of 10%, resulting in a value of US$ 273.60 for a reduction in sediment deposition of one cubic meter every year in perpetuity.

5. REFERENCES

(NatCap) The Natural Capital Project. 2013. "Sediment and Nutrient Model Parameter Database." Stanford, CA. http://www.naturalcapitalproject.org/invest/.

Bank, Asian Development. 2004. "PROJECT COMPLETION REPORT ON THE KALI GANDAKI 'A' HYDROELECTRIC PROJECT."

Bishwakarma, Meg B. 2012. "Performance Improvement of Headworks: A Case of Kalignadaki A Hydropweor Project through Physical Hydraulic Modelling."

Cardinael, Rémi, Viviane Umulisa, Anass Toudert, Alain Olivier, Louis Bockel, and Martial Bernoux. 2018. "Revisiting IPCC Tier 1 Coefficients for Soil Organic and Biomass Carbon Storage in Agroforestry Systems." *Environmental Research Letters* 13 (12): 124020. https://doi.org/10.1088/1748-9326/aaeb5f.

Chhetry, Balendra, and Kumar Rana. 2015a. "Effect of Sand Erosion on Turbine Components: A Case Study of Kali Gandaki 'A' Hydroelectric Project (144 MW), Nepal." *Hydro Nepal: Journal of Water, Energy and Environment* 17: 24–33. https://doi.org/10.3126/hn.v17i0.13270.

———. 2015b. "Effect of Sand Erosion on Turbine Components: A Case Study of Kali Gandaki 'A' Hydroelectric Project (144 MW), Nepal." *Hydro Nepal: Journal of Water, Energy and Environment*. https://doi.org/10.3126/hn.v17i0.13270.

Dahal, Nagmindra, and Roshan M Bajracharya. 2013. "Effects of Sustainable Soil Management Practices on Distribution of Soil Organic Carbon in Upland Agricultural Soils of Mid-Hills of Nepal." *Nepal Journal of Science and Technology* 13 (1): 133–41. https://doi.org/10.3126/njst.v13i1.7452.

Freeman, Myrick A, Joseph A Herriges, and Catherine L Kling. 2014. *The Measurement of Environmental Resource Values: Theory and Methods. The Measurement of Environmental Resource Values.*

IHA. n.d. "Nepal - Kali Gandaki Case Study."

Kamien, Morton S, and Nancy L. Schwartz. 1981. *Dynamic Optimization: The Calculus of Variations and Optimal Control in Economics and Management*. New York: Elsevier.

Karki, Nava Raj, Arbind Kumar Mishra, and Jayandra Shrestha. 2010. "Industrial Customer Outage Cost Analysis: A Case Study of Nepal." *International Journal of Systems Assurance Engineering and Management*. https://doi.org/10.1007/s13198-010-0011-z.

Kawashima, Shigekazu. 2007. "Conserving Reservoir Water Storage: An Economic Appraisal." *Water Resources Research*. https://doi.org/10.1029/2006WR005090.

Kolstad, Charles. 2011. *Intermediate Environmental Economics: International Edition. Oxford University Press.*

Morgan, R.P.C., D.D.V. Morgan, and H.J. Finney. 1982. "Stability of Agricultural Ecosystems: Documentation of a Simple Model for Soil Erosion Assessment." Collaborative Paper CP-82–59.

Morris, Gregory. 2014. "Sustainable Sediment Management: Kali Gandaki 144 MW Hydropower Dam, Nepal."

Rickenmann, Dieter. 1999. "Empirical Relationships for Debris Flows." *Natural Hazards* 19 (1): 47–77. https://doi.org/10.1023/A:1008064220727.

Ruesch, Aaron, and Holly K. Gibbs. 2008. "New IPCC Tier-1 Global Biomass Carbon Map For the Year 2000." Oak Ridge, Tennessee.

Shrestha, Jayandra Prasad, and Namrata Tusuju Shrestha. 2016. "Expansion Planning of Electricity Generating System Using the VALORAGUA and WASP-IV Models in Nepal." *Hydro Nepal: Journal of Water, Energy and Environment.* https://doi.org/10.3126/hn.v19i0.15352.

Shrestha, Ratna Sansar. 2011. "Electricity Crisis (Load Shedding) in Nepal, Its Manifestations and Ramifications." Hydro Nepal: Journal of Water, Energy and Environment. https://doi.org/10.3126/hn.v6i0.4187.

Timilsina, Govinda R., and Mike Toman. 2016. "Potential Gains from Expanding Regional Electricity Trade in South Asia." *Energy Economics*. https://doi.org/10.1016/j.eneco.2016.08.023.

Wischmeier, W H, and D Smith. 1978. "Predicting Rainfall Erosion Losses: A Guide to Conservation Planning." Washington DC: U.S. Department of Agriculture, Agriculture Handbook No. 537.

APPENDIX 5: SUMMARY OF DATA SOURCES AND PARAMETER VALUES, KALI GANDAKI

HILLSLOPE EROSION (INVEST SDR MODEL)

Table A5.1. Baseline USLE C (crop) factors used in hillslope erosion modeling

Land use/land cover class	Baseline USLE C value	USLE C value source
Airport	0.2853	Global average value for built up areas, from InVEST coefficient literature database (NatCap 2013)
Barren land	0.45	Wischmeier and Smith 1978, Table 10, "no appreciable canopy" with 0% ground cover
Built up	0.2853	Global average value for built up areas, from InVEST coefficient literature database (NatCap 2013)
Bush	0.08	Wischmeier and Smith 1978, Table 10, "appreciable brush or bushes" with 50-75% cover, 40% ground cover
Cliff	0.45	Wischmeier and Smith 1978, Table 10, "no appreciable canopy" with 0% ground cover
Forest	0.004	Global average value for forest, from InVEST coefficient literature database (NatCap 2013)
Forest - degraded	0.0154	Forest value (0.004) divided by 0.26, to match literature findings of forest rehabilitation impacts
Glacier	0.0001	Assumed extremely little erosion from glaciers
Grass	0.091	Wischmeier and Smith 1978, Table 10, Herbaceous (based on studies of species composition in Mustang) "no appreciable canopy" with 60% ground cover
Nursery	0.246	Average value for bare ground and grass
Orchard	0.2	Average value from global studies of orchards and tree plantations
Pond or Lake	0.04	Global average values for different water body types
Sand	0.45	Wischmeier and Smith 1978, Table 10, "no appreciable canopy" with 0% ground cover
Scattered tree	0.45	Wischmeier and Smith 1978, Table 10, "no appreciable canopy" with 0% ground cover
Snow	0.0001	Assuming extremely little erosion from permanent snow
Waterbody	0.04	Global average values for different water body types
Cultivation - Kaski	0.2799	Average of C values by crop type, weighted by the area grown in that crop in Kaski district, according to the Nepal Department of Irrigation. C values from (Morgan, Morgan, and Finney 1982).
Cultivation - Syangja	0.2909	Average of C values by crop type, weighted by the area grown in that crop in Syangja district, according to the Nepal Department of Irrigation. C values from (Morgan, Morgan, and Finney 1982).

Land use/land cover class	Baseline USLE C value	USLE C value source
Cultivation - Gulmi	0.2085	Average of C values by crop type, weighted by the area grown in that crop in Gulmi district, according to the Nepal Department of Irrigation. C values from (Morgan, Morgan, and Finney 1982).
Cultivation - Mustang	0.1988	Average of C values by crop type, weighted by the area grown in that crop in Mustang district, according to the Nepal Department of Irrigation. C values from (Morgan, Morgan, and Finney 1982).
Cultivation - Myagdi	0.2413	Average of C values by crop type, weighted by the area grown in that crop in Myagdi district, according to the Nepal Department of Irrigation. C values from (Morgan, Morgan, and Finney 1982).
Cultivation - Parbat	0.2954	Average of C values by crop type, weighted by the area grown in that crop in Parbat district, according to the Nepal Department of Irrigation. C values from (Morgan, Morgan, and Finney 1982).
Cultivation - Baglung	0.3427	Average of C values by crop type, weighted by the area grown in that crop in Baglung district, according to the Nepal Department of Irrigation. C values from (Morgan, Morgan, and Finney 1982).

Table A5.2: Baseline USLE P (practice) factors used in hillslope erosion modeling

Land use/land cover class	Baseline USLE P value	USLE P value source
Airport	1	Assumes that no erosion control practices are done
Barren land	1	Assumes that no erosion control practices are done
Built up	1	Assumes that no erosion control practices are done
Bush	1	Assumes that no erosion control practices are done
Cliff	1	Assumes that no erosion control practices are done
Forest	1	Assumes that no erosion control practices are done
Forest - degraded	1	Assumes that no erosion control practices are done
Glacier	1	Assumes that no erosion control practices are done
Grass	0.8	Assumes little to no management
Nursery	1	Assumes that no erosion control practices are done
Orchard	1	Assumes that no erosion control practices are done
Pond or Lake	1	Assumes that no erosion control practices are done
Sand	1	Assumes that no erosion control practices are done
Scattered tree	1	Assumes that no erosion control practices are done
Snow	1	Assumes that no erosion control practices are done
Waterbody	1	Assumes that no erosion control practices are done
Cultivation - Kaski <=5% slope	0.48	Assumes some soil management practices and terracing in place. Value is equal to average of p-factors reported in Shrestha 2016, Maskey et al. 1992, Atreya et al. 2008, Chalise et al. 2019, Tiwari et al. 2009, Das and Bauer 2012, Narain et al. 1998, Munish 2002, Ban et al. 2016, based on application in equivalent slope class.

Land use/land cover class	Baseline USLE P value	USLE P value source
Cultivation - Kaski >5% slope	0.46	Assumes some soil management practices and terracing in place. Value is equal to average of p-factors reported in Shrestha 2016, Maskey et al. 1992, Atreya et al. 2008, Chalise et al. 2019, Tiwari et al 2009 Das and Bauer 2012, Narain et al. 1998, Munish 2002, Ban et al. 2016, based on application in equivalent slope class.
Cultivation - Syangja <=5% slope	0.48	Assumes some soil management practices and terracing in place. Value is equal to average of p-factors reported in Shrestha 2016, Maskey et al. 1992, Atreya et al. 2008, Chalise et al. 2019, Tiwari et al. 2009, Das and Bauer 2012, Narain et al. 1998, Munish 2002, Ban et al. 2016, based on application in equivalent slope class.
Cultivation - Syangja >5% slope	0.46	Assumes some soil management practices and terracing in place. Value is equal to average of p-factors reported in Shrestha 2016, Maskey et al. 1992, Atreya et al. 2008, Chalise et al. 2019, Tiwari et al. 2009, Das and Bauer 2012, Narain et al. 1998, Munish 2002, Ban et al. 2016, based on application in equivalent slope class.
Cultivation - Gulmi <=5% slope	0.48	Assumes some soil management practices and terracing in place. Value is equal to average of p-factors reported in Shrestha 2016, Maskey et al. 1992, Atreya et al. 2008, Chalise et al. 2019, Tiwari et al. 2009, Das and Bauer 2012, Narain et al. 1998, Munish 2002, Ban et al. 2016, based on application in equivalent slope class.
Cultivation - Gulmi >5% slope	0.46	Assumes some soil management practices and terracing in place. Value is equal to average of p-factors reported in Shrestha 2016, Maskey et al. 1992, Atreya et al. 2008, Chalise et al. 2019, Tiwari et al. 2009, Das and Bauer 2012, Narain et al. 1998, Munish 2002, Ban et al. 2016, based on application in equivalent slope class.
Cultivation - Mustang <=5% slope	0.48	Assumes some soil management practices and terracing in place. Value is equal to average of p-factors reported in Shrestha 2016, Maskey et al. 1992, Atreya et al. 2008, Chalise et al. 2019, Tiwari et al. 2009, Das and Bauer 2012, Narain et al. 1998, Munish 2002, Ban et al. 2016, based on application in equivalent slope class.
Cultivation - Mustang >5% slope	0.46	Assumes some soil management practices and terracing in place. Value is equal to average of p-factors reported in Shrestha 2016, Maskey et al. 1992, Atreya et al. 2008, Chalise et al. 2019, Tiwari et al. 2009, Das and Bauer 2012, Narain et al. 1998, Munish 2002, Ban et al. 2016, based on application in equivalent slope class.
Cultivation - Myagdi <=5% slope	0.48	Assumes some soil management practices and terracing in place. Value is equal to average of p-factors reported in Shrestha 2016, Maskey et al. 1992, Atreya et al. 2008, Chalise et al. 2019, Tiwari et al. 2009, Das and Bauer 2012, Narain et al. 1998, Munish 2002, Ban et al. 2016, based on application in equivalent slope class.
Cultivation - Myagdi >5% slope	0.46	Assumes some soil management practices and terracing in place. Value is equal to average of p-factors reported in Shrestha 2016, Maskey et al. 1992, Atreya et al. 2008, Chalise et al. 2019, Tiwari et al. 2009, Das and Bauer 2012, Narain et al. 1998, Munish 2002, Ban et al. 2016, based on application in equivalent slope class.

Land use/land cover class	Baseline USLE P value	USLE P value source
Cultivation - Parbat <=5% slope	0.48	Assumes some soil management practices and terracing in place. Value is equal to average of p-factors reported in Shrestha 2016, Maskey et al. 1992, Atreya et al. 2008, Chalise et al. 2019, Tiwari et al. 2009, Das and Bauer 2012, Narain et al. 1998, Munish 2002, Ban et al. 2016, based on application in equivalent slope class.
Cultivation - Parbat >5% slope	0.46	Assumes some soil management practices and terracing in place. Value is equal to average of p-factors reported in Shrestha 2016, Maskey et al. 1992, Atreya et al. 2008, Chalise et al. 2019, Tiwari et al. 2009, Das and Bauer 2012, Narain et al. 1998, Munish 2002, Ban et al. 2016, based on application in equivalent slope class.
Cultivation - Baglung <=5% slope	0.48	Assumes some soil management practices and terracing in place. Value is equal to average of p-factors reported in Shrestha 2016, Maskey et al. 1992, Atreya et al. 2008, Chalise et al. 2019, Tiwari et al. 2009, Das and Bauer 2012, Narain et al. 1998, Munish 2002, Ban et al. 2016, based on application in equivalent slope class.
Cultivation - Baglung >5% slope	0.46	Assumes some soil management practices and terracing in place. Value is equal to average of p-factors reported in Shrestha 2016, Maskey et al. 1992, Atreya et al. 2008, Chalise et al. 2019, Tiwari et al. 2009, Das and Bauer 2012, Narain et al. 1998, Munish 2002, Ban et al. 2016, based on application in equivalent slope class.

Table A5.3: USLE C (crop) factors for management activities

Land use/land cover class	Activity USLE C value	USLE C value source
Cultivation - Kaski <=5% slope with soil and water conservation practices	0.2799	Same as baseline
Cultivation - Kaski >5% slope with terrace improvement	0.2799	Same as baseline
Cultivation - Syangja <=5% slope with soil and water conservation practices	0.2909	Same as baseline
Cultivation - Syangja >5% slope with terrace improvement	0.2909	Same as baseline
Cultivation - Gulmi <=5% slope with soil and water conservation practices	0.2085	Same as baseline
Cultivation - Gulmi >5% slope with terrace improvement	0.2085	Same as baseline
Cultivation - Mustang <=5% slope with soil and water conservation practices	0.1988	Same as baseline
Cultivation - Mustang >5% slope with terrace improvement	0.1988	Same as baseline
Cultivation - Myagdi <=5% slope with soil and water conservation practices	0.2413	Same as baseline
Cultivation - Myagdi >5% slope with terrace improvement	0.2413	Same as baseline
Cultivation - Parbat <=5% slope with soil and water conservation practices	0.2954	Same as baseline
Cultivation - Parbat >5% slope with terrace improvement	0.2954	Same as baseline
Cultivation - Baglung <=5% slope with soil and water conservation practices	0.3427	Same as baseline
Cultivation - Baglung >5% slope with terrace improvement	0.3427	Same as baseline
Forest - degraded with rehabilitation	0.004	Global average value for forest, from InVEST coefficient literature database (NatCap 2013)
Grass with rangeland management	0.043	Wischmeier & Smith (1978), value for 80% ground cover
Barren land with landslide rehabilitation	0.45	Same as baseline

Table A5.4. USLE P (practice) factors for management activities

Land use/land cover class	Activity USLE P value	USLE P value source
Cultivation - Kaski <=5% slope with soil and water conservation practices	0.11	Value is equal to minimum of p-factors reported in Shrestha 2016, Maskey et al. 1992, Atreya et al. 2008, Chalise et al. 2019, Tiwari et al. 2009, Das and Bauer 2012, Narain et al. 1998, Munish 2002, Ban et al. 2016, based on application in equivalent slope class.
Cultivation - Kaski >5% slope with terrace improvement	0.11	Value is equal to minimum of p-factors reported in Shrestha 2016, Maskey et al. 1992, Atreya et al. 2008, Chalise et al. 2019, Tiwari et al. 2009, Das and Bauer 2012, Narain et al. 1998, Munish 2002, Ban et al. 2016, based on application in equivalent slope class.
Cultivation - Syangja <=5% slope with soil and water conservation practices	0.11	Value is equal to minimum of p-factors reported in Shrestha 2016, Maskey et al. 1992, Atreya et al. 2008, Chalise et al. 2019, Tiwari et al 2009., Das and Bauer 2012, Narain et al. 1998, Munish 2002, Ban et al. 2016, based on application in equivalent slope class.
Cultivation - Syangja >5% slope with terrace improvement	0.11	Value is equal to minimum of p-factors reported in Shrestha 2016, Maskey et al. 1992, Atreya et al. 2008, Chalise et al. 2019, Tiwari et al. 2009, Das and Bauer 2012, Narain et al. 1998, Munish 2002, Ban et al. 2016, based on application in equivalent slope class.
Cultivation - Gulmi <=5% slope with soil and water conservation practices	0.11	Value is equal to minimum of p-factors reported in Shrestha 2016, Maskey et al. 1992, Atreya et al. 2008, Chalise et al. 2019, Tiwari et al. 2009, Das and Bauer 2012, Narain et al. 1998, Munish 2002, Ban et al. 2016, based on application in equivalent slope class.
Cultivation - Gulmi >5% slope with terrace improvement	0.11	Value is equal to minimum of p-factors reported in Shrestha 2016, Maskey et al. 1992, Atreya et al. 2008, Chalise et al. 2019, Tiwari et al. 2009, Das and Bauer 2012, Narain et al. 1998, Munish 2002, Ban et al. 2016, based on application in equivalent slope class.
Cultivation - Mustang <=5% slope with soil and water conservation practices	0.11	Value is equal to minimum of p-factors reported in Shrestha 2016, Maskey et al. 1992, Atreya et al. 2008, Chalise et al. 2019, Tiwari et al. 2009, Das and Bauer 2012, Narain et al. 1998, Munish 2002, Ban et al. 2016, based on application in equivalent slope class.
Cultivation - Mustang >5% slope with terrace improvement	0.11	Value is equal to minimum of p-factors reported in Shrestha 2016, Maskey et al. 1992, Atreya et al. 2008, Chalise et al. 2019, Tiwari et al. 2009, Das and Bauer 2012, Narain et al. 1998, Munish 2002, Ban et al. 2016, based on application in equivalent slope class.
Cultivation - Myagdi <=5% slope with soil and water conservation practices	0.11	Value is equal to minimum of p-factors reported in Shrestha 2016, Maskey et al. 1992, Atreya et al. 2008, Chalise et al. 2019, Tiwari et al. 2009, Das and Bauer 2012, Narain et al. 1998, Munish 2002, Ban et al. 2016, based on application in equivalent slope class.
Cultivation - Myagdi >5% slope with terrace improvement	0.11	Value is equal to minimum of p-factors reported in Shrestha 2016, Maskey et al. 1992, Atreya et al. 2008, Chalise et al. 2019, Tiwari et al. 2009, Das and Bauer 2012, Narain et al. 1998, Munish 2002, Ban et al. 2016, based on application in equivalent slope class.

Land use/land cover class	Activity USLE P value	USLE P value source
Cultivation - Parbat <=5% slope with soil and water conservation practices	0.11	Value is equal to minimum of p-factors reported in Shrestha 2016, Maskey et al. 1992, Atreya et al. 2008, Chalise et al. 2019, Tiwari et al. 2009, Das and Bauer 2012, Narain et al. 1998, Munish 2002, Ban et al. 2016, based on application in equivalent slope class.
Cultivation - Parbat >5% slope with terrace improvement	0.11	Value is equal to minimum of p-factors reported in Shrestha 2016, Maskey et al. 1992, Atreya et al. 2008, Chalise et al. 2019, Tiwari et al. 2009, Das and Bauer 2012, Narain et al. 1998, Munish 2002, Ban et al. 2016, based on application in equivalent slope class.
Cultivation - Baglung <=5% slope with soil and water conservation practices	0.11	Value is equal to minimum of p-factors reported in Shrestha 2016, Maskey et al. 1992, Atreya et al. 2008, Chalise et al. 2019, Tiwari et al. 2009, Das and Bauer 2012, Narain et al. 1998, Munish 2002, Ban et al. 2016, based on application in equivalent slope class.
Cultivation - Baglung >5% slope with terrace improvement	0.11	Value is equal to minimum of p-factors reported in Shrestha 2016, Maskey et al. 1992, Atreya et al. 2008, Chalise et al. 2019, Tiwari et al. 2009, Das and Bauer 2012, Narain et al. 1998, Munish 2002, Ban et al. 2016, based on application in equivalent slope class.
Forest - degraded with rehabilitation	1	Same as baseline
Grass with rangeland management	0.8	Assumes some management practices in place.
Barren land with landslide rehabilitation	0.125	Value is equal to p-factors reported for similar activities in Shrestha 2016.

For assessing the degraded scenario, all USLE P values were set to 1, indicating that no management activities are done.

Carbon storage

Table A5.5: Land cover and land use-based baseline carbon stock values used in this study.

LULC class	Carbon stored (Mg/ha)	Source(s)
Cliff	1	Ruesch and Gibbs 2008
Cultivation	34.25	Ruesch and Gibbs 2008 Dahal and Bajracharya 2013
Grass	35.25	Ruesch and Gibbs, 2008 Dahal and Bajracharya 2013
Barren Land	1	Ruesch and Gibbs, 2008
Bush	37	Ruesch and Gibbs, 2008
Pond or Lake	0	Ruesch and Gibbs, 2008
Sand	1	Ruesch and Gibbs, 2008
Waterbody	0	Ruesch and Gibbs, 2008
Built Up	1	Ruesch and Gibbs, 2008
Nursery	5	Ruesch and Gibbs, 2008
Airport	0	Ruesch and Gibbs, 2008
Scattered Tree	27.48	MoFSC 2016 Ruesch and Gibbs, 2008 Dahal and Bajracharya, 2013
Snow	0	Ruesch and Gibbs, 2008
Glacier	0	Ruesch and Gibbs, 2008
Orchard	92.25	Ruesch and Gibbs 2008 Dahal and Bajracharya, 2013
Forest - Middle Mountains	102.92	MoFSC, 2016 Dahal and Bajracharya, 2013
Forest - High Mountains	178.23	MoFSC, 2016 Dahal and Bajracharya, 2013
Forest - High Himal	178.23	MoFSC, 2016 Dahal and Bajracharya, 2013

To calculate the carbon sequestration from watershed management interventions, we assume changes in above- and below-ground and soil organic carbon pools based on the type of land use land cover at the intervention site and the type of intervention. For soil and water conservation, hill terrace improvement, degraded forest rehabilitation, and degraded grazing land rehabilitation, we use data from (Cardinael et al. 2018), which give a mean response ratio reflecting the ratio of soil organic carbon (SOC) before and after implementation of a variety of agroforestry practices (e.g. hedgerows, tree species intercropped with annual crops).

We apply the mean response ratio of 1.4 from Cardinael et al. (2018) to soil and water conservation and terrace improvement activities, based on studies of conversion from cropland to silvoarable practices in warm temperate Asia (n=7). This value is similar to one reported by (Dahal and Bajracharya 2013), who found a mean response ratio of 1.5 from adoption of sustainable soil management practices across four

districts of Nepal. For grassland rehabilitation, we use the mean response ratio of 1.05 reported by Cardinael et al. (2018) for conversion of grassland to silvopasture in temperate regions (n=9). For rehabilitation of degraded forest, mean response ratio values were not available, so we assume a response ratio of 1.4 for forests rehabilitated in the middle mountain region. We opted to use Cardinael et al. (2018) values over the Dahal and Bajracharya (2013) study in Nepal, because there are a larger number of study sites included in the Cardinael study, and because the reported coefficients have recently been included in the improved 2006 IPCC National GHG Inventory Guidelines. We convert tons of C stored to CO_2 equivalents (CO_2e) using the standard conversion factor of 3.667.

REFERENCES

(MoFSC) Ministry of Forests and Soil Conservation. 2016. "National Forest Reference Level of Nepal (2000 – 2010)." Kathmandu, Nepal. https://redd.unfccc.int/files/nepal_frl_jan_8__2017.pdf.

(NatCap) The Natural Capital Project. 2013. "Sediment and Nutrient Model Parameter Database." Stanford, CA. http://www.naturalcapitalproject.org/invest/.

Atreya, Kishor, Subodh Sharma, Roshan M. Bajracharya, and Neeranjan P. Rajbhandari. 2008. "Developing a Sustainable Agro-System for Central Nepal Using Reduced Tillage and Straw Mulching." *Journal of Environmental Management*. https://doi.org/10.1016/j.jenvman.2007.03.017.

Ban, Jeevan, Insang Yu, and Sangman Jeong. 2016. "Estimation of Soil Erosion Using RUSLE Model and GIS Techniques for Conservation Planning from Kulekhani Reservoir Catchment, Nepal." *Journal of Korean Society of Hazard Mitigation* 16: 323–30. https://doi.org/10.9798/KOSHAM.2016.16.3.323.

Cardinael, Rémi, Viviane Umulisa, Anass Toudert, Alain Olivier, Louis Bockel, and Martial Bernoux. 2018. "Revisiting IPCC Tier 1 Coefficients for Soil Organic and Biomass Carbon Storage in Agroforestry Systems." *Environmental Research Letters* 13 (12): 124020. https://doi.org/10.1088/1748-9326/aaeb5f.

Chalise, Devraj, Lalit Kumar, and Paul Kristiansen. 2019. "Land Degradation by Soil Erosion in Nepal: A Review." *Soil Systems* . https://doi.org/10.3390/soilsystems3010012.

Dahal, Nagmindra, and Roshan M Bajracharya. 2013. "Effects of Sustainable Soil Management Practices on Distribution of Soil Organic Carbon in Upland Agricultural Soils of Mid-Hills of Nepal." *Nepal Journal of Science and Technology* 13 (1): 133–41. https://doi.org/10.3126/njst.v13i1.7452.

Das, Romy, and Siegfried Bauer. 2012. "Bio-Economic Analysis of Soil Conservation Technologies in the Mid-Hill Region of Nepal." *Soil and Tillage Research*. https://doi.org/10.1016/j.still.2012.01.016.

K, Munish. 2002. "Impact of Soil & Water Conservation on Erosion Loss and Yield of Kharif Crops under Ravenous Watershed." *Proceedings of Indian Association of Soil & Water Conservationists* Dehradun c: 301–3.

Maskey, R.B., D. Joshi, and P.L. Maharjan. 1992. "Management of Slopping Lands for Sustainable Agriculture in Nepal." In: IBSRAM (International Board for Soil Research, Management) (Ed.), Technical Report on the Management of Slopping Lands for Sustainable Agriculture in Asia. Phase I, 1988-1991, Network Document No. 2. Thailand.

Morgan, R.P.C., D.D.V. Morgan, and H.J. Finney. 1982. "Stability of Agricultural Ecosystems: Documentation of a Simple Model for Soil Erosion Assessment." Collaborative Paper CP-82–59.

Narain, Pratap, R.K. Singh, N.S. Sindhwal, and P. Joshie. 1998. "Agroforestry for Soil and Water Conservation in the Western Himalayan Valley Region of India 1. Runoff, Soil and Nutrient Losses." *Agroforestry Systems* 39: 175–189. https://link-springer-com.stanford.idm.oclc.org/content/pdf/10.1007%2F978-94-007-7723-1.pdf.

Ruesch, Aaron, and Holly K. Gibbs. 2008. "New IPCC Tier-1 Global Biomass Carbon Map For the Year 2000." Oak Ridge, Tennessee.

Shrestha, Ser Bahadur. 2016. "Soil erosion and payment for sediment retention in kulekhani watershed." Agricultural and Forestry University (Nepal).

Tiwari, Krishna R, Bishal K Sitaula, Roshan M Bajracharya, and Trond B∅rresen. 2009. "Runoff and Soil Loss Responses to Rainfall, Land Use, Terracing and Management Practices in the Middle Mountains of Nepal." *Acta Agriculturae Scandinavica, Section B — Soil & Plant Science* 59 (3): 197–207. https://doi.org/10.1080/09064710802006021.

Wischmeier, W H, and D Smith. 1978. "Predicting Rainfall Erosion Losses: A Guide to Conservation Planning."

Washington DC: U.S. Department of Agriculture, Agriculture Handbook No. 537.

APPENDIX 6: SUMMARY OF DATA SOURCES AND PARAMETER VALUES, MANGLA

HILLSLOPE EROSION (INVEST SDR MODEL)

Table A6.1. Baseline USLE C (crop) factors used in hillslope erosion modeling

Land use/land cover class	Baseline USLE C value	USLE C value source
Cropland: rainfed	0.2654	Average of C values from (Morgan, Morgan, and Finney 1982)
Herbaceous cover	0.091	Wischmeier and Smith 1978, Table 10, Herbaceous "no appreciable canopy" with 60% ground cover
Tree or shrub cover	0.0765	Average of Shrubland and Tree cover: mixed leaf type
Cropland: irrigated or post-flooding	0.2654	Wischmeier and Smith 1978, Table 10, "appreciable brush or bushes" with 50-75% cover, 40% ground cover
Mosaic cropland (>50%) / natural vegetation (tree: shrub: herbaceous cover) (<50%)	0.2087	Weighted average of Cropland: rainfed (70%) and Tree or shrub cover, Shrubland and Tree cover: mixed leaf type (30%)
Mosaic natural vegetation (tree: shrub: herbaceous cover) (>50%) / cropland (<50%)	0.1332	Weighted average of Tree or shrub cover, Shrubland and Tree cover: mixed leaf type (70%) and Cropland: rainfed (30%)
Tree cover: broadleaved: evergreen: closed to open (>15%)	0.0192	Low value from InVEST coefficient literature database (NatCap 2013), modified to assume degraded condition by dividing by 0.26, to match literature findings of forest rehabilitation impacts (Shrestha 2016)
Tree cover: broadleaved: deciduous: closed to open (>15%)	0.0308	High value from InVEST coefficient literature database (NatCap 2013), modified to assume degraded condition by dividing by 0.26, to match literature findings of forest rehabilitation impacts (Shrestha 2016)
Tree cover: broadleaved: deciduous: closed (>40%)	0.0269	Mid-high value from InVEST coefficient literature database (NatCap 2013), modified to assume degraded condition by dividing by 0.26, to match literature findings of forest rehabilitation impacts (Shrestha 2016)
Tree cover: needleleaved: evergreen: closed to open (>15%)	0.0192	Low value from InVEST coefficient literature database (NatCap 2013), modified to assume degraded condition by dividing by 0.26, to match literature findings of forest rehabilitation impacts (Shrestha 2016)
Tree cover: needleleaved: evergreen: closed (>40%)	0.0154	Mid-low value from InVEST coefficient literature database (NatCap 2013), modified to assume degraded condition by dividing by 0.26, to match literature findings of forest rehabilitation impacts (Shrestha 2016)

Land use/land cover class	Baseline USLE C value	USLE C value source
Tree cover: needleleaved: deciduous: closed to open (>15%)	0.0308	High value from InVEST coefficient literature database (NatCap 2013), modified to assume degraded condition by dividing by 0.26, to match literature findings of forest rehabilitation impacts (Shrestha 2016)
Tree cover: needleleaved: deciduous: closed (>40%)	0.0269	Mid-high value from InVEST coefficient literature database (NatCap 2013), modified to assume degraded condition by dividing by 0.26, to match literature findings of forest rehabilitation impacts (Shrestha 2016)
Tree cover: mixed leaf type (broadleaved and needleleaved)	0.0231	Middle value from InVEST coefficient literature database (NatCap 2013), modified to assume degraded condition by dividing by 0.26, to match literature findings of forest rehabilitation impacts (Shrestha 2016)
Mosaic tree and shrub (>50%) / herbaceous cover (<50%)	0.0809	Weighted average of Shrubland and Tree cover: mixed leaf type (70%) and Herbaceous (30%)
Mosaic herbaceous cover (>50%) / tree and shrub (<50%)	0.0867	Weighted average of Herbaceous (70%) and Shrubland and Tree cover: mixed leaf type (30%)
Shrubland	0.13	Wischmeier and Smith 1978, Table 10, average of "appreciable brush or bushes" with 75% & 25% cover, 40% ground cover
Grassland	0.091	Wischmeier and Smith 1978, Table 10, Herbaceous "no appreciable canopy" with 60% ground cover
Sparse vegetation (tree: shrub: herbaceous cover) (<15%)	0.4131	Weighted average of Bare areas (90%) and Shrubland, Tree cover: mixed leaf type, and Herbaceous (10%)
Tree cover: flooded: saline water	0.001	Assumed that very minimal erosion is possible.
Shrub or herbaceous cover: flooded: fresh/ saline/brackish water	0.001	Assumed that very minimal erosion is possible.
Urban areas	0.2853	Global average value for built up areas, from InVEST coefficient literature database (NatCap 2013)
Bare areas	0.45	Wischmeier and Smith 1978, Table 10, "no appreciable canopy" with 0% ground cover
Water b odies	0	Assumed that no erosion is possible.
Permanent snow and ice	0.0001	Assumed that very minimal erosion is possible.

Table A6.2: Baseline USLE P (practice) factors used in hillslope erosion modeling

Land use/land cover class	Baseline USLE P value	USLE P value source
Cropland: rainfed	0.88	Assumes little to no management practices currently in place. Value is equal to max of p-factors reported in Shrestha 2016, Maskey et al. 1992, Atreya et al. 2008, Chalise et al. 2019, Tiwari et al. 2009, Das and Bauer 2012, Narain et al. 1998, Munish 2002, Ban et al. 2016.
Herbaceous cover	1	Assumes that no erosion control practices are done
Tree or shrub cover	1	Assumes that no erosion control practices are done
Cropland: irrigated or post-flooding	0.88	Assumes little to no management practices currently in place. Value is equal to max of p-factors reported in Shrestha 2016, Maskey et al. 1992, Atreya et al. 2008, Chalise et al. 2019, Tiwari et al. 2009, Das and Bauer 2012, Narain et al. 1998, Munish 2002, Ban et al. 2016.
Mosaic cropland (>50%) / natural vegetation (tree: shrub: herbaceous cover) (<50%)	0.916	Weighted average of 75% of cropland value and 25% of average of Mixed trees and Shrubland.
Mosaic natural vegetation (tree: shrub: herbaceous cover) (>50%) / cropland (<50%)	0.964	Weighted average of 25% of cropland value and 75% of average of Mixed trees and Shrubland.
Tree cover: broadleaved: evergreen: closed to open (>15%)	1	Assumes that no erosion control practices are done
Tree cover: broadleaved: deciduous: closed to open (>15%)	1	Assumes that no erosion control practices are done
Tree cover: broadleaved: deciduous: closed (>40%)	1	Assumes that no erosion control practices are done
Tree cover: needleleaved: evergreen: closed to open (>15%)	1	Assumes that no erosion control practices are done
Tree cover: needleleaved: evergreen: closed (>40%)	1	Assumes that no erosion control practices are done
Tree cover: needleleaved: deciduous: closed to open (>15%)	1	Assumes that no erosion control practices are done

Land use/land cover class	Baseline USLE P value	USLE P value source
Tree cover: needleleaved: deciduous: closed (>40%)	1	Assumes that no erosion control practices are done
Tree cover: mixed leaf type (broadleaved and needleleaved)	1	Assumes that no erosion control practices are done
Mosaic tree and shrub (>50%) / herbaceous cover (<50%)	1	Assumes that no erosion control practices are done
Mosaic herbaceous cover (>50%) / tree and shrub (<50%)	1	Assumes that no erosion control practices are done
Shrubland	1	Assumes that no erosion control practices are done
Grassland	1	Assumes that no erosion control practices are done
Sparse vegetation (tree: shrub: herbaceous cover) (<15%)	1	Assumes that no erosion control practices are done
Tree cover: flooded: saline water	1	Assumes that no erosion control practices are done
Shrub or herbaceous cover: flooded: fresh/ saline/brackish water	1	Assumes that no erosion control practices are done
Urban areas	1	Assumes that no erosion control practices are done
Bare areas	1	Assumes that no erosion control practices are done
Water bodies	1	Assumes that no erosion control practices are done
Permanent snow and ice	1	Assumes that no erosion control practices are done

Table A6.3: USLE C (crop) factors for management activities

Land use/land cover class	Activity USLE C value	USLE C value source
Cropland: rainfed <=5% slope with soil and water cons	0.2654	Same as baseline
Cropland: rainfed >5% slope with terrace improvement	0.2654	Same as baseline
Cropland: irrigated or post-flooding <=5% slope with soil and water cons	0.2654	Same as baseline
Cropland: irrigated or post-flooding >5% slope with terrace improvement	0.2654	Same as baseline
Mosaic cropland (>50%) / natural vegetation (tree: shrub: herbaceous cover) (<50%) <=5% slope with soil and water cons	0.2087	Same as baseline
Mosaic cropland (>50%) / natural vegetation (tree: shrub: herbaceous cover) (<50%) >5% slope with terrace improvement	0.2087	Same as baseline
Mosaic natural vegetation (tree: shrub: herbaceous cover) (>50%) / cropland (<50%) <=5% slope with soil and water cons	0.1332	Same as baseline
Mosaic natural vegetation (tree: shrub: herbaceous cover) (>50%) / cropland (<50%) >5% slope with terrace improvement	0.1332	Same as baseline
Mosaic cropland (>50%) / natural vegetation (tree: shrub: herbaceous cover) (<50%) <=5% slope with forest rehabilitation	0.1876	Changed C factor for 30% of area that is natural vegetation to 0.006, value of "mixed forest" in good condition.
Mosaic cropland (>50%) / natural vegetation (tree: shrub: herbaceous cover) (<50%) >5% slope with forest rehabilitation	0.1876	Changed C factor for 30% of area that is natural vegetation to 0.006, value of "mixed forest" in good condition.
Mosaic natural vegetation (tree: shrub: herbaceous cover) (>50%) / cropland (<50%) <=5% slope with forest rehabilitation	0.0838	Changed C factor for 70% of area that is natural vegetation to 0.006, value of "mixed forest" in good condition.
Mosaic natural vegetation (tree: shrub: herbaceous cover) (>50%) / cropland (<50%) >5% slope with forest rehabilitation	0.0838	Changed C factor for 70% of area that is natural vegetation to 0.006, value of "mixed forest" in good condition.
Mosaic cropland (>50%) / natural vegetation (tree: shrub: herbaceous cover) (<50%) <=5% slope with soil and water cons AND forest rehabilitation	0.1876	Changed C factor for 30% of area that is natural vegetation to 0.006, value of "mixed forest" in good condition. C factor for 70% of area that is cropland remains same as baseline.

Land use/land cover class	Activity USLE C value	USLE C value source
Mosaic cropland (>50%) / natural vegetation (tree: shrub: herbaceous cover) (<50%) >5% slope with terrace AND forest rehabilitation	0.1876	Changed C factor for 30% of area that is natural vegetation to 0.006, value of "mixed forest" in good condition. C factor for 70% of area that is cropland remains same as baseline.
Mosaic natural vegetation (tree: shrub: herbaceous cover) (>50%) / cropland (<50%) <=5% slope with soil and water cons AND forest rehabilitation	0.0838	Changed C factor for 70% of area that is natural vegetation to 0.006, value of "mixed forest" in good condition. C factor for 30% of area that is cropland remains same as baseline.
Mosaic natural vegetation (tree: shrub: herbaceous cover) (>50%) / cropland (<50%) >5% slope with terracing AND forest rehabilitation	0.0838	Changed C factor for 70% of area that is natural vegetation to 0.006, value of "mixed forest" in good condition. C factor for 30% of area that is cropland remains same as baseline.
Tree cover: broadleaved: evergreen: closed to open (>15%) with forest rehabilitation	0.005	InVEST coefficient literature database (NatCap 2013), assuming forest in good condition
Tree cover: broadleaved: deciduous: closed to open (>15%) with forest rehabilitation	0.008	InVEST coefficient literature database (NatCap 2013), assuming forest in good condition
Tree cover: broadleaved: deciduous: closed (>40%) with forest rehabilitation	0.007	InVEST coefficient literature database (NatCap 2013), assuming forest in good condition
Tree cover: needleleaved: evergreen: closed to open (>15%) with forest rehabilitation	0.005	InVEST coefficient literature database (NatCap 2013), assuming forest in good condition
Tree cover: needleleaved: evergreen: closed (>40%) with forest rehabilitation	0.004	InVEST coefficient literature database (NatCap 2013), assuming forest in good condition
Tree cover: needleleaved: deciduous: closed to open (>15%) with forest rehabilitation	0.008	InVEST coefficient literature database (NatCap 2013), assuming forest in good condition
Tree cover: needleleaved: deciduous: closed (>40%) with forest rehabilitation	0.007	InVEST coefficient literature database (NatCap 2013), assuming forest in good condition
Tree cover: mixed leaf type (broadleaved and needleleaved) with forest rehabilitation	0.006	InVEST coefficient literature database (NatCap 2013), assuming forest in good condition
Grassland with rangeland mgmt.	0.043	Change C factor to Wischmeier and Smith 1978, grassland with 80% vegetation cover
Cropland: rainfed <=5% slope with soil and water cons	0.2654	Same as baseline
Cropland: rainfed >5% slope with terrace improvement	0.2654	Same as baseline

Table A6.4. USLE P (practice) factors for management activities

Land use/land cover class	Activity USLE P value	USLE P value source
Cropland: rainfed <=5% slope with soil and water cons	0.48	Average of p-factors reported in Ahmad and Khan 2001, Shrestha 2016, Maskey et al. 1992, Atreya et al. 2008, Chalise et al. 2019, Tiwari et al. 2009, Das and Bauer 2012, Narain et al. 1998, Munish 2002, Ban et al. 2016, based on application in equivalent slope class.
Cropland: rainfed >5% slope with terrace improvement	0.46	Average of p-factors reported in Ahmad and Khan 2001, Shrestha 2016, Maskey et al. 1992, Atreya et al. 2008, Chalise et al. 2019, Tiwari et al. 2009, Das and Bauer 2012, Narain et al. 1998, Munish 2002, Ban et al. 2016, based on application in equivalent slope class.
Cropland: irrigated or post-flooding <=5% slope with soil and water cons	0.48	Average of p-factors reported in Ahmad and Khan 2001, Shrestha 2016, Maskey et al. 1992, Atreya et al. 2008, Chalise et al. 2019, Tiwari et al. 2009, Das and Bauer 2012, Narain et al. 1998, Munish 2002, Ban et al. 2016, based on application in equivalent slope class.
Cropland: irrigated or post-flooding >5% slope with terrace improvement	0.46	Average of p-factors reported in Ahmad and Khan 2001, Shrestha 2016, Maskey et al. 1992, Atreya et al. 2008, Chalise et al. 2019, Tiwari et al. 2009, Das and Bauer 2012, Narain et al. 1998, Munish 2002, Ban et al. 2016, based on application in equivalent slope class.
Mosaic cropland (>50%) / natural vegetation (tree: shrub: herbaceous cover) (<50%) <=5% slope with soil and water cons	0.636	Weighted average of p-factor for cropland and natural vegetation. P-factor for cropland is average of p-factors reported in Ahmad and Khan 2001, Shrestha 2016, Maskey et al. 1992, Atreya et al. 2008, Chalise et al. 2019, Tiwari et al. 2009, Das and Bauer 2012, Narain et al. 1998, Munish 2002, Ban et al. 2016, based on application in equivalent slope class.
Mosaic cropland (>50%) / natural vegetation (tree: shrub: herbaceous cover) (<50%) >5% slope with terrace improvement	0.622	Weighted average of p-factor for cropland and natural vegetation. P-factor for cropland is average of p-factors reported in Ahmad and Khan 2001, Shrestha 2016, Maskey et al. 1992, Atreya et al. 2008, Chalise et al. 2019, Tiwari et al. 2009, Das and Bauer 2012, Narain et al. 1998, Munish 2002, Ban et al. 2016, based on application in equivalent slope class.
Mosaic natural vegetation (tree: shrub: herbaceous cover) (>50%) / cropland (<50%) <=5% slope with soil and water cons	0.844	Weighted average of p-factor for cropland and natural vegetation. P-factor for cropland is average of p-factors reported in Ahmad and Khan 2001, Shrestha 2016, Maskey et al. 1992, Atreya et al. 2008, Chalise et al. 2019, Tiwari et al. 2009, Das and Bauer 2012, Narain et al. 1998, Munish 2002, Ban et al. 2016, based on application in equivalent slope class.
Mosaic natural vegetation (tree: shrub: herbaceous cover) (>50%) / cropland (<50%) >5% slope with terrace improvement	0.838	Weighted average of p-factor for cropland and natural vegetation. P-factor for cropland is average of p-factors reported in Ahmad and Khan 2001, Shrestha 2016, Maskey et al. 1992, Atreya et al. 2008, Chalise et al. 2019, Tiwari et al. 2009, Das and Bauer 2012, Narain et al. 1998, Munish 2002, Ban et al. 2016, based on application in equivalent slope class.
Mosaic cropland (>50%) / natural vegetation (tree: shrub: herbaceous cover) (<50%) <=5% slope with forest rehabilitation	0.916	Weighted average of p-factor for cropland (70%) and natural vegetation (30%). P-factor for forest rehabilitation = 1.

Land use/land cover class	Activity USLE P value	USLE P value source
Mosaic cropland (>50%) / natural vegetation (tree: shrub: herbaceous cover) (<50%) >5% slope with forest rehabilitation	0.916	Weighted average of p-factor for cropland (70%) and natural vegetation (30%). P-factor for forest rehabilitation = 1.
Mosaic natural vegetation (tree: shrub: herbaceous cover) (>50%) / cropland (<50%) <=5% slope with forest rehabilitation	0.964	Weighted average of p-factor for cropland (30%) and natural vegetation (70%). P-factor for forest rehabilitation = 1.
Mosaic natural vegetation (tree: shrub: herbaceous cover) (>50%) / cropland (<50%) >5% slope with forest rehabilitation	0.964	Weighted average of p-factor for cropland (30%) and natural vegetation (70%). P-factor for forest rehabilitation = 1.
Mosaic cropland (>50%) / natural vegetation (tree: shrub: herbaceous cover) (<50%) <=5% slope with soil and water cons AND forest rehabilitation	0.636	Weighted average of p-factor for cropland with soil and water conservation (70%) and natural vegetation (30%). P-factor for forest rehabilitation = 1.
Mosaic cropland (>50%) / natural vegetation (tree: shrub: herbaceous cover) (<50%) >5% slope with terrace AND forest rehabilitation	0.622	Weighted average of p-factor for cropland with soil and water conservation (70%) and natural vegetation (30%). P-factor for forest rehabilitation = 1.
Mosaic natural vegetation (tree: shrub: herbaceous cover) (>50%) / cropland (<50%) <=5% slope with soil and water cons AND forest rehabilitation	0.844	Weighted average of p-factor for cropland with soil and water conservation (30%) and natural vegetation (70%). P-factor for forest rehabilitation = 1.
Mosaic natural vegetation (tree: shrub: herbaceous cover) (>50%) / cropland (<50%) >5% slope with terracing AND forest rehabilitation	0.838	Weighted average of p-factor for cropland with soil and water conservation (30%) and natural vegetation (70%). P-factor for forest rehabilitation = 1.
Tree cover: broadleaved: evergreen: closed to open (>15%) with forest rehabilitation	1	Default value, assumes no active sediment management practices.

Land use/land cover class	Activity USLE P value	USLE P value source
Tree cover: broadleaved: deciduous: closed to open (>15%) with forest rehabilitation	1	Default value, assumes no active sediment management practices.
Tree cover: broadleaved: deciduous: closed (>40%) with forest rehabilitation	1	Default value, assumes no active sediment management practices.
Tree cover: needleleaved: evergreen: closed to open (>15%) with forest rehabilitation	1	Default value, assumes no active sediment management practices.
Tree cover: needleleaved: evergreen: closed (>40%) with forest rehabilitation	1	Default value, assumes no active sediment management practices.
Tree cover: needleleaved: deciduous: closed to open (>15%) with forest rehabilitation	1	Default value, assumes no active sediment management practices.
Tree cover: needleleaved: deciduous: closed (>40%) with forest rehabilitation	1	Default value, assumes no active sediment management practices.
Tree cover: mixed leaf type (broadleaved and needleleaved) with forest rehabilitation	1	Default value, assumes no active sediment management practices.
Grassland with rangeland mgmt.	0.8	Assumes some sediment management practices in place.

Carbon storage

TABLE A6.5: LAND COVER AND LAND USE-BASED BASELINE CARBON STOCK VALUES USED IN THIS STUDY, FROM RUESCH AND GIBBS (2008).

LULC class	Carbon stored (Mg/ha) by Eco floristic Zone	
	Subtropical Mountain	Subtropical Steppe
Cropland: rainfed	5	5
Herbaceous cover	5	4
Tree or shrub cover	47.43	46.36
Cropland: irrigated or post-flooding	5	5
Mosaic cropland (>50%) / natural vegetation (tree: shrub: herbaceous cover) (<50%)	13.49	13.17
Mosaic natural vegetation (tree: shrub: herbaceous cover) (>50%) / cropland (<50%)	24.8	24.07
Tree cover: broadleaved: evergreen: closed to open (>15%)	57.86	55.71
Tree cover: broadleaved: deciduous: closed to open (>15%)	57.86	55.71
Tree cover: broadleaved: deciduous: closed (>40%)	57.86	55.71
Tree cover: needleleaved: evergreen: closed to open (>15%)	57.86	55.71
Tree cover: needleleaved: evergreen: closed (>40%)	57.86	N/A
Tree cover: needleleaved: deciduous: closed to open (>15%)	57.86	N/A
Tree cover: needleleaved: deciduous: closed (>40%)	57.86	N/A
Tree cover: mixed leaf type (broadleaved and needleleaved)	57.86	N/A
Mosaic tree and shrub (>50%) / herbaceous cover (<50%)	34.7	33.65
Mosaic herbaceous cover (>50%) / tree and shrub (<50%)	17.73	16.71
Shrubland	37	N/A
Grassland	4.5	4
Sparse vegetation (tree: shrub: herbaceous cover) (<15%)	4.23	N/A
Tree cover: flooded: saline water	57.86	55.71
Shrub or herbaceous cover: flooded: fresh/saline/brackish water	21	20.5
Urban areas	1	1
Bare areas	1	N/A
Water bodies	0	0
Permanent snow and ice	0	N/A

To calculate the carbon sequestration from watershed management interventions, we assume changes in above- and below-ground and soil organic carbon pools based on the type of land use land cover at the intervention site and the type of intervention. For soil and water conservation, hill terrace improvement, degraded forest rehabilitation, and degraded grazing land rehabilitation, we use data from Cardinael et al. (2018), which give a mean response ratio reflecting the ratio of soil organic carbon (SOC) before and after implementation of a variety of agroforestry practices (e.g. hedgerows, tree species intercropped with annual crops).

We apply the mean response ratio of 1.4 from Cardinael et al. (2018) to soil and water conservation and terrace improvement activities, based on studies of conversion from cropland to silvoarable practices in warm temperate Asia (n=7). For grassland rehabilitation, we use the mean response ratio of 1.05 reported by Cardinael et al. (2018) for conversion of grassland to silvopasture in temperate regions (n=9). For rehabilitation of degraded forest, mean response ratio values were not available, so we assume a response ratio of 1.4 for forests. We convert tons of C stored to CO_2 equivalents (CO_2e) using the standard conversion factor of 3.667.

REFERENCES

(NatCap) The Natural Capital Project. 2013. "Sediment and Nutrient Model Parameter Database." Stanford, CA. http://www.naturalcapitalproject.org/invest/.

Atreya, Kishor, Subodh Sharma, Roshan M. Bajracharya, and Neeranjan P. Rajbhandari. 2008. "Developing a Sustainable Agro-System for Central Nepal Using Reduced Tillage and Straw Mulching." *Journal of Environmental Management*. https://doi.org/10.1016/j.jenvman.2007.03.017.

Ban, Jeevan, Insang Yu, and Sangman Jeong. 2016. "Estimation of Soil Erosion Using RUSLE Model and GIS Techniques for Conservation Planning from Kulekhani Reservoir Catchment, Nepal." *Journal of Korean Society of Hazard Mitigation* 16: 323–30. https://doi.org/10.9798/KOSHAM.2016.16.3.323.

Cardinael, Rémi, Viviane Umulisa, Anass Toudert, Alain Olivier, Louis Bockel, and Martial Bernoux. 2018. "Revisiting IPCC Tier 1 Coefficients for Soil Organic and Biomass Carbon Storage in Agroforestry Systems." *Environmental Research Letters* 13 (12): 124020. https://doi.org/10.1088/1748-9326/aaeb5f.

Chalise, Devraj, Lalit Kumar, and Paul Kristiansen. 2019. "Land Degradation by Soil Erosion in Nepal: A Review." *Soil Systems* . https://doi.org/10.3390/soilsystems3010012.

Das, Romy, and Siegfried Bauer. 2012. "Bio-Economic Analysis of Soil Conservation Technologies in the Mid-Hill Region of Nepal." *Soil and Tillage Research*. https://doi.org/10.1016/j.still.2012.01.016.

K, Munish. 2002. "Impact of Soil & Water Conservation on Erosion Loss and Yield of Kharif Crops under Ravenous Watershed." *Proceedings of Indian Association of Soil & Water Conservationists* Dehradun c: 301–3.

Maskey, R.B., D. Joshi, and P.L. Maharjan. 1992. "Management of Slopping Lands for Sustainable Agriculture in Nepal." In: IBSRAM (International Board for Soil Research, Management) (Ed.), Technical Report on the Management of Slopping Lands for Sustainable Agriculture in Asia. Phase I, 1988-1991, Network Document No. 2. Thailand.

Morgan, R.P.C., D.D.V. Morgan, and H.J. Finney. 1982. "Stability of Agricultural Ecosystems: Documentation of a Simple Model for Soil Erosion Assessment." Collaborative Paper CP-82–59.

Narain, Pratap, R.K. Singh, N.S. Sindhwal, and P. Joshie. 1998. "Agroforestry for Soil and Water Conservation in the Western Himalayan Valley Region of India 1. Runoff, Soil and Nutrient Losses." *Agroforestry Systems* 39: 175–189. https://link-springer-com.stanford.idm.oclc.org/content/pdf/10.1007%2F978-94-007-7723-1.pdf.

Ruesch, Aaron, and Holly K. Gibbs. 2008. "New IPCC Tier-1 Global Biomass Carbon Map For the Year 2000." Oak Ridge, Tennessee.

Shrestha, Ser Bahadur. 2016. "Soil erosion and payment for sediment retention in Kulekhani watershed." Agricultural and Forestry University (Nepal).

Tiwari, Krishna R, Bishal K Sitaula, Roshan M Bajracharya, and Trond BØrresen. 2009. "Runoff and Soil Loss Responses to Rainfall, Land Use, Terracing and Management Practices in the Middle Mountains of Nepal." *Acta Agriculturae Scandinavica, Section B — Soil & Plant Science* 59 (3): 197–207. https://doi.org/10.1080/09064710802006021.

Wischmeier, W H, and D Smith. 1978. "Predicting Rainfall Erosion Losses: A Guide to Conservation Planning." Washington DC: U.S. Department of Agriculture, Agriculture Handbook No. 537.

1818 H Street, NW
Washington, D.C. 20433 USA
Telephone: 202-473-1000
Internet: www.worldbank.org/environment